ABSTRACT

Title of Document:	SMART FABRIC SENSORS FOR FOOT MOTION MONITORING Lina Maria Castano Salcedo, Masters of Science, 2010.
Directed By:	Dr. Alison Flatau, Clark School Dean of Research and Aerospace Engineering Professor

Smart Fabrics or fabrics that have the characteristics of sensors are a wide and emerging field of study. This thesis summarizes an investigation into the development of fabric sensors for use in sensorized socks that can be used to gather real time information about the foot such as gait features. Conventional technologies usually provide 2D information about the foot. Sensorized socks are able to provide angular data in which foot angles are correlated to the output from the sensor enabling 3D monitoring of foot position. Current angle detection mechanisms are mainly heavy and cumbersome; the sensorized socks are not only portable but also non-invasive to the subject who wears them. The incorporation of wireless features into the sensorized socks enabled a remote monitoring of the foot.

SMART FABRIC SENSORS FOR FOOT MOTION MONITORING

By

Lina Maria Castano Salcedo

Thesis submitted to the Faculty of the Graduate School of the
University of Maryland, College Park, in partial fulfillment
Of the requirements for the degree of
Master of Science
2010

Advisory Committee:
Professor Alison B. Flatau, Chair
Professor David Akin
Professor Allen E. Winkelmann

Dedication

I would like to thank the Almighty for allowing me to work in such a great school, it is truly a blessing to have the best professors and be part of this wonderful dynamic engine of knowledge. It is certainly a privilege to learn and be part of it. To my parents and uncle, and specially my mom, who has been there by the minute, always providing her voice of wisdom, love and support. To them, my deepest gratitude. I cannot thank you enough for being such an amazing family.

Acknowledgements

I would like to thank everyone who has kindly contributed to this project in one way or the other. First, thanks to Dr. Alison Flatau for allowing me to work in this wonderful and highly motivational research topic, also for her support with presentations and during conferences. Special thanks to the National Science Foundation for supporting this project [1]. Many thanks to Dr. Allen Winkelmann for providing a place for the experimental setups (Aerolab) presented in this thesis and for his invaluable help with their design and construction, which required a lot of time and effort. His technical expertise and input made a substantial contribution towards the completion of this work. Special thanks to Dr. Shim, from the Kinesiology department for his advice, insight and for allowing us to use some of his lab equipment. Thanks to Dr. Schork from Chemical Engineering, who kindly provided access for one of our first experiments. Thanks also to Andrew Elsberry for his help with the wireless hardware. Many thanks to Zohaib Hasnain for his savvy technical advice and collaboration in computational schemes, and for being a great colleague and friend. Special thanks to Rosalia who was part of the Aerospace Department and who was always a warm, friendly and understanding person you could always talk to. Thanks to all my aerospace friends who have been great people to share with during the course of these two years.

Table of contents

List of Tables

List of Figures

Overview

Fabrics are part of our daily lives. They are present in our clothing, our furniture, and many other articles of common use. More than 70% of the materials we constantly interact with are textiles. They are a perfect target to be turned into sensors due to their high compliance and adaptability to the ergonomics of the human body and the advantages over conventional kinematic and dynamic sensor systems, which can be bulky, heavy and/or rigid. The modification of fabrics to give them sensor characteristics entitles them to the generic name 'Smart Fabrics' or 'Smart textiles'. This is an emerging field with many potential applications, especially in wearable sensor systems, which could be useful in human health monitoring, rehabilitation [2], and sports and multimedia [3]. 'Smart Fabrics' is a broad term that comprises many different or associate subfields such as flexible electronics, pervasive computing and wearable technology. In general, these sensorized fabrics can be categorized according to the different levels of integration of sensing capabilities. These characteristics may be electrical [4, 5], capacitive [6, 7], or optical [8, 9] properties, among others. This thesis addresses sensorizing fabrics mainly with conductive-resistive properties.

Chapter 1: Introduction

1.1 Why smart or sensorized fabrics

The application of sensorized or smart fabrics in aerospace has a range of possibilities, especially in the limb monitoring of astronauts while they are wearing a space suit. It is critical to know what the motion and posture state of the limbs are while the astronauts are performing tasks. Astronauts in microcravity reveal an impaired ability to judge their elbow angles [10] and rate of change of position of the ankles, knees and hip joints [11]. This is due to the effect of microgravity on the proprioceptive sensory receptors, tactile receptors and joint receptors, a fluid shift or sudden release of muscle tone. For instance, the Golgi tendon organs are force transducers and they do not sense weight when in microgravity, only inertial loads acting on the body. An example of this phenomenon is presented in Figure 1.

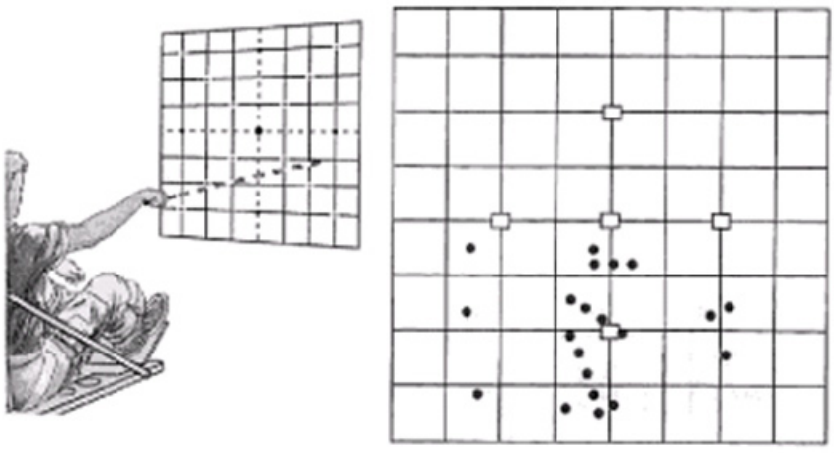

Figure 1. Decrease in position sense accuracy [11], boxes represent targets, dots represent in-flight perceptions of the targets. The divisions represent inches.

In this experiment the astronauts looked at one of the five cardinal targets on a screen (boxes), then closed their eyes and pointed a laser beam at the remembered target position. The results obtained during flight, dots, and show that there is a downward pointing bias when the subjects are in microgravity. Not only limb perception problems but also complete posture perceptions get affected in microgravity; astronauts lean forward showing difficulty in maintaining posture perpendicular to the foot support.

Sensorized fabrics could provide a solution to these aerospace challenges by monitoring position of the legs and feet. Furthermore, not only the monitoring of the lower limbs is possible with this technology but also, a monitoring of other joints and the hands is possible, and even the entire body. The sensorized fabrics may also be used in gloves or other garments to assist motion of exoskeletons or space suite prototypes. The sock prototype that will be presented in this thesis is based on the premise of being able not only to contribute to astronaut gait analysis but also to provide aid in the rehabilitation of patients with walking disabilities such as diabetes and Parkinson disease. The vision for this thesis is that sensorized socks can be used alone as interactive rehabilitation aids for the physical therapist, as well as a complement to smart shoes, which can measure GCF's or ground contact forces for the same purposes. The smart socks could complement the 2D data currently available for obtaining foot data by providing dynamic data about the foot, and joint angles. The conformability and lightweight of the sensorized fabrics make them also an ideal wearable gait analysis tool for characterizing and monitoring gait, assisting in the rehabilitation of patients with lower limb disabilities.

1.2 E-textiles and smart fabrics overview

E-textiles and smart fabrics are the result of an increasing interest in human-technology integration. The goal is to have a computer integrated into every aspect of life providing useful information and useful tools without hindering motion or interrupting normal activities. One could imagine having a shirt that would display the current weather, or a jacket that could play music after touching a button [12]; a t-shirt that would display the heart rate and our favorite news while we are exercising [13], or even a garment that would heat up or cool down as a reaction to the environment, in order to keep the internal body temperature constant. Soldiers could have garments that would outpour healing medicines [14] when broken or cut, or even self camouflage when needed. A hat that could be a cell phone itself, leotards that could correct our posture while we are seating, or even the aesthetic possibility of having a color changing garment in response to our mood or according to the occasion [15]. All these are possible with the newest developments in e-textiles, which are a continuously growing field.

This overview intends to provide a conceptual panoramic of the available techniques and provide a framework for the sensors used for the sock prototypes built in this project. The field of smart fabrics is very broad and can be categorized according to different parameters. First, from a major development motivator point of view we can identify commercial (civilian, sports), medical, research and military applications. An example of each is displayed in Figure 2. More examples on each of these categories can be found in Appendix A. Second, from the sensing element integration perspective we can categorize e-textiles according to the levels of sensor element integration with the fabrics. The

sensors used may be made of conventional electronic materials or they can be made of adapted fabric constitutive components acting as electronic components. It is also important to mention that these technologies do not intend to replace the mainstream hard electronics, but to expand the functionality of fabrics as sensors and to provide a new environment of human-technology interaction. Smart fabrics should be regarded as complimentary in expanding interaction environments and in enabling technology features that could not be carried in any other way. The rising interest in these technologies stems from their physical flexibility and large surface area characteristics which would be unachievable with conventional electronics fabrication methods.

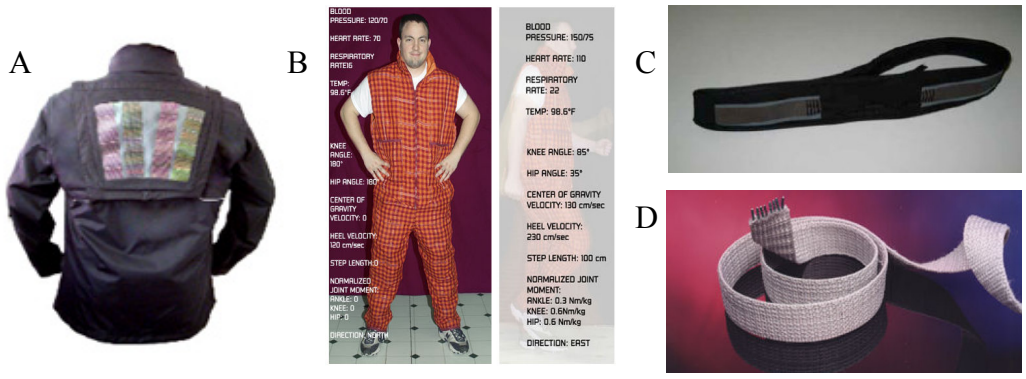

Figure 2. E-textiles and smart fabrics major development motivators: a. Civilian (Solar Jacket)[16], b. Research (Hookie suit)[17], c. Medical (Chest strap)[18], d. Military (Fabrics information cable.)[14]

E-textiles range from very superficially attached electronic components to substitution of fibers and yarns with sensing properties inserted in normal fabrics, to electronic components made of fabric materials. A schematic of the increasing sensing integration into fabrics is shown in Figure 3. From this figure, intrinsically functional elements are adapted to the human in the first two steps (from left to right), Kopin Golden-I [19] and MiThrill vest [20], and are basically still in the realm of portable computers. The next

two steps, hybrid clothing (network of light emitting diodes-LED's sewn into fabric) and hybrid yarns (silk organza) are commonly referred to as e-textiles and comprise a wide range of fabric adapted electronic components, ranging from microcontrollers to PCB boards which can be surface mounted on textiles. The Konarka photovoltaic cell, presented in the last step, is the ideal smart fabric component, namely, an electronic component made of compliant materials or new materials which can have the same functionality as electronic components but with different mechanical properties. In particular, Konarka technologies built the photovoltaic cell using dye-sensitized titanium and electrolyte on a metal wire core using fiber optics principles. The result is a flexible photovoltaic fiber array. A detailed presentation of the elements presented here and more smart fabric devices can be found in Appendix A.

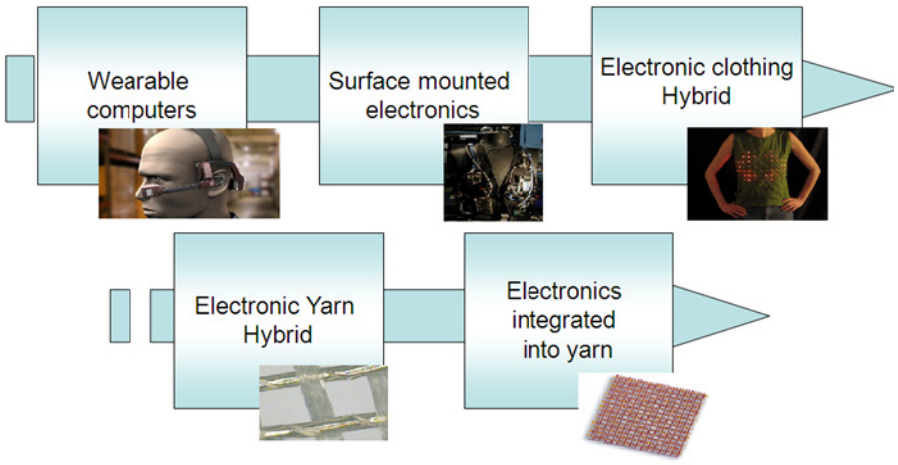

Figure 3. Levels of smart fabric component integration (after [4]) Golden-i[19], MiThril[20], LED shirt [21], hybrid yarn [5], photovoltaic fabric [8]

This thesis focuses on smart fabrics sensorized by coating. Coatings can be intrinsically or extrinsically conductive. Inherently conductive polymers, like doped polypyrrole [22],

polyaniline and PEDOT [23], are used to coat fabric substrates in order to give them sensing capabilities. There is also a method that deals with electrostatic self assembly of conductive nanoparticles onto fabric layers, where the surface of the fibers is infused with combinations of polymers and metals or metal oxides or semiconductors [24]. Extrinsically conductive polymers consist of mixtures of metal particles and non-conductive matrices. Coatings of these mixtures can be applied to fabrics to give them sensing properties. In particular, fabrics can become 'smart' by applying piezoresistive [25], piezoelectric [26] or piezocapacitive [27] materials, usually in the form of polymers due to their elastic properties. Different polymeric materials can be used as coatings and they are chosen according to the sensing property that is desired for a particular application. For example, the piezoresistive properties are present in polymers which can partially or totally conduct electric current. Carbon doped polymers are extrinsically modified polymers with piezoresistive properties. These will be studied in Chapters 2 and 3 of this thesis, where they are experimentally characterized. A theoretical model of their behavior can be found in the gesture monitoring section, section 1.3.

1.2.1 Fabrication, materials and connections

New techniques have to be used in order to obtain good circuit integration into the fabrics (Figure 4). New mechanical requirements associated with, for instance compliance (non-brittle), weight, large sensorized areas, etc., have lead to a series of novel fabrication methods. Electronic components and connections need to be smaller in size, compact, flexible and encapsulated. Conductive threads of different kinds, conductive inks and conductive fabric itself may all be used as compliant interconnects. All these components

may have different techniques of encapsulation, printing and joint connection. Electronic components can be made of fabric materials or they can be conventional components attached with novel methods. An example of the former includes yarns of different electrical resistances that can be used to replace standard capacitors, resistors, and inductors.

The circuits on fabrics are designed as being of low power consumption and high input impedance. A primary method for textile circuitry is called e-broidery, which is used to define circuit traces, component connection pads or sensing surfaces by basically sewing the circuit components on to the fabric. Another technique for building circuits on fabrics consists of soldering the electronic components to fabric conduction lines. A third technique consists of 'ironing on' the circuits on to the fabric, where a printing technique is used to generate a Sn/Cu laser cut fabric circuit. Other alternatives for textile circuitry include conductive inks that are painted on the fabric to create the conductive patterns, such as the process of ink-jet printing.

As for the interfaces or connections of the electronic components (details in Appendix A), several different methods can be used, such as soldering conventional electronic components to embedded conduction lines. Fabric component holders can be sewn and used as holders for i.e. batteries. Components are then easy to sew into the textile. Gripper snaps can also be used as mechanical contacts between components. Conductive adhesives can also be used to attach the components to the fabric. Encapsulation of

conductive lines and components go from thread encapsulation, to epoxy, to fabric paint, these techniques vary according to the intended application.

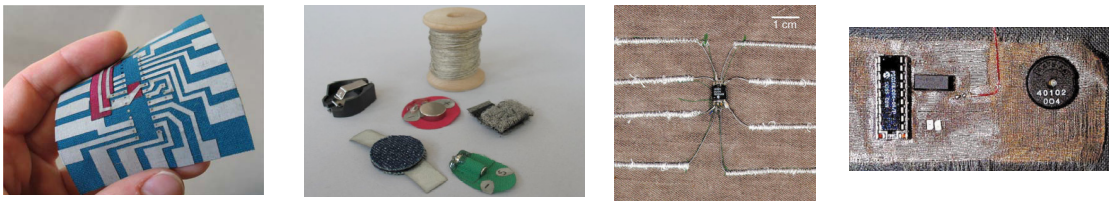

A B C D

Figure 4. Textile circuitry enabling technologies: a. Ironed-on fabric circuit [28], b. Stitchable holders [28], c. Encapsulated conduction lines [5], d. Soldered electronic components [4]

There is a growing number of enabling technologies and materials which are being developed given the flexibility, portability and water resistant requirements of body worn sensors. Novel materials such as QTC, flexible transistors, and carbon nanotubes, and novel techniques such as energy harvesting devices, for instance the body thermoelectric generator chip, can be found in Appendix A.

When sensorizing fabrics, not only should the compliance of components, connections and encapsulation should be taken into consideration but also the mechanics of the fabric itself. Fabrics have different types of construction: woven, knitted, non-woven, nets, braided, and tufted. Appendix C contains a detailed discussion on the properties of the construction of fabrics. Each type of construction has a number of properties associated to them. In particular, socks are mainly knitted, this gives them a natural stretchability, which is enhanced by mixing resilient polymers in the knit. Given these properties, a conductive polymer that reacts or gives a change in output when strained is a good candidate to coat on knit fabrics. The response of the sensors will depend on the combined properties of the fabric and the coated polymer. In this thesis, carbon sensors

are coated on knitted fabrics with the purpose of characterizing human motion, in particular foot angles.

1.3 Posture and gesture monitoring works (mainly carbon printed sensors)

Human posture and gesture studies are an important component of human recognition systems with application to surveillance, identification and human-machine interaction. However, these studies also are important as a way to quantify and characterize the human body for the purpose of aiding in the rehabilitation of patients with impairments. Posture is an arrangement of the body and its limbs, a gesture is a sequence of postures with semantic content. Posture is sometimes a general term for static posture, which was described by [29], however, the term may refer to any arrangement of either the entire body or a particular limb. These studies are usually carried on the human hand or on the entire body. Some of the techniques used are optical, either planar (photographic, video graphic) or 3D, while others deal with clothes which have been sensorized for that purpose. The latter is investigated in this thesis.

In particular, printing carbon based polymers onto stretchable fabrics such as Lycra can provide a perfect body sensor due to its compliant qualities and the piezoresistive behavior of the polymer [30]. Its low cost compared to precious metal powder mixtures [31] is an advantage. The sensor characteristics, such as gauge factor of carbon sensors will be studied in the experimental section of this work. These sensors have been placed on gloves, leotards, and other garment sections in the work of de Rossi et al. [32]. In their works, the sensors are printed on Lycra, a fabric which has been knitted with spandex in

order to enhance resilience properties. However, these sensors present a drift which gives the signal a long settling time, in addition to nonlinearities which become a challenge for real-time processing. These nonlinearities can be seen from the response of a sensor strip to a strain impulse [33] [34], as can be seen in Figure 5. The output depends on both the velocity and acceleration or second rate of change of the sensor length. A first important observation from this figure is that the response of the sensor is positive when the strain is applied and when the strain is released.

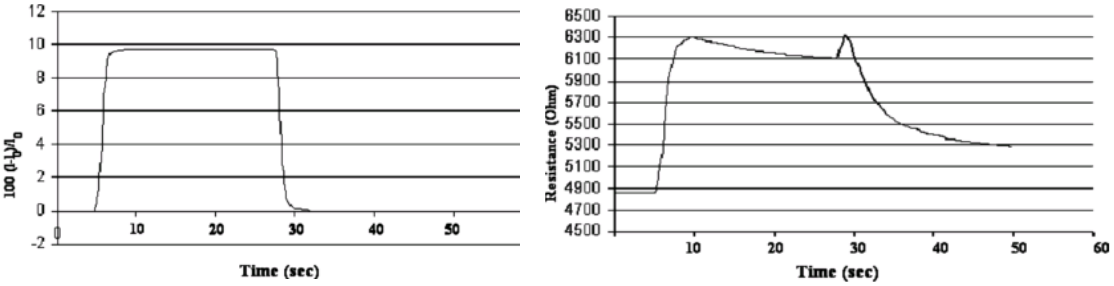

a. Square strain input b. Carbon sensor response

Figure 5. a. Square strain input, b. Carbon sensor response [34]

This behavior is typical of these types of sensors. The second thing to notice is the roll off in resistance. According to the work of [33], the drift can be predicted by acquiring the poles of a linear system that models the behavior of the sensor. These poles are then used to predict the final value of resistance (c_0) after the settling time. The positive peak indicates that the approximation should have a square component in terms of the length of the sensor as an input (see appendix B).

When a garment is worn by the user, the sensors on the garment acquire values that are strictly related to the sensor configuration. A better characterization is obtained with a larger number of sensors. If the number of sensors is large enough and a sufficient

number of sensor locations are used then the values obtained from the sensors can uniquely characterize the considered posture or configuration. A system identification, which maps the space of kinematic configurations into the sensor space, can be constructed. Its inverse will yield the angles when a set of sensor data is provided as an input. Detail of the models used by [33] are included in Appendix B.

1.4 Foot anatomy, articulation and characteristics

Need for monitoring of lower limbs: a clinical perspective.

There are many technologies that aim towards the monitoring of the limbs. However none of them have been completely successful in aiding in problems such as diabetes. Diabetes can cause nerve damage on the feet, making them insensitive to heat, cold or pain. This lack of feeling is called sensory neuropathy and may affect the lower limb motor abilities. The muscles of the foot may also get affected as a consequence of affected nerves and possibly cause the foot to not align properly and create too much pressure in one area of the foot. This might generate a sore which is at risk of infection. About 10% of diabetics generate sores on their feet. In the United States, as of the year 2007, there were a total of 23.6 million people, that is, about 7.8 % of the population with diabetes, where 17.9 million people were diagnosed to have diabetes and 5.7 million had undiagnosed diabetes.

Not only people with diabetes are prone to having foot problems, but also Parkinson patients [35] and stroke patients. Each year about 795,000 people experience a new or

recurrent stroke. Similarly, tens of thousands of people are diagnosed with Parkinson disease per year. These diseases can cause serious damage to the motor abilities of the limbs. Among several motor problems, there are gait and motion disturbances that occur. These include shuffling gait, dystonia (abnormal muscle contractions), and festination (combination of imbalance and short steps that accelerates gait and usually ends in a fall).

Foot anatomy and articulation

Given the premise for this thesis, which entails the possibility of tracking the motion of the foot, we proceed to looking at some of its anatomic aspects, which are determinants of its motion mechanism. The major function of the human foot is locomotion, it cannot grasp but it is adapted for running and striding. It consists of 26 bones (Figure 6a) connected by ligaments: seven tarsal bones, five metatarsal bones and fourteen phalanges.

The bones are articulated by 33 joints and more than a hundred muscles to achieve mobility. In a first simplified model only the ankle joint and two hinged rigid segments are considered. The ankle joint consists of all the bones and tendons around the talus. In a second simplified model two joints are considered: the ankle joint and the metatarsal-phalangeal joint, which is the first joint that connects the forefoot to the midfoot and includes all the meta-phalanx joints of the five fingers. In this second model the foot is viewed as three functional segments: hindfoot (heel), midfoot (arch) and forefoot (toes).

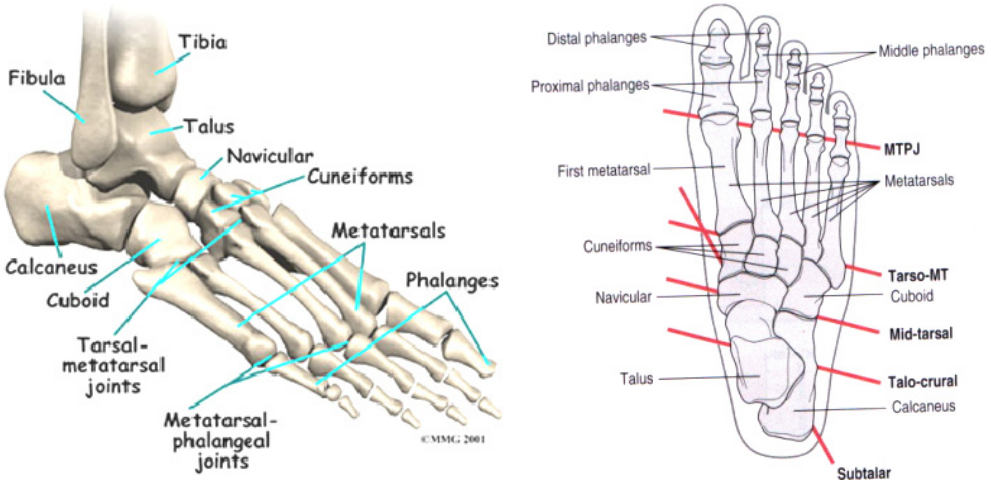

a. Human foot bones b. Major human foot joints

Figure 6. Anatomy of the human foot: a. bones [36], b. joints [37].

The first model (two segment description) is used to define the general types of foot motion (Figure 7a). The two rightmost types depicted in this figure correspond to motion on the saggital plane. It is on this plane where the experimental studies of this thesis will take place. Even though this one joint model is a good approximation to foot motion on the saggital plane, the actual external motion of the foot also includes motion in the frontal and lateral planes. It is way more complex also because there is some internal motion of the foot constituents such as the expansion or contraction of the foot when loaded or unloaded, respectively.

More complex studies consist of dividing the foot into even more segments, such as the ones in Figure 6b (five joints) and from [30], where the foot is divided into: hindfoot, talus, midfoot and medial, and lateral forefoot segments. These complex models enable measurement of the foot's internal motion. However, models with numerous degrees of freedom, which are useful for a precise characterization, are often impractical to

implement and require complex hardware setups. Therefore a simplified foot model was adopted for the study presented henceforth. All the other types of foot motion, such as the different directions in which the foot may be flexed or rotated can be found in Appendix B.

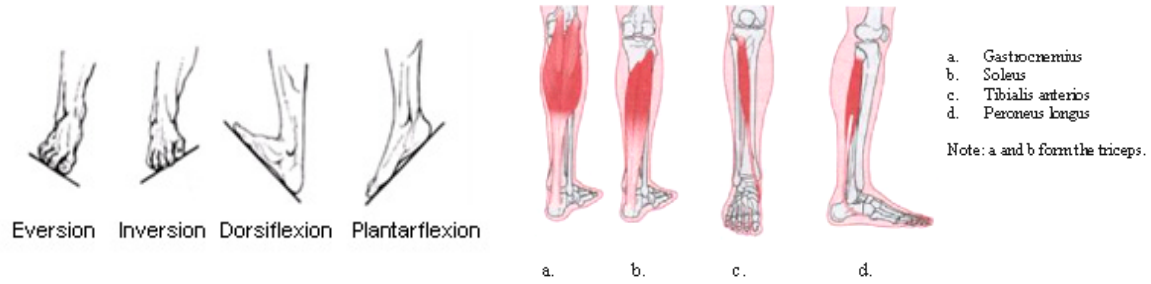

a. Main foot motion types b. Main leg muscles

Figure 7.a. Main types of foot motion [38], b. Main leg muscles involved in foot motion [37]

There are hip, knee and ankle muscle groups involved in the foot motion mechanism. The main leg muscles (Figure 7b) [37] which directly affect foot motion in the saggital plane, are a *dorsiflexor*, Tibialis anterior and two *plantarflexors*, Gastrocnemius and Soleus. The muscles that produce foot motion in the frontal plane are, an *inverter,* Tibialis anterior, posterior, and the *everter*, Peronei. Since these are a vital part of gait, a portable system should not hinder the action of these muscles. A detailed description of all the foot muscles involved can be found in Appendix B.

1.5 Human Gait Analysis

The biomechanics of human motion were already being conceptualized and mathematically enabled by the end of the 19th century. The start of photography led to the documentation of human motion, leading to sequence studies, such as those of Eadweard

Muybridge [39], where photography became an essential part in the study of motion. With computer technology it is possible to build models based on information acquired from visual systems. It is also possible to digitize images, place them into sequences and track objects within the sequences, either in 2D-local features or 3D-global features. Optical three-dimensional techniques are currently being widely used for characterization of human motion [40]. Developments in this area have been mainly driven by the gaming and graphics industry [37].

Human gait is defined as the manner of walking or moving on foot; that is, achieving locomotion using human limbs. It can be described in two major cycle phases: stance (60%) and swing (40%). Gait is usually characterized by looking at the phases through which one foot goes; therefore the stance and swing phases refer only to one foot at a time. Stance begins when the heel first touches the ground. During stance, the portion of the weight that corresponds to one foot shifts from being exerted completely at the heel to being exerted at the metatarsophalangeal joint and then to being partially transferred to the big toe. Following this last event toe-off takes place marking the end of stance and at the same time the beginning of the swing phase, where the foot is not touching the ground. The end of the cycle occurs with the next contact of the same foot or heel-strike. The double support phase is an overall phase where both feet are on the ground. The complete gait cycle comprises two steps (step length=s), and a stride or step period equals two steps (stride=2s). The frequency is the inverse of the step period. The entire gait cycle is illustrated in Figure 8 [41]. The sensorized socks may be used as a tool to characterize normal gait and abnormal gait.

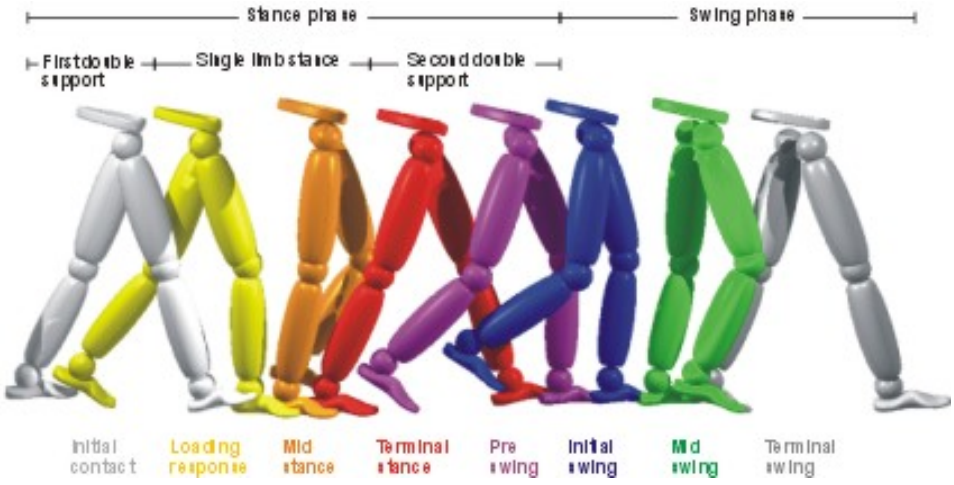

Figure 8. Human gait phases [41]

Gait is the study of the pattern of motion of the limbs of animals, including humans. From the literature, it has been said that the driving aim of gait is to minimize vertical and transverse motion and maximize forward motion of the center of mass, while maximizing energy efficiency. This mechanism is complex and is determined by several factors, such as pelvic rotation, and leg segment rotations. Three sets of physical variables are important in studying human locomotion: kinematic (velocities, positions), dynamic (forces and moments), and bioelectrical (muscle activity). Efforts have been made to characterize gait in all these variables theoretically and experimentally but always with the axiom of minimizing the energy expenditure via cost of transport, or metabolic cost, or energy expenditure. The musculoskeletal forces exerted during walking are considered of little importance during the swing phase, due to Electromyographic (EMG) studies on the leg undergoing swing. However, EMG studies can be used to measure muscle activity during the entire gait cycle. The metabolic, energetic and electromyographic aspects of gait are rather presented as part of the background information on human gait, i.e. its origin or cause, but these will not take part in the studies presented later in this document.

This thesis is mainly concerned with development of a sensor capable of complementing the information gathered on 2D plantar pressure insoles by the determination of out-of-plane foot motion characterization parameters, such as the variation of the main sagittal angle of the foot when in motion.

1.6 Current practices for Gait measurement

Gait analysis entails systems to capture kinematics, and motion characteristics during gait. The kinematics comprise a description of motion in terms of the angles, displacements, velocities and accelerations of the body segments and joints. Several techniques are available to achieve such measurements. Systems can measure relative changes or they can measure global changes. Potentiometers and electrogoniometers measure the relative change of angle. However, for global measurements, where the absolute motion of body segments is measured, a fixed reference system is needed. This can be done with four general techniques:

1. Optical: Such as in Vicon Motion Systems [42], CODA, Optotrak, etc;
2. Electromagnetic: Such as FasTrak [43];
3. Ultrasonic: Such as Zebris [44];
4. Inertial: Such as a combination of inertial MEMS [45];

Some comments on these methods; Muscle activity can be obtained by EMG as mentioned before, or it can be deduced from the kinematics by using Newton's equations

and constructing inverse dynamics. In this process, a link-segment model of the foot is constructed and each of the lower limb segments is treated as a rigid body. To model foot motion with visual systems one could go to unnecessary extremes, for example a too complicated route would require placing of markers on each of the 26 bones but it is unlikely to assume that this configuration could actually reflect the underlying bone motion. Miniature electromagnetic tracking such as the 'Flock of Birds' system [46] can yield measurements for these more sophisticated models. However, a reasonable way to proceed is to place markers according to more simplified foot models, as discussed earlier.

Gait kinematics consists of the motion of the lower limbs and therefore of three major lower limb joints: ankle, knee and hip.The kinematics of these major joints in normal gait can be seen in Figure 9.

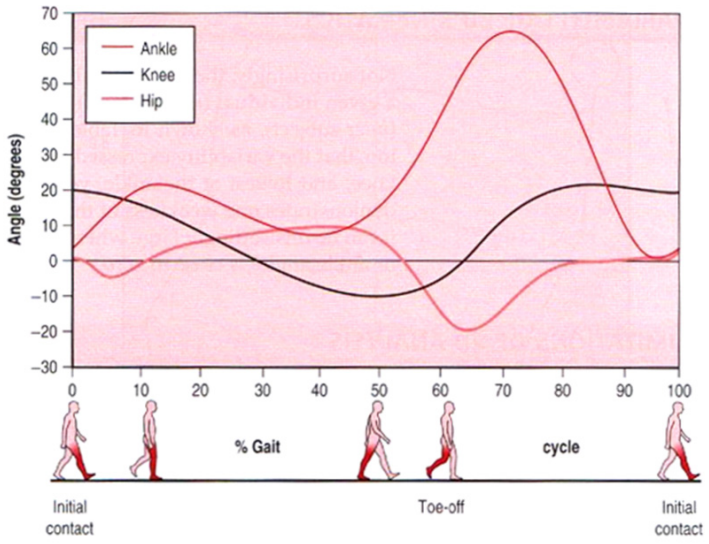

Figure 9. 2D Joint kinematics during normal gait [37]

There are limitations however to optical 2D gait analysis, and as a result, 3D techniques are now accepted as standard. Optical 3D gait analysis eliminates 2D parallax errors by using skin markers and placing them on the underlying bone. However, these systems require complex setups and are quite expensive in their simplest form. A portable gait measurement system, such as the proposed sensorized socks, would greatly help to monitor subjects in their natural environment without all the equipment that is conventionally required for such systems in measuring angles for instance.

Measurement of human angles has been possible by means of different techniques. These include goniometers, electrogoniomers [47], optical fiber goniometers [48], refractive optical fibers [49], gyroscope-accelerometer systems [50], visual techniques such as camera-based systems [51], *vicon* camera systems, etc… Goniometers and electrogoniometers are a common method for measuring body joint angles. Mechanical goniometers are usually resistive linear potentiometers which have linearly proportional change in resistance with a change in angle spanned. However, none of these methods is completely portable and light. Some of these devices are cumbersome to wear for long periods of time and have intrusive methodologies that affect the patient and the data intended to be gathered. An electrogoniometer [52] and a mechanical goniometer were used in this project to provide calibration data for the smart fabric sock. The sensorized sock could act then as a portable gait system by producing out of plane information of the main foot angle on the saggital plane.

1.6.1 Plantar pressure and improvement of sensorized socks

Besides the angular behavior, during gait, the foot undergoes pressure due to the weight of the individual. This pressure is caused by ground reaction forces which change according to the place in the gait cycle. The vertical ground reaction force during normal gait cycle is shown in Figure 10. Before initiating the gait cycle, that is, when standing, the total ground reaction is constant, equal and opposite to body weight, it is depicted by the red dotted line. If the weight is balanced between the two feet, then each foot gets half of the total weight. The figure depicts a process where during initial support the force quickly rises as the weight is transferred from the other limb. The force rises above resting body weight in early stance, then falls below resting body weight during mid-stance and rises again during late stance, falling again when the weight gets transferred back to the other limb. The center of pressure exerted by body weight goes from the border of the heel at initial contact to the hallux (big-toe).

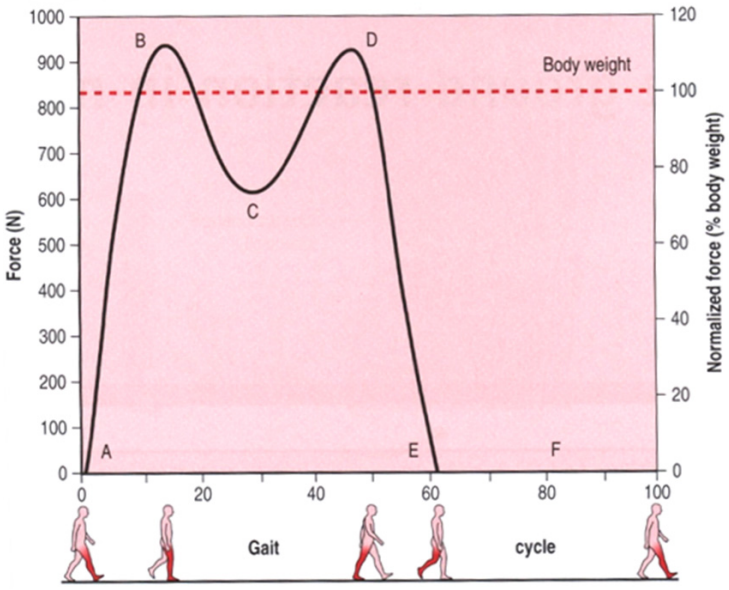

Figure 10. Vertical ground reaction force during normal gait [37]

This pathway is depicted in Figure 11 for a normal gait pattern. It can be measured by force platforms, which can also detect the shear and vertical load components, since the force is not just vertical.

A schematic of the ground force vectors exerted on the foot and their proportional intensities are shown in the Pedotti diagram, where each vector represents the ground force exerted on each foot at different progressive and sequential points in the gait cycle (actually half of the gait cycle). Notice from this diagram that the vectors have vertical (load) and horizontal (shear) components. Numerous devices for measuring force vertical components and corresponding pressures account for a large amount of commercial products, such as pressure sensitive insoles. Some of these applications are reviewed in Appendix A.

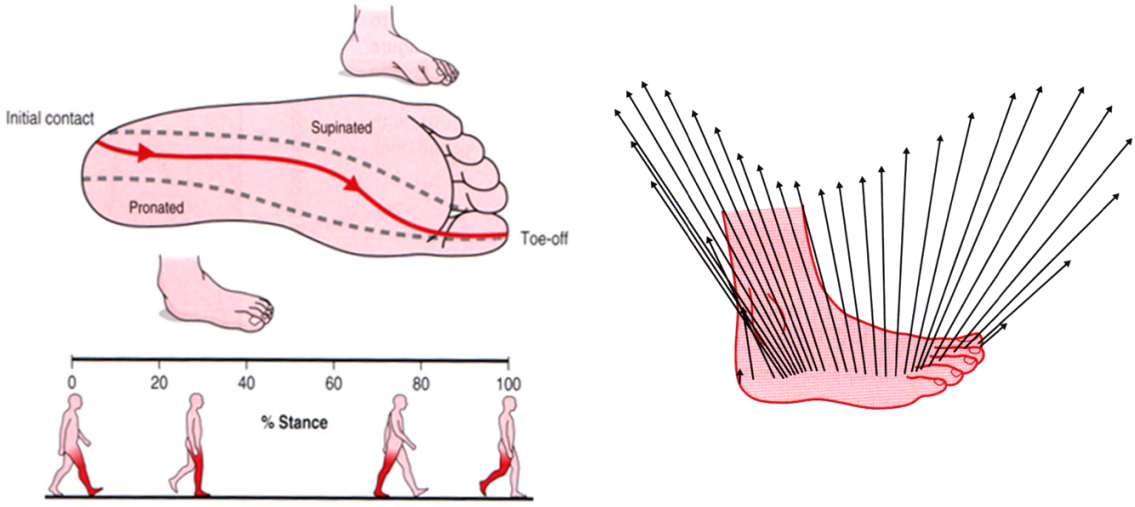

a. Center of Pressure pathway b. Pedotti Diagram

Figure 11. Pathway of the center of pressure (CoP) in normal gait [37].

However, plantar pressures only provide a 2D depiction of the foot. It is also worth mentioning that there are currently no commercial methods to assess shear forces of the foot. An out-of-plane motion measurement could complement the existing insole devices with a more complete perspective of the foot. This is the technical objective of the sensorized socks in this project. The medical applications of the socks were mentioned in an earlier section and have as the main purpose to aid in the rehabilitation of people with lower limb disabilities.

Chapter 2: Sensorized fabric development: Sensor Materials, Substrates and Connections.

2. 1 Initial study with elastic bands-stretch bands and other materials

As a first attempt to choose a sensor material for the proposed research objective, several ideas were examined. For this purpose, semiconductors such as graphite were chosen as first candidates for the coatings due to their convenient availability. First, several materials were coated (Figure 12) in order to investigate the effects of their potential use as fabric sensors or as sensors applicable to fabrics. Different concentrations of graphite were applied on rubbers, strings and foams of different kinds. Mold rubber was also filled with graphite in the attempt of looking for a sensor material.

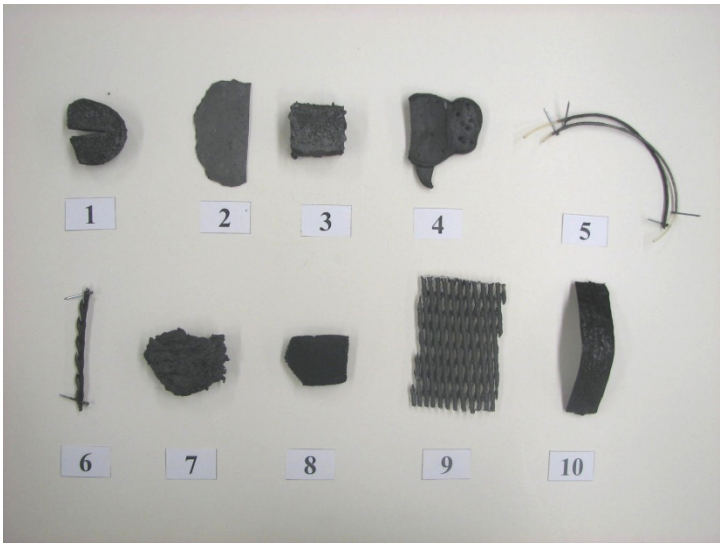

Figure 12. Different conductive enabled materials: 1. Synthetic sponge and rubber cement, 2. Rubber cement and graphite 50%, 3. Thick foam, 4. Mold rubber and graphite at 10%, 5. Rubber strings coated with rubber cement, 6. Expanded polyethylene foam net strand, 7. Mold rubber and graphite

at 20%, 8. Synthetic sponge and carbon black solution, 9. Expanded polyethylene foam net, 10. PDMS and carbon black strip.

Some of these materials had different surface structures, and therefore caused the coating to have different behaviors. These are shown in Figure 13, where the labels correspond to those of Figure 12.

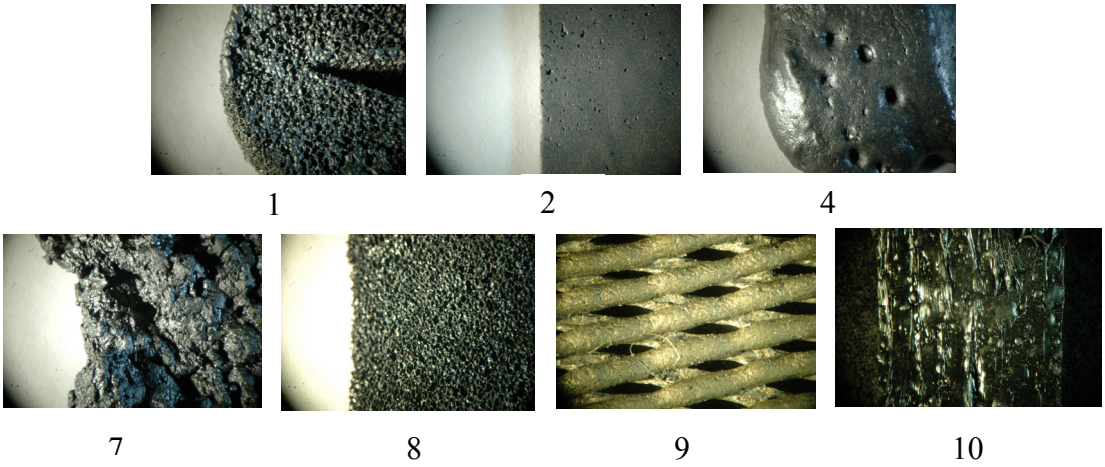

Figure 13. Microstructures of different conductive coated materials.

The conductivity of these coatings was examined as well on an acrylic board (Figure 14). Paint sprays and other mixtures were painted on the board and electrodes were placed on opposite ends of the painted strips to determine their conductivity.

Figure 14. Acrylic board with raw materials to be tested for their conductive properties.

From all of these materials, a subgroup was selected to do some testing which will be described in what follows. The paints, sealants and the lower concentrations of graphite did not present good conductive properties. The only ones with a good conductivity were the 50% graphite and rubber cement and the carbon black/PDMS strip. Samples were also evaluated with respect to their elastic properties. Even the rubber cement and graphite mixture, which will later be coated on strings, looked rather brittle. The only material that presented ideal elastic properties was the carbon black and PDMS mixture. The mold rubber and graphite did not show good signal properties when placed between electrodes. The resistance ranges were too high as well. The 20% graphite in mold rubber hardened while it was still being mixed and acquired an irregular morphology. However, it seemed to be mildly responsive to pressure, as is shown in Figure 15. At 10% graphite, the sample was compliant but the resistance signals were noisy and extremely non uniform. It was also found that the electrical response was a little better when the electrodes were closer to each other.

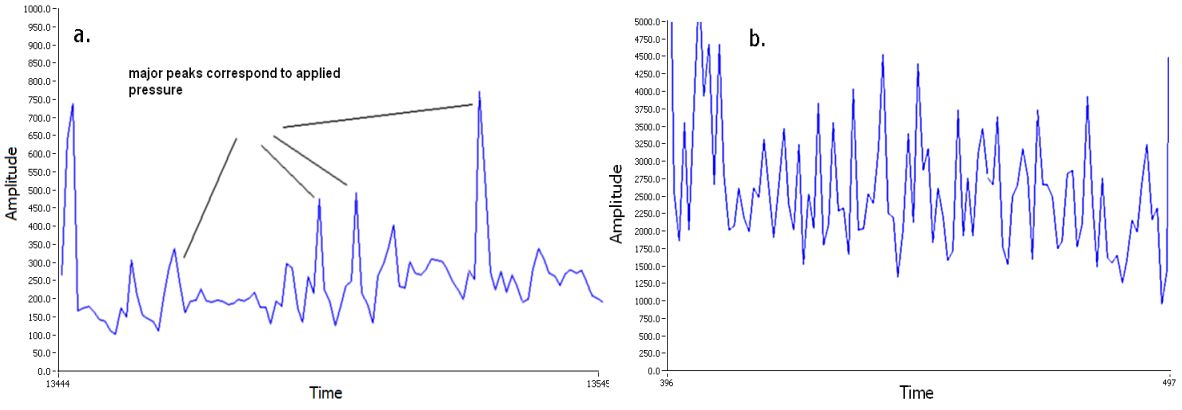

Figure 15. Mold rubber and graphite signal response: a. at 20% graphite, peaks show mild response to pressure, b. at 10% graphite though compliant, signal is noisy.

The sample with a somewhat constant value of resistance was the 50% graphite in rubber cement. This was the case regardless of the location of the electrodes (Figure 16).

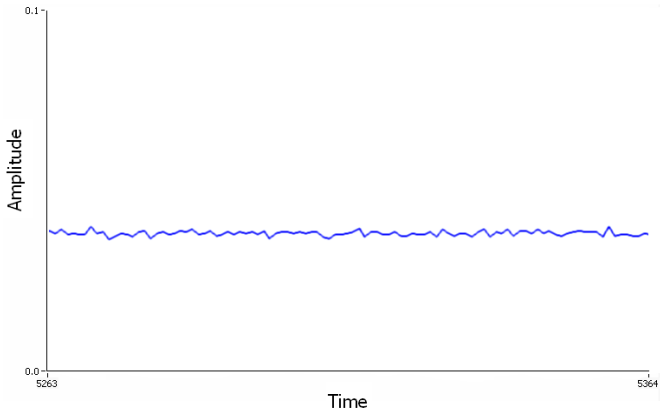

Figure 16. Bulk conductive response of 50% graphite and rubber cement

The 20% carbon black in mold rubber coagulated faster than expected, ending in a rigid uneven morphology. This mixture however was able to produce somewhat even signals when the electrodes were close enough, about half an inch apart. Overall, the signal was less noisy and it was responsive to pressure in a repeatable pattern (Figure 17).

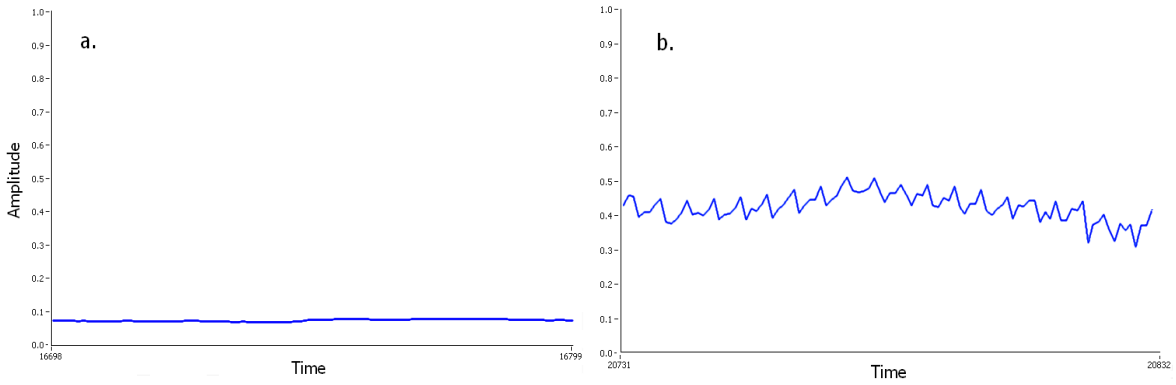

Figure 17. Carbon black and mold rubber (blue signal): a. signal across sample, b. responsiveness to pressure applied

Combinations of graphite and PDMS on the other hand, did not cure even after subjecting them to curing temperatures for more than 15 minutes. The resistance measurements were infinite at first. This is probably due to the lack of surfactants used in the raw mixture. However, after two days it showed a decreased resistance, though still high, and it did not present any reaction to strain. The sample was repeatedly stretched during this time but the signal continued to be the same. This is shown in Figure 18. A similar mixture: 20% carbon black and PDMS had a very rubbery and completely cured consistency. For this last mixture, the overall resistance is lower than the 20% graphite-PDMS sample. It was seen from a small strip of this material that its resistance goes down with stretching; this could be due to the particles coming closer together in the thickness direction while being stretched. Both mixtures had resistances in the lower MΩ range and needed auxiliary (or fixed/ballast) resistors in this order to balance the voltage divider in the acquisition setup.

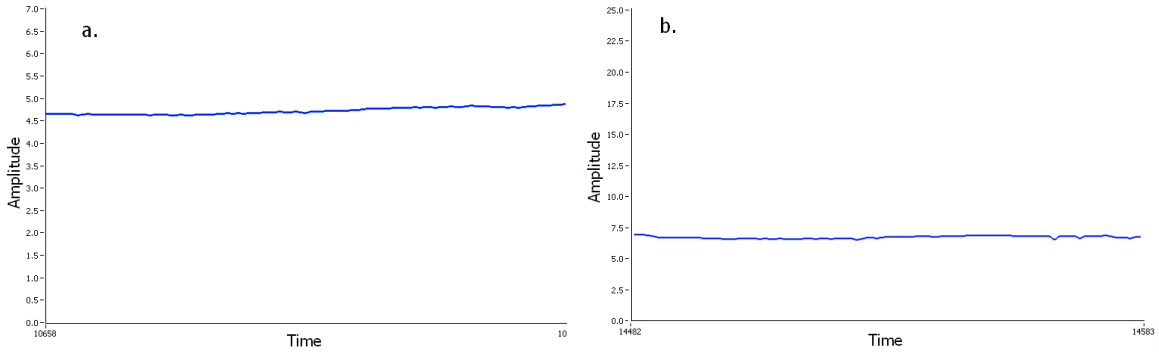

Figure 18. Resistance vs time: a. 20% graphite and PDMS, and b. 20% carbon black and PDMS.

Images of the graphite and carbon particles were captured with an SEM microscope before being mixed with the polymer. The nature of the particles is very different and

could account for their miscibility characteristics. The images are shown below in Figure 19.

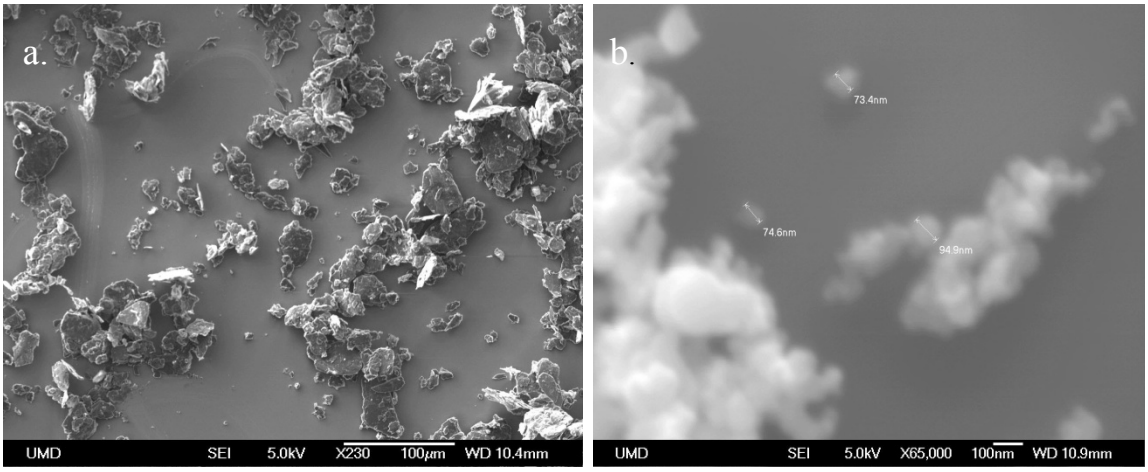

Figure 19. SEM images of conductive particles: a. Graphite micro-flakes (X230) and b. Carbon black nanoparticles (X65000).

A second idea entailed coating strings and stretch bands. The materials chosen were commercial brands of stretch cloth materials. Some of the materials studied are shown in the following pictures (Figure 20). The first material to be coated was the white elastic stretch string shown in part b of Figure 20, and subsequently, the elastic band (white) shown in part a. of the same figure.

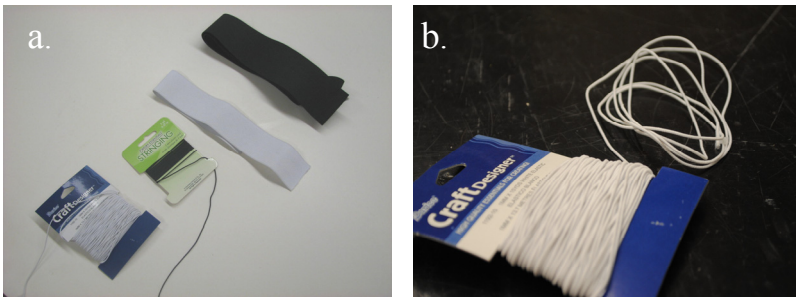

Figure 20. Stretch materials: a. Different materials and b. Stretch string

In order to have an appreciation of the mechanical behavior of the strings, a graph of strain vs. weight was obtained for each strip by hanging weights on one end of the string, with the other end fixed, under the acceleration of gravity. In this setup, the strain was taken by means of a scale and the resistance was taken as a quasi-static measurement after the exertion of the force used to stretch the string. The resistance was taken by direct measurement using a two probe multimeter. The force was added using dead weights mounted on a strip of aluminum which exerted the final force on one end of the string. The setup for these sets of experiments is shown in Figure 21.

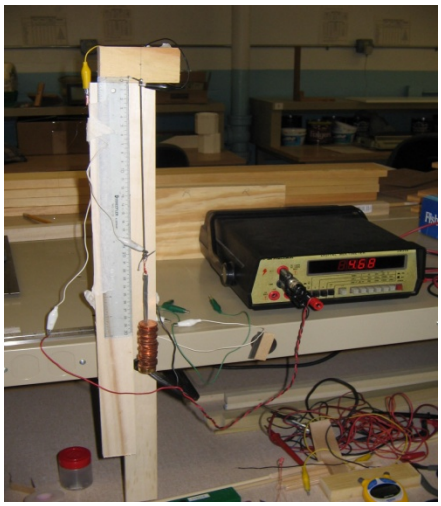

Figure 21. Setup for resistance vs. strain measurements

Several strips of the same length were subjected to the same loads; an average curve error bar graph was obtained considering that all the strips should have had similar behaviors. This is shown in Figure 22. In this case and in what follows we will be referring to a 'sensor strip' as the combination of elastic substrate and semi conductive or fully conductive coatings.

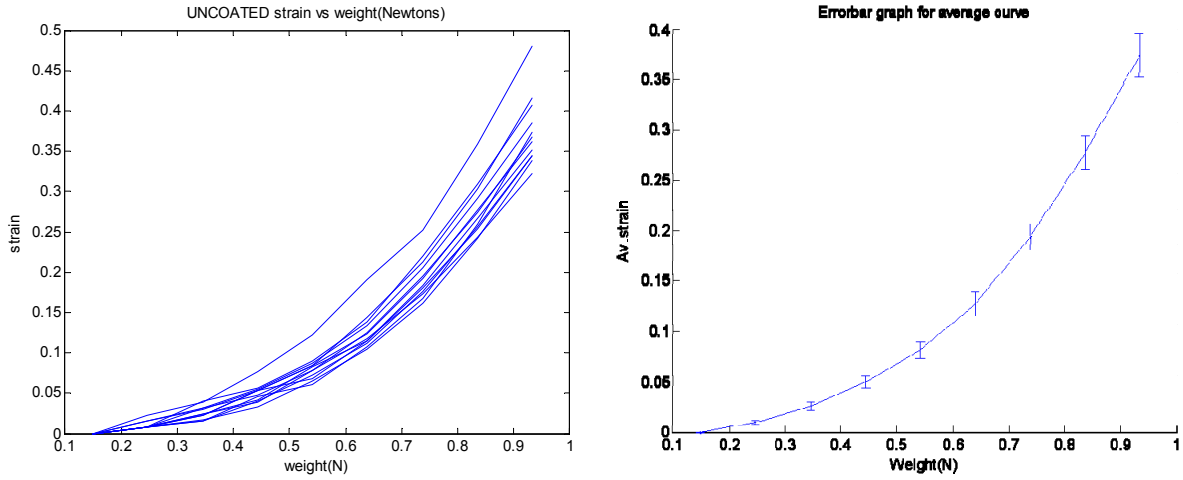

a. Strain vs weight load

b. Average error graph

Figure 22. Uncoated elastic strings: a. Strain vs weight load and b. Average error graph

The same strands were coated with a mixture of graphite flakes of micron dimensions and rubber cement at 50%. This percentage was chosen due to its good conductive characteristics. Micrographs of a small percentage and one of a larger percentage will be shown in what follows. The pictures indicate why the larger percentages allow for better conduction. The coating was manual and it was carried out as consistently as it could physically be given the settings. The initial approach to coating the strings was to clamp their ends with small nails and coat them while in tension, just enough for them not to bend. Similar strain vs weight measurements were followed for the coated strings to visualize how the coating affects the structure of the string. Figure 23 illustrates results, showing that the coating modified the mechanical response of the strings. The differences were more noticeable with increasing strain. Given the premise of creating a stretch sensitive fabric sensor mainly with electrically conductive characteristics, the coated strings were placed on a fixture similar to the one used for the strain vs. weight

measurements but this time two electrodes were placed at the ends of the string and the resistance was taken at each strain step.

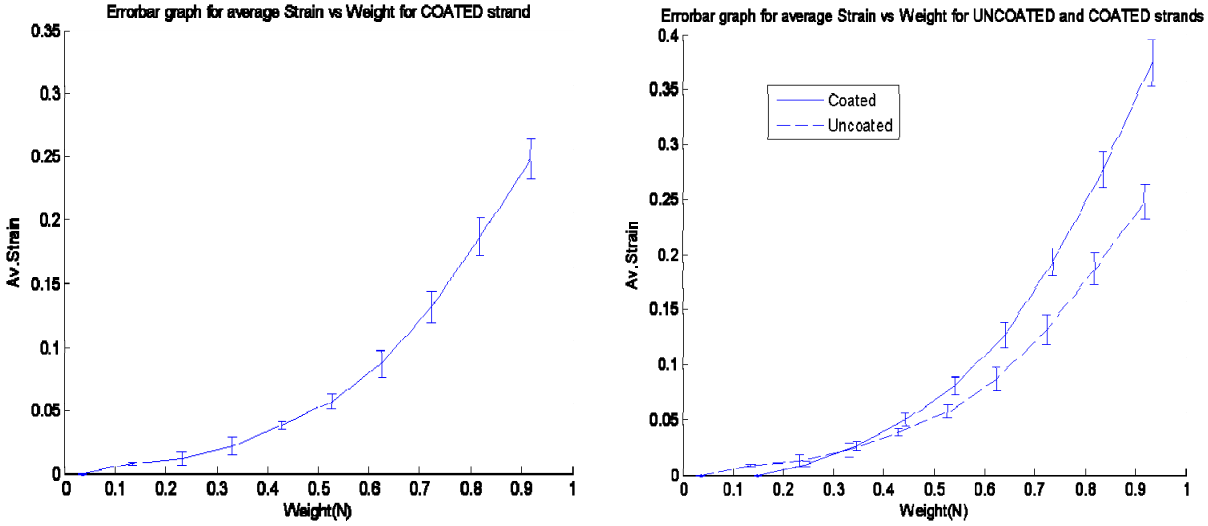

a.Average error graph b.Coated and uncoated strings

Figure 23. Coated elastic strings: a. average error bar graph for strain vs. weight and b. comparison of coated and uncoated strings

The results for these experiments are shown in the following plots. Figure 24b shows a larger scatter of the resistance as the strain increased.

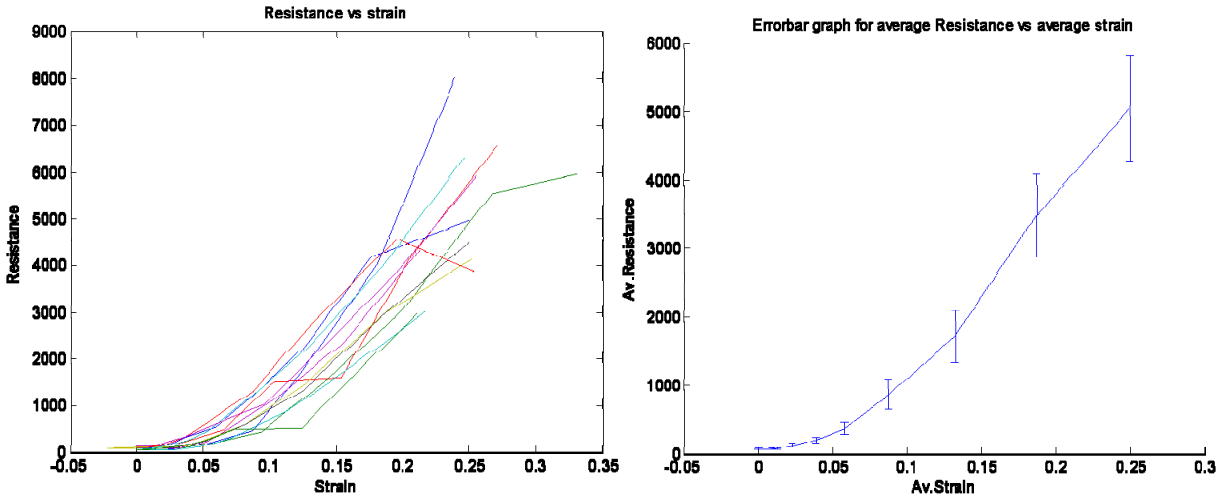

a. Resistance vs strain b. average error graph

Figure 24. Coated elastic Strings: a. Resistance vs. Strain and b. average error bar graph.

The different concentrations of graphite coatings were also captured in surface micrographs. There are mainly two distinctive forms, the 0.5% and the 10% graphite. The 50% graphite is similar to the 10% and the 0.5% to the lower concentrations. These major differences can be viewed in Figure 25 below.

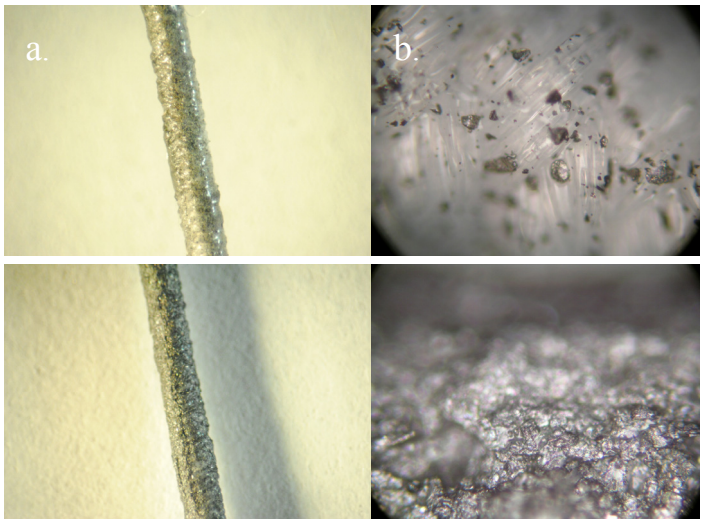

Figure 25. Graphite coated string micrographs at different concentrations: a. 0.5%, b. 10%

A setup was built in order to apply dynamic loads on some of the materials that were coated. This setup, as shown in Figure 26, consisted of a cantilever beam with a calibrated strain gauge, a strain gauge box, a shaker and a motor. The samples were clamped at first with gator jaws, followed by a clip holder with a copper strip attached to it as an electrode. The motor ran at a fixed rate of 20rpm and the voltage divider circuit was powered up with 5V. In this setup, a voltage divider circuit, shown in detail in section 3.1, was used to measure resistance. The auxiliary (or fixed/series) resistor was in the order of tens of MOhms.

The strain gauge outputs force in the acquisition program. In Figure 27 the red signal corresponds to the cyclic loading of the motor, outputting pounds. The blue signal

corresponds to the response from a 50% graphite coated rubber band and the amplitude is scaled per 100MOhms.

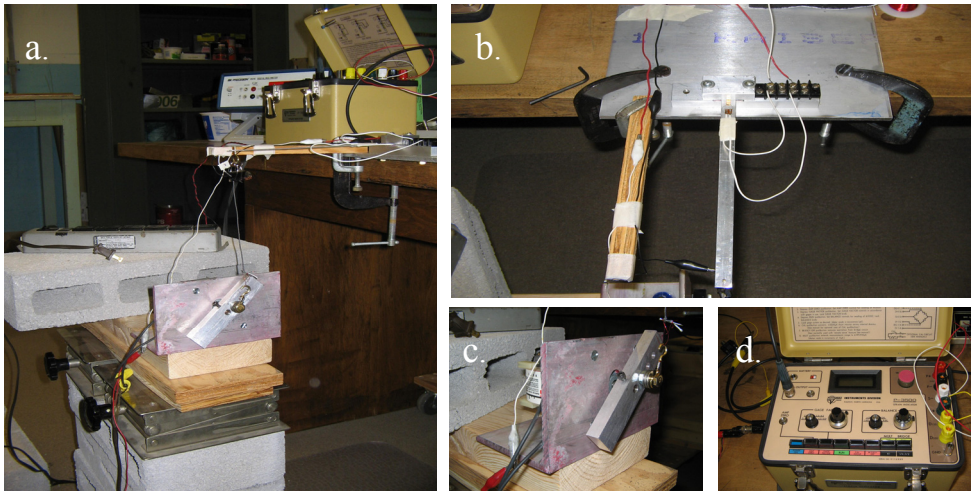

Figure 26. Dynamic loading setup: a. Complete setup, b. cantilever beam, c. rotating shaft, d. strain gauge box

The first peak corresponds to the stretch at the beginning of the stretch cycle. The second peak corresponds to a response from the sensor to the unloading phase. The second peak is noticeable because the end of the string was not pinned but rather anchored and free to rotate, therefore augmenting the unloading response.

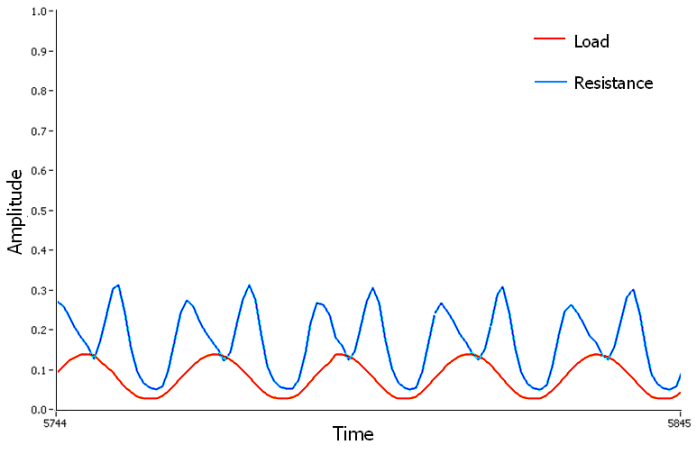

Figure 27. Cyclic loading response of a 50% graphite coated rubber band.

The rubber band surface was captured in the following micrograph (Figure 28). It shows a rather uneven surface; however, the signal was very well behaved, probably due to the pure rubber substrate.

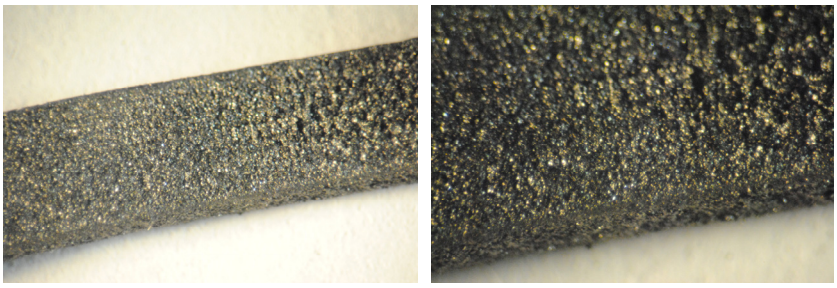

a.10x b.20x

Figure 28. Micrograph of 50% graphite on a rubber band: a. magnified 10 times, b. Magnified 20 times.

This same test was performed for graphite coated elastic strings. A representative graph of the behavior of this system is show in the left portion of Figure 29. The two figures differ in that the clamping to the motor is different. Curves are smoother with the enhanced clamping. Again, two peaks are present, one for loading and the other one for unloading, that is when the sample gets released or unstrained.

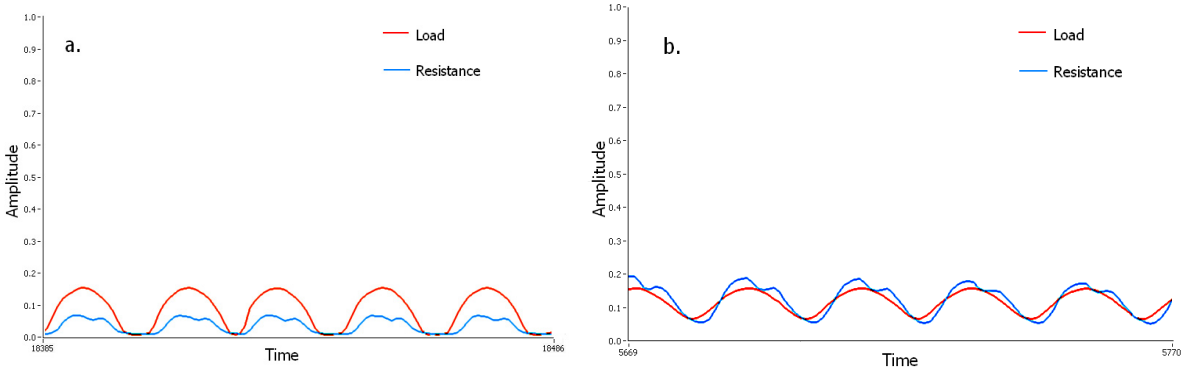

Figure 29. 50% graphite coated string subjected to a 20rpm loading: a. loose clamping, and b. clip clamping.

Due to some induced stretching in the horizontal direction by the motor mechanism, an electrodynamic shaker was used instead of the motor to produce an entirely vertical stretch. The settings for the strain gauge box which aided in the calculation of the force being applied by the shaker were around 692 micro-in/in to 752 micro-in/in. A digital signal generator was used to generate different waveforms: sinusoidal, square, etc. The response to the coated string to a square input eliminated the second peak. This is shown in Figure 30. The blue signal is the resistance divided by 3MΩ, the auxiliary resistance is 2MΩ, and the amplitude of the signal generator was set to 50mVpp. A 1 Hz square signal was applied to a string which had a 1/16th of an inch in maximum vertical displacement, where the un-stretched length was 3 and 10/16 inches. The signals on part b of this figure correspond to a sinusoid impulse applied with a signal generator of amplitude 100mVpp and a maximum displacement of 1/8th of an inch. The un-stretched length was the same for both graphs.

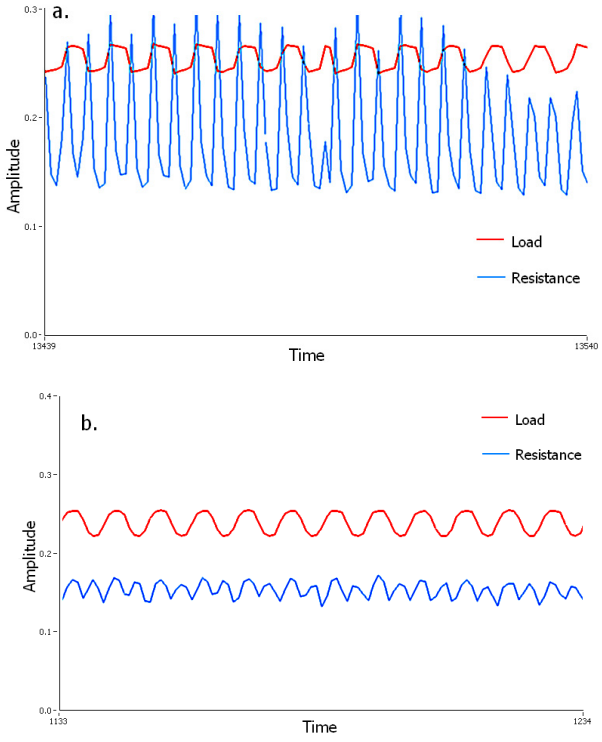

Figure 30. a. Graphite coated string loaded by a square signal and b. loaded by a sinusoid.

Several strings were coated and subjected to the same procedure; however, the signals were noticeably different, even though the strings were of equal dimensions. The coating technique could have been responsible for the differences in electrical response. Several techniques for coating were tested. Two, three and four coatings were applied on to the different strings, in different alternating directions and in one single direction. The four coatings gave too much graphite to the sample, making it more brittle. The samples coated in alternating directions ended up curling after they dried out. The one technique which seemed to work best was the three coatings in the same direction. These coatings were done using a synthetic sponge since it provides better uniformity in spreading the mixture over the string. This was also the result of trying out other coating appliers, such as brushes or just soaking the string in the graphite mixture. The one which worked the best was the sponge, considering the equipment constraints. Combining these results the sponge coating repeated three times was used in subsequent studies.

After deciding on the coating mechanism, another consideration was made on the coating technique. It entailed the actual tension under which the strings were coated. Therefore a setup that made this concept distinguishable was built. Two and three washers acted as the load under which the strings were coated. The setup is shown in Figure 31; strings were attached to a wood mount and then stretched by dead weights (washers). It was seen from the resulting experiments that the better signal responses seemed to have a tradeoff between the integrity of the string and how high the resistance ended up being. For strings coated being pulled by two washers, the resistance had a higher overall value,

while for the ones coated under the exerted force of three washers, the resistance had a lower value but the strings looked physically more curled up, which is undesirable in stretch sensors.

Figure 31. Washer setup for coating elastic strings under a certain tension

The graphite coated strings also presented drift in the signals (Figure 32), this was seen when the strings were subjected to a 1 Hz signal generated by the shaker, with amplitude 100mVpp and a maximum vertical displacement of 1/8. The un-stretched length was the same as for the previous examples. The resistance is scaled by 3MΩ. This drift could be corrected if the mechanics of the elastic thread supporting it did not have as much elastic creep.

The next material that was analyzed was a 'knit heavy stretch elastic' of 68% polyester and 32% rubber. A different conductive mixture was also taken into consideration due to the high brittleness of the graphite mixture. Graphite and PDMS was not considered, as was mentioned before, because the mixture did not completely cure. The mold rubber was too sturdy to be coated. The following section entails carbon black coatings.

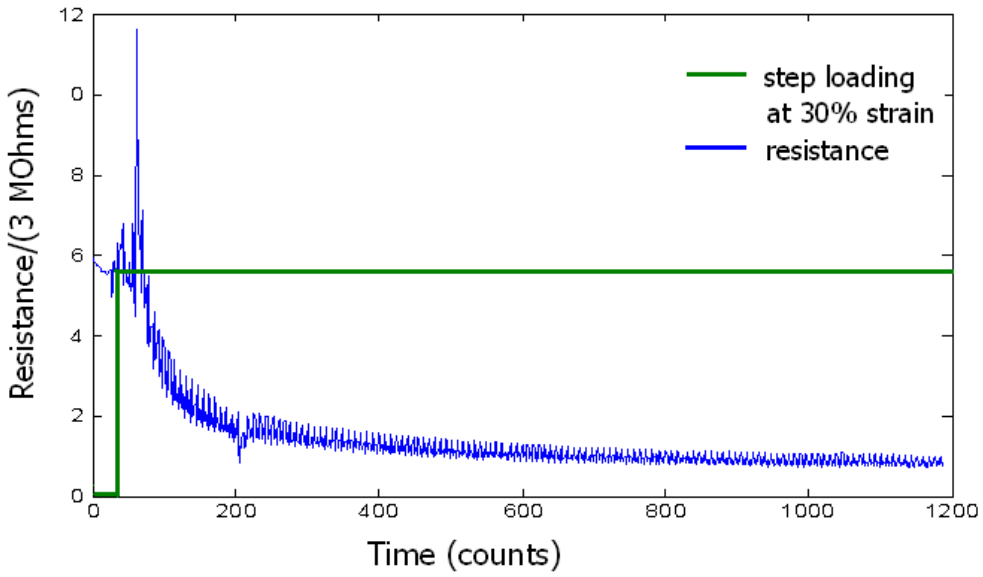

Figure 32. Resistance vs. time: Drift in the 50% graphite coated elastic strings

Mixing carbon black with a polymeric matrix needs precise proportions. The following figure illustrates some carbon black sensors which were damaged as a product of different errors. In Figure 33 part a, the first strip shows how printing very thin sensors on a coarse substrate produced the leakage of carbon black. The second strip ended up being too brittle due to excess solvent, and the third strip shows how very liquid carbon black diffused beyond targeted gauge region of fabric.

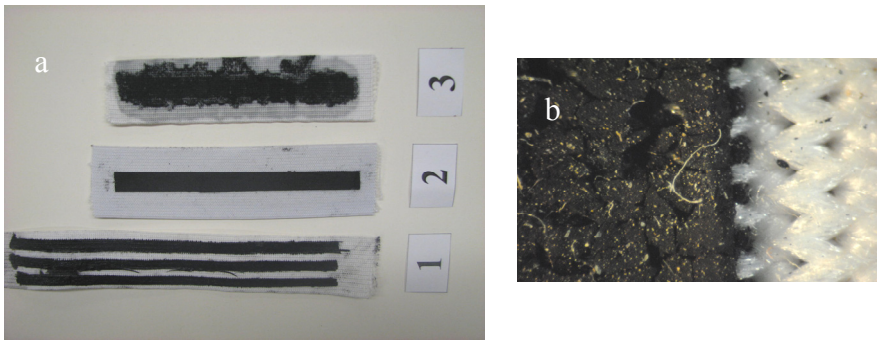

Figure 33. a. Failure modes of carbon black sensors, b. micrograph of 2.

Also, a commercial form of carbon black was adopted for the main portion of this thesis since the mixtures prepared in the lab showed much higher resistance ranges. This might be due to the lack of a proper polymeric mixer. The new conductive material Elastosil, was acquired as a courtesy from Wacker Ltd. This composite was originally created for the tire industry.

Elastosil was applied to the 'knit heavy stretch elastic' from Figure 33. The coated section was masked with high temperature tape and Elastosil was applied by hand and was smoothed out with a blade. A dead load test was carried to determine the level of drift. This setup is shown in the following schematic of Figure 34. Five samples (B1..B5) of length 11.5 cm, width 10mm and thickness of 4 mils, were placed in this setup (Figure 35).

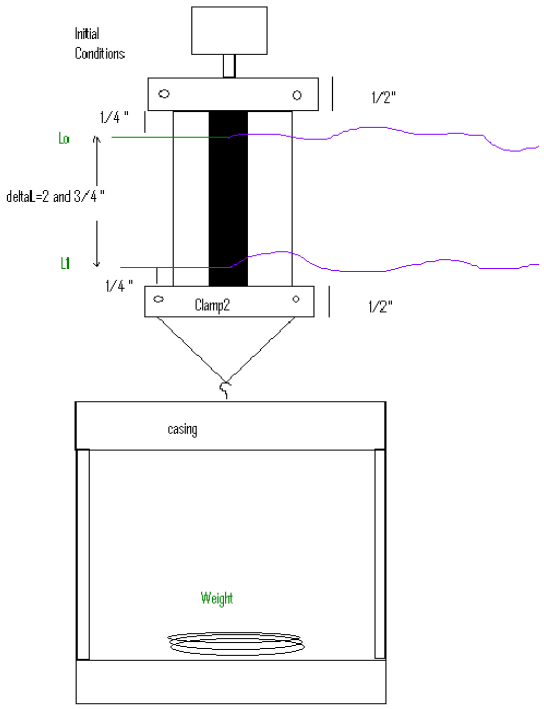

Figure 34. Schematic of dead load setup for heavy knit elastic and carbon black.

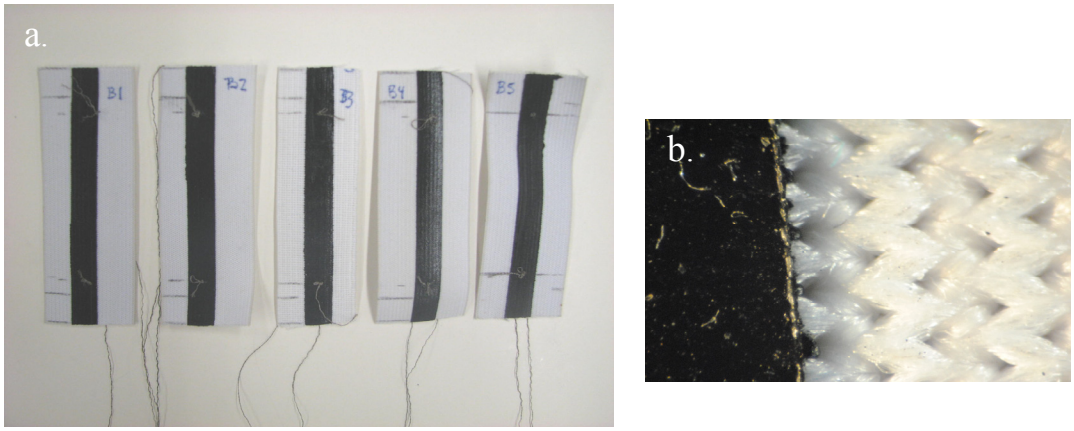

Figure 35. a. Heavy knit strips with coated carbon black, b. micrograph of strip.

The resulting resistance profiles behaved similar to that of Figure 36 which shows the resistance profile of sample B3 under the different loads. The graph shows the different mass values used to generate force under the effect of gravity. The drift is less than the one shown by the elastic strings coated by the graphite flakes and rubber cement. The only other observation was the mild deterioration of the signal with bigger weights; more noise was present than in the lower weights. Elastosil was chosen for most part of the studies presented in Chapter 4 since it had better properties than the materials previously studied. Such properties include fabric integration, and lower resistance overall values.

Other materials considered to act as the sensor or perhaps as connective lines, were the conductive fabrics courtesy of Eeonyx (Figure 37). These were all mixtures and coatings of polypyrrole and other pi-conjugated polymers. A PI-coated fabric was chosen to be implemented in one of the sock prototypes presented in section 3.2.7.

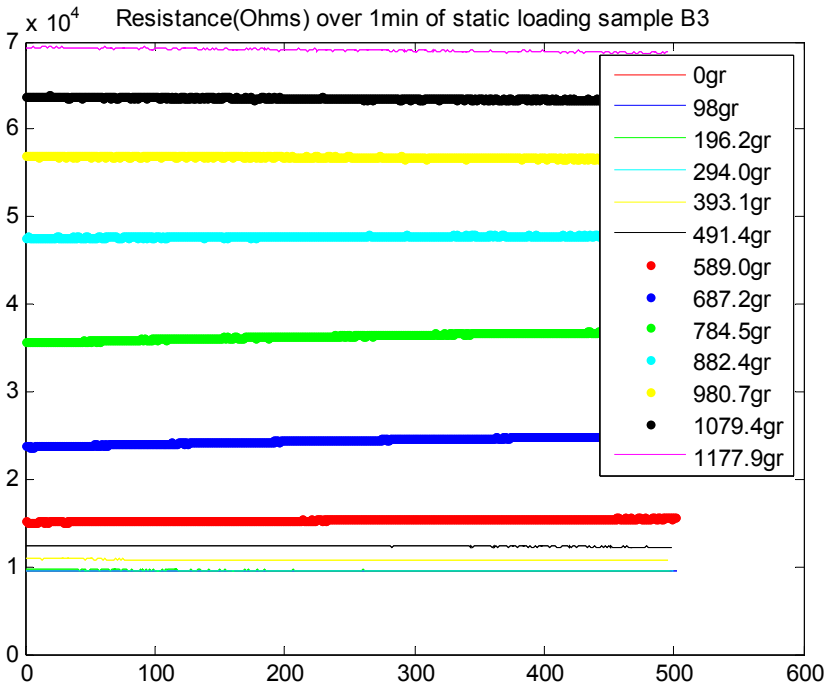

Figure 36. Static loading for sample B3 of heavy knit elastic.

Figure 37. Eeonyx conductive fabric samples-courtesy of Eeonyx

A novel material considered was a quantum tunneling composite (QTC) polymer material. However, this material acted more like a switch, eliminating the possibility of having ranges of values that varied in proportion to fabric stretch. Another form of QTC was a conductive sheet (Figure 38), but it was paper-like and very brittle, therefore not directly applicable to this study.

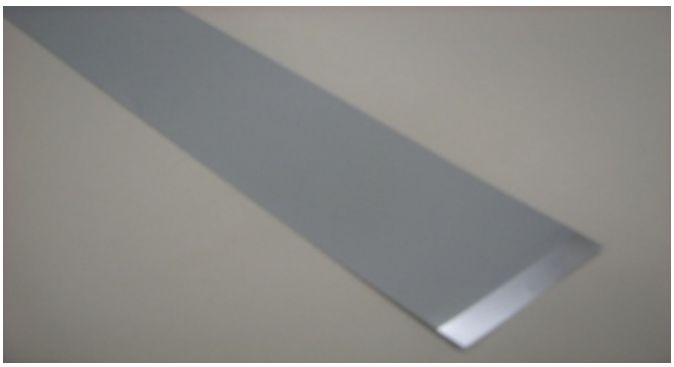

Figure 38. QTC conductive sheet

2.2 Conductive polymer sensors

A number of methods for making fabric-based sensors were investigated. This included studies of conductive additions to elastic matrix materials and assessment of suitability for the proposed application. Based on these results, the sensor material chosen for most part of the experimental studies in this thesis was the conductive elastomer Elastosil LR3162 A/B, as mentioned in section 2.2. This elastomer comes in two parts and can be diluted in trycholoroethylene. The sensors used in this thesis were produced from the mixture of equal parts of Elastosil and trichloroethylene [34]. Different methods to obtain a uniform and viscous mixture of these components were tested. First, equal parts of Elastosil's components were mixed with a higher quantity of trychloroethylene to gain

more solubility and less viscosity, aiming at a complete evaporation of the solvent with sufficient curing time. With this very liquid inhomogeneous mixture, several methods for mixing were tested: The first was a magnetic bar stirrer as part of a sonicator. In this method the substance is placed in a beaker and a magnetic bar is placed inside. Then the beaker is placed on top of a motor that moves the magnetic bar. This approach did not give good results because the substance was not liquid enough to undergo an ideal cyclic recirculation from bottom to top of the beaker. Therefore the stirrer was only mixing a part of the substance but not all of it. Also, as time passed by and the solvent evaporated it was difficult to have the stirrer mix at a constant rate, it increasingly slowed down as the viscosity increased. The other method that was used was a hand stirrer, which stirred the substance with a shear mechanism. The high temperatures generated during this procedure made the mixture crosslink locally with a non-homogenous result. A third approach to mixing the components was to use a mechanical drill where a small shaft was inserted. The shaft had a rectangular piece attached to act as a rotor with variable velocities. This approach did not manage to give an even mixture because the substance had the tendency to be centrifuged and therefore accumulate on the walls of the beaker, a place difficult to reach for the stirrer. Therefore, hand mixing was followed for the diluted sample. However, the mixture didn't crosslink completely even after curing and waiting for several days. It also lost its luster. The most consistent way that was found, within reachable scale, was to thoroughly hand mix the three parts of the mixture on a beaker. The polymer was then put into a desiccator to eliminate possible air defects, which did not seem to have an impact on the sensor. It is worth to mention that the ideal method would have been a commercial type mixer, such as a shear mill mixer.

2.3 Substrates

This mixture was then applied by hand on the different substrates (Figure 39), with the long direction of the fabric parallel to the stretch direction. The desired shape of the sensors was achieved by masking the stretchable fabric with high temperature tape. A squeegee or a razor blade was used to uniformly spread the substance over the substrate. All the strips were scraped flush against the high temperature tape that was used as an adhesive removable mask and which had a thickness of 4 mils. Following the work of [34], the sensors were baked at 130° C for about 10 min in a convection oven. The baking shape of the sensors was 1cm by 12 cm by 4 mils. After letting the sensors cool off, the fabric on which they were baked was cut to a width of about one inch, using ASTM standards for textile testing as a guideline [53-55].

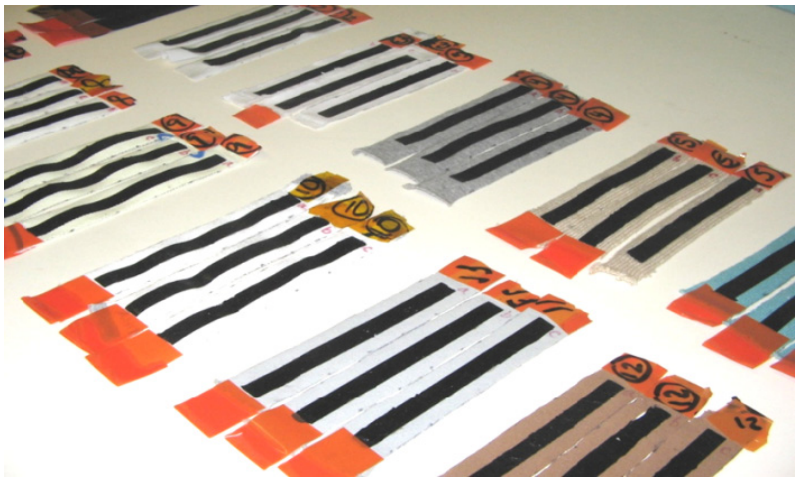

Figure 39.Sample strips with applied conductive polymer

The substrates were composed of different mixtures of fibers that are commercially used for socks. Table 1 identifies the first substrates studied (substrates I). They are all knitted fabrics where Spandex has been blended to enhance stretchable properties. Three samples

of each substrate were prepared. A second batch of substrates (substrates II), used for a feasibility study, is described in detail in Table 2.

Table 1. Sample substrates I: knits

Sample	Fabric composition	Microstructure characteristic
1	94%cotton 6%spandex	Plain knit-double sided stockinette- single plied
2	95%rayon 5%spandex	Plain knit-double sided stockinette
3	95%polyester 5%spandex	Double sided knit-reverse stockinette-dense-high twist
4	87%Nylon 13%spandex	Double sided knit –stockinette dense-ribbed-high resilience
5*	96%Tactel Nylon 4%Lycra Elastane	Double sided knit-coarse-low twist
6	79%Rayon 20%Polyester 1%Spandex	Plain knit-double sided stockinette-multiple yarn
7	73%Cotton 24%Polyester 2%Spandex 1%other fiber	Plain knit-double sided-bulky
8	66%Polyester 29%Cotton, 2%Spandex, 3%Other Fiber	Plain knit-double sided-bulky
9**	62%Microdenier nylon, 36%nylon, 2%Lycra Spandex	Plain knit-double sided stockinette
10***	85% Soft cotton, 15%nylon	Plain knit-double sided stockinette- plied yarn-loose stitch

*, ** used for sensorized sock prototype ***Diabetic sock

The first four substrates correspond to commercially available stretchable cloth. Substrate 5 is composed of Tactel Nylon, which is lightweight, breathable and is said to dry eight times as faster than cotton. It is also at least twice as soft as most of other fibers and three times as resilient as comparable natural fibers. Substrates 7 and 8 correspond to sports socks. Substrate 9 has microdenier (less than one denier per filament) fibers, being the smallest fiber fabric among all the ten substrates. Substrate 10 corresponds to a sock made for diabetics and it has the thickest fiber of the study. Substrates 9 and 5 are noticeable in their comfort and fit.

Table 2. Sample Substrates II: knit fabrics and sock knits

Sample	Fabric composition	Microstructure characteristic
1*	60% cotton, 40% polyester	Classic knit-interlock-low twist
2*	90% polyester, 10% spandex	Double sided knit-purl stich-dense-fine
3*	100%polyester	Classic knit-loose stitch
4	75% cotton, 24%nylon, 1%spandex	Stockinette-loose stitch
5	47% Organic cotton, 46% Lyocell, 6% Nylon, 1%Spandex	Stockinette stitch with ply yarn
6	68% polyester, 28% cotton, 2% spandex, 2%other fiber	Stockinette with single yarn
7	94%Nylon, 6%spandex	Stockinette-fine stitch
8	61% Acrylic, 24%polyester, 13%Nylon, 2% spandex	Ribbed stockinette
9	73% nylon, 24%polyester, 2% spandex, 1%natural latex rubber	Double sided knit
10	94%polyester, 4%natural latex rubber, 2%spandex	Stockinette
11	97% nylon, 3% spandex	Flat knit
12	86% nylon, 14% spandex	Stockinette-low twist

*knit fabrics

For the second batch of substrates, most of the substrates consist of samples taken from commercially available socks. The first three substrates are commercially available stretchable cloth. Substrates 4, 5, 6 had some cotton in their composition. Substrates 2,3,7 and 12 had very thin fibers. Substrates 8, 9, 10 corresponded to sports socks and therefore rather thicker structures. The last substrate, 12, behaved similarly to the rayon from the first batch (Substrates I) in that the coating was particularly uneven due to the thin nature of the fibers.

2.4 Study of Substrates (microphotographs)

An optical Bausch & Lomb stereo zoom microscope (max. 30X), was used to view the fabric constructions of all the substrates. The fabrics have noticeably different microstructures. An SEM microscope was used to look at some of the cross sections of the sensors. Some distinctive substrates are shown in their microstructures in the following pictures (Figure 40).

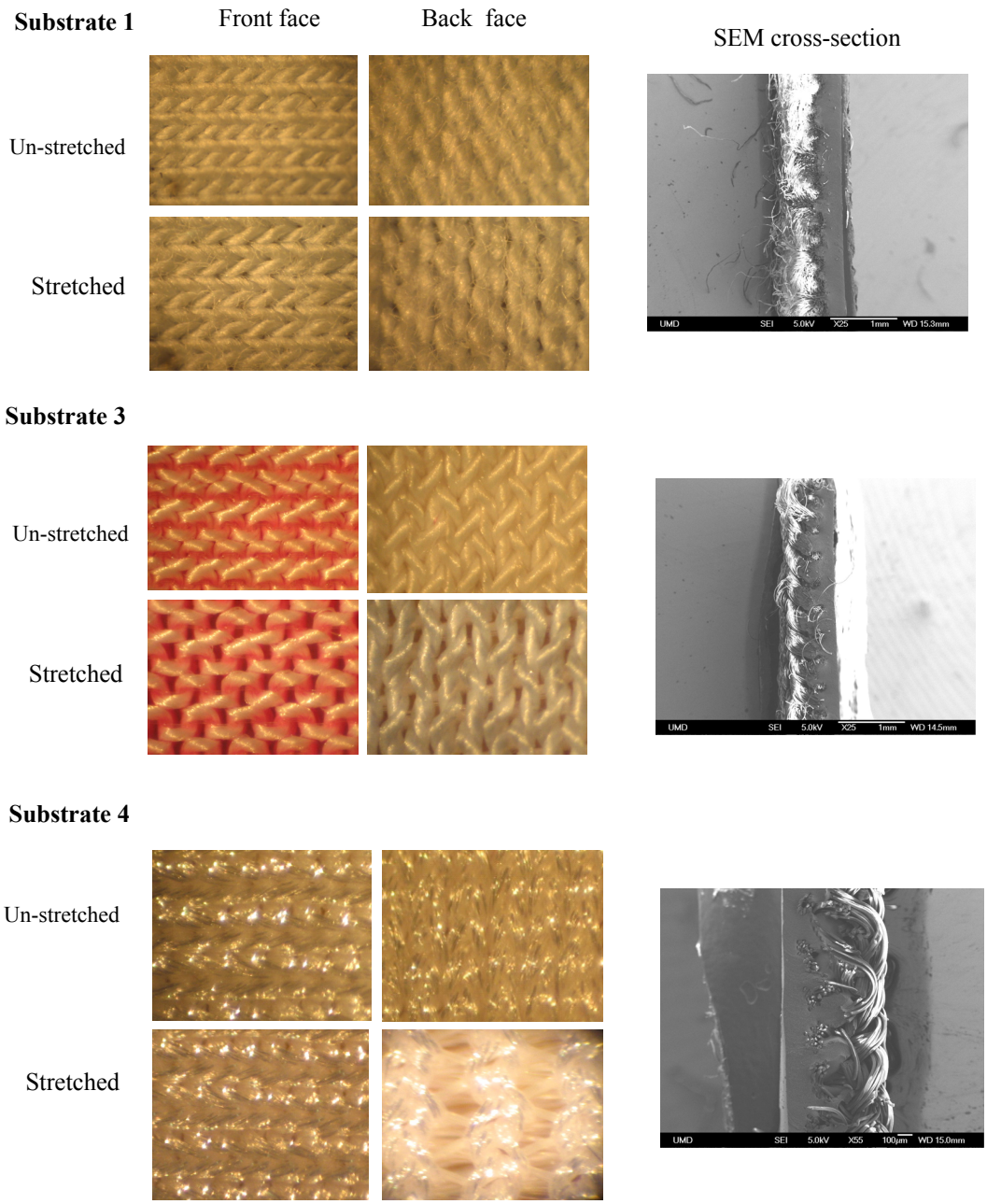

Substrate 5

Un-stretched

Stretched

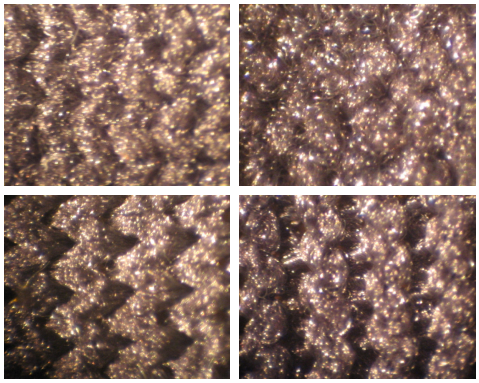

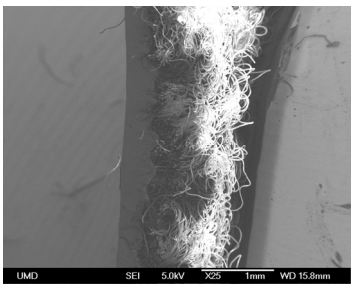

Substrate 6

Un-stretched

Stretched

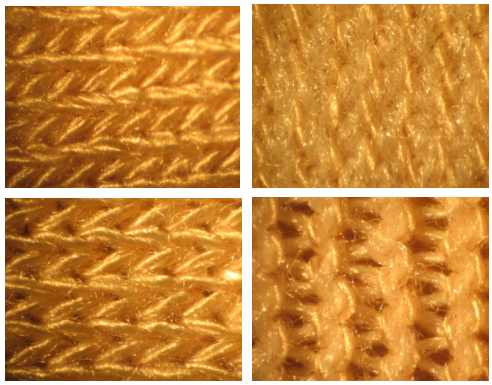

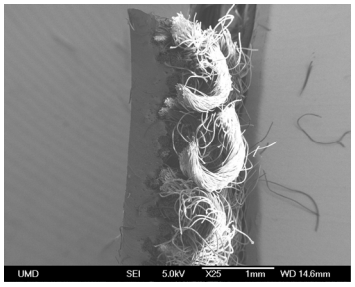

Substrate 7

Un-stretched

Stretched

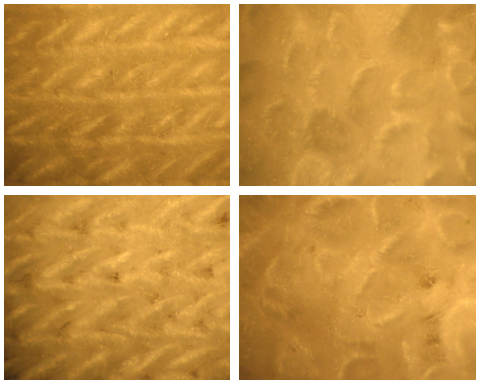

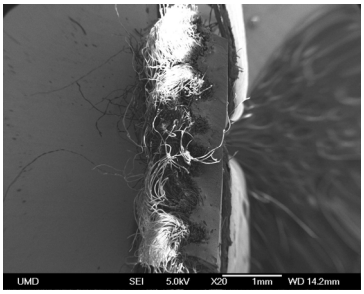

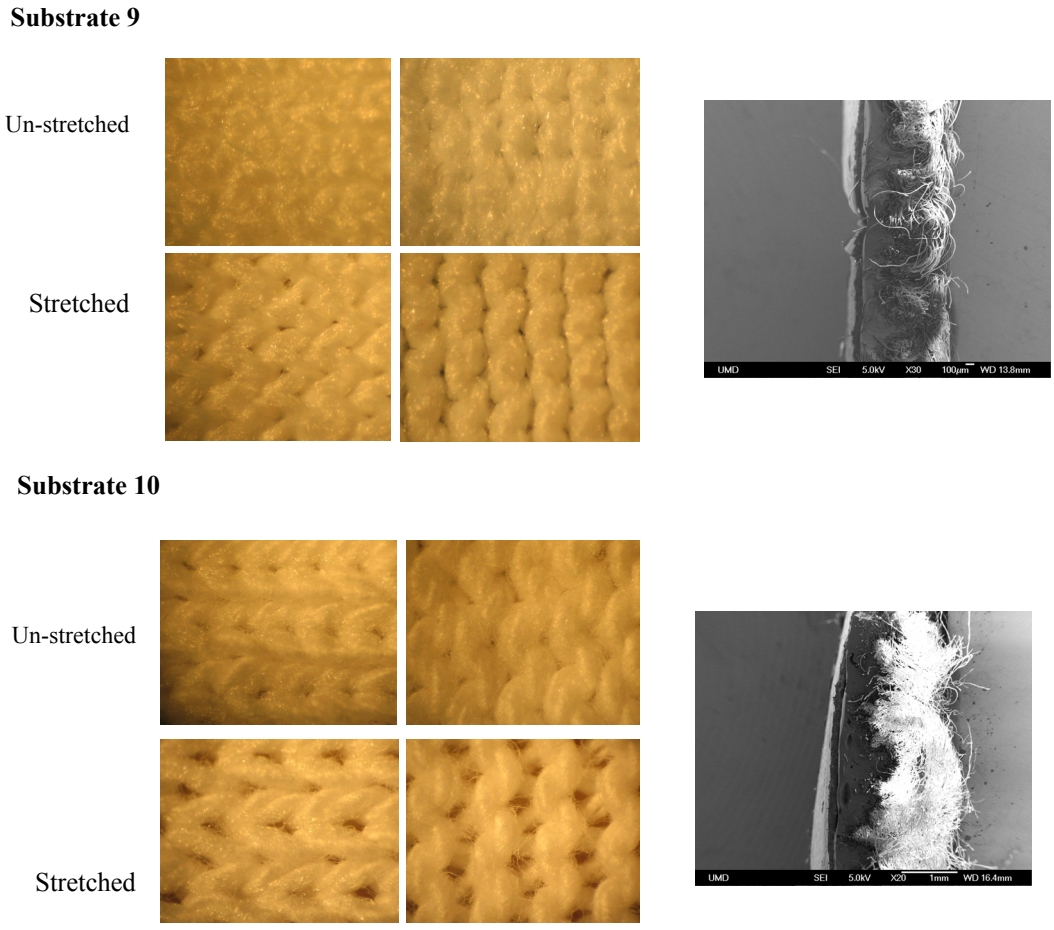

Figure 40. Different knit microstructures from Substrates I (face side, backside, stretched and un-stretched) magnified approx. 30 times.

Some interesting observations can be made from these microscope images of the substrate textures. Luster is characteristic of fibers with high resilience and high twist, such as that of Substrates 3 and 4. Very thin synthetic fibers such as that of substrates 5 and 9 make the surface of the fabric be noticeably filled, unlike substrate 10 which had a thicker fabric. The substrates with thinner fabrics and loose stitch are softer to the touch. It is a desirable characteristic for materials in contact with the human body that they be soft and compliant.

A second batch of substrates -Substrates II (Figure 41) was coated with the carbon-based component to look into the feasibility of using such coating on other knitted fabrics. The table with a description of these substrates is provided in Table 2. This time, most of the substrates correspond to commercial socks of different materials.

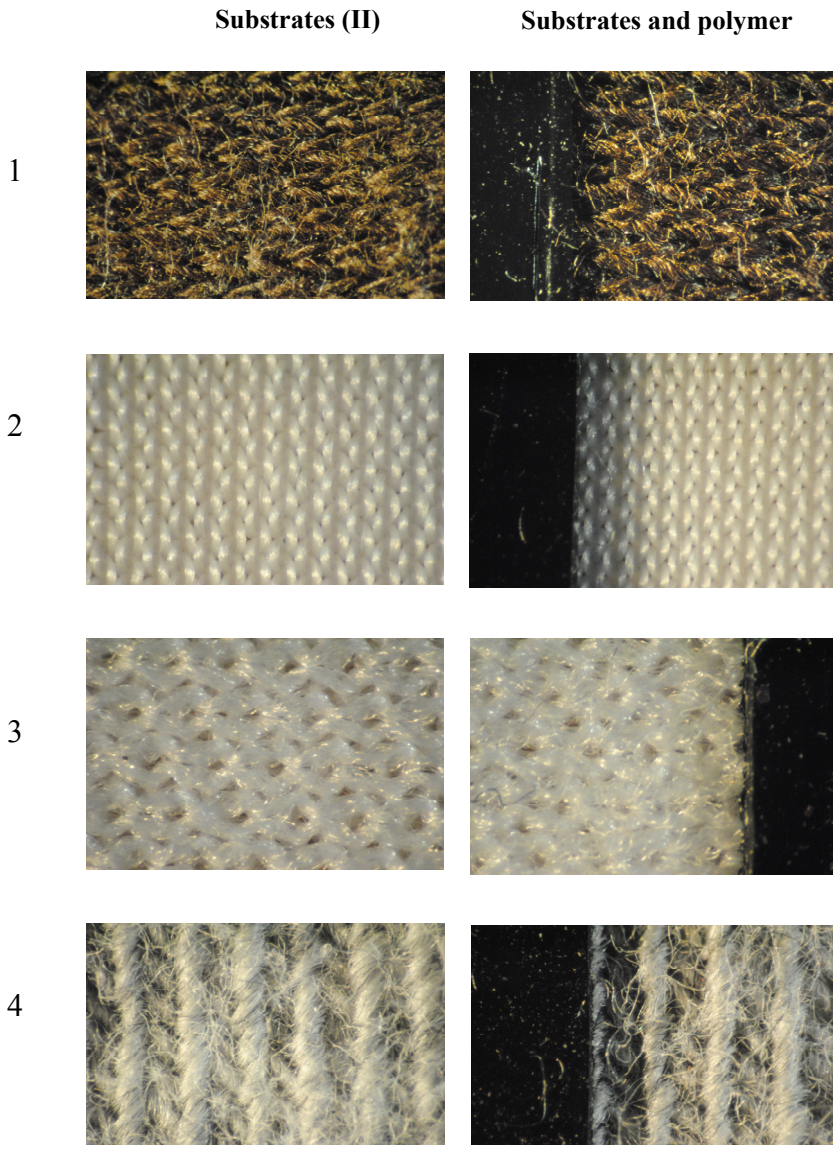

5


6

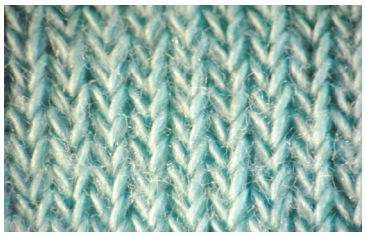
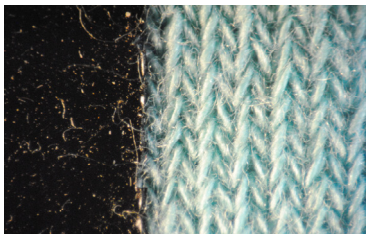

7

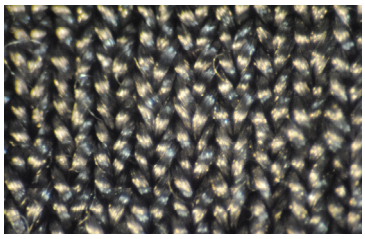
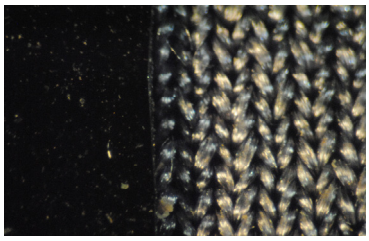

8


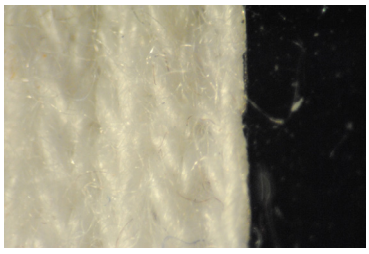

9

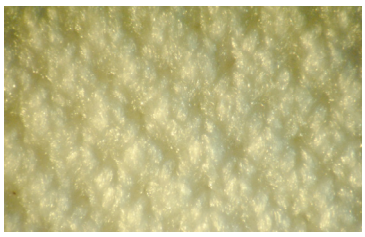
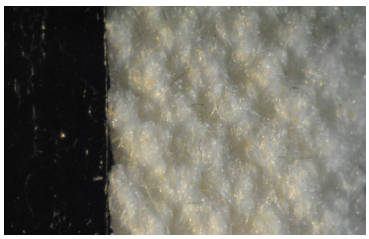

10

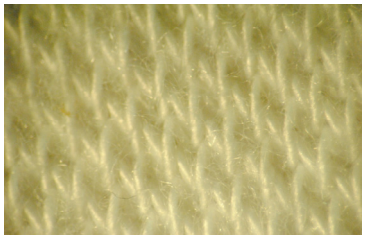
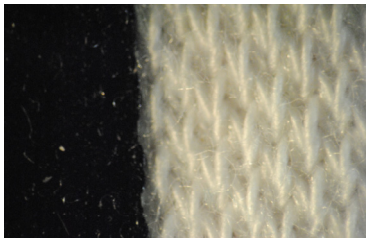

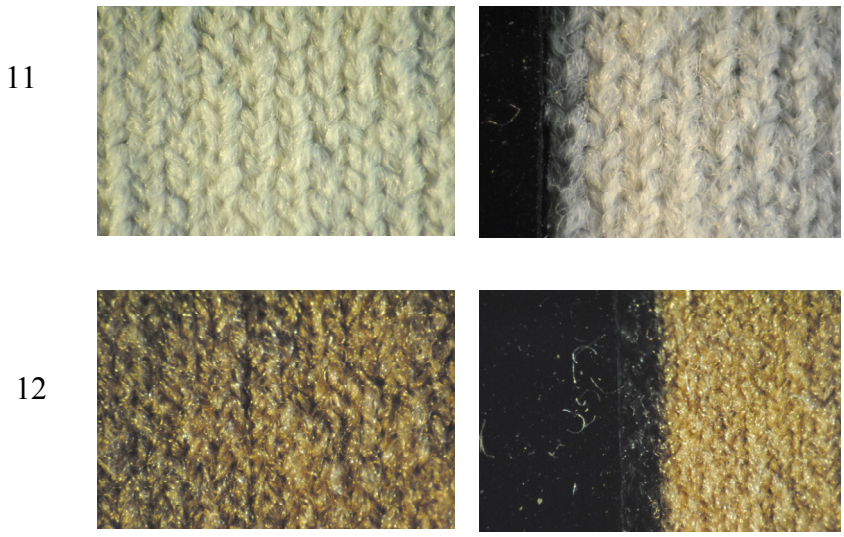

Figure 41. Micrographs of all Substrates II: left column shows the fabric structure and right column shows the coated substrate.

From these micrographs of substrates II (Figure 41) it can be noted that fabrics with low twist, such as substrate 1 and substrate 12 are prone to letting the polymer diffuse out of the masked area which is used to shape the sensor. Also, if substrate fibers are too thin the coating might not even be feasible due to a mechanical alteration of the fibers during the application process. This effect was seen with substrate 12 (substrates II) and substrate 2 (substrates I). This last one, rayon based, also presented a chemical reaction with the polymer, increasing the effect of the mechanical modification by growing a noticeable unevenness or swollen areas. Extremely loose stitch knits are also not favorable since the polymer may permeate completely through the substrate, not allowing the substrate to provide stability. This effect was seen with substrate 3 (II), where the knit had big fibers but were not tightly knit.

2.5 Study of Connections

Several methods for establishing electrical connections from the sensors to the acquisition board were investigated. The goal for this study was to find a compliant material, adaptable to fabrics with the least resistance possible. Several different materials such as silver paint, thin wires, carbon paint, and conductive thread were analyzed (Figure 42).

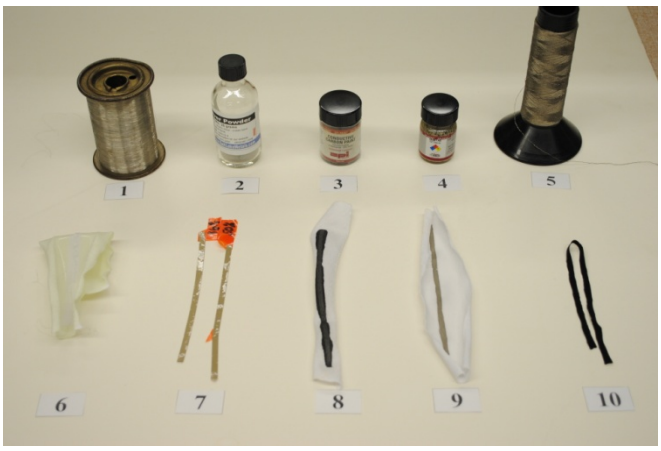

Figure 42. Connection materials

The materials shown in Figure 42 correspond to: 1. Chrome ultra thin wire, 2. Silver powder, 3. Carbon paint, 4. Silver paint, 5. Conductive thread, 6. Wire attached to fabric with PDMS, 7. Silver powder in PDMS, 8. Fabric coated with carbon paint, 9. Fabric coated with silver paint, 10. Eeontex PI coated conductive fabric. The fabric used as substrate for the coated connection samples was a 87% Nylon and Spandex knit.

The conductive silver paint had a great conductivity if it remained un-stretched. The silver sensor strip, which was of dimensions 13.5cm by 3mm presented a resistance of

210 Ohms. However, after the slightest of stretches its resistance climbed to the MOhm range. The conductive carbon paint strip of the same dimensions as the silver strip had a resistance of about 170 kOhms, which was too high for its purpose. Another material tested was the PI coated conductive fabric courtesy of Eeontex which showed a resistance in the order of a few thousand Ohms.

A mixture of PDMS and silver powder was investigated, however, given the constraints of not having a proper chemical hood, the mixture was done without the silane coupling agent (for silicone rubber), the chemical responsible for acting as a surfactant of the particles to be scattered in the polymer matrix. As a result, the bulk strips that came out of this mixture had resistances as high as 10MOhms per 5mm in a strip that was 4mm wide. This mixture was also coated on the nylon fabric to test whether the conductive properties would have a change or not. The mixture showed to be so inhomogeneous for lack of proper chemical treatment, which was mentioned before, that the particles were left on top of the fabric and the PDMS leaked and sank onto the mold use for holding everything in place. These strips can be seen in Figure 43.

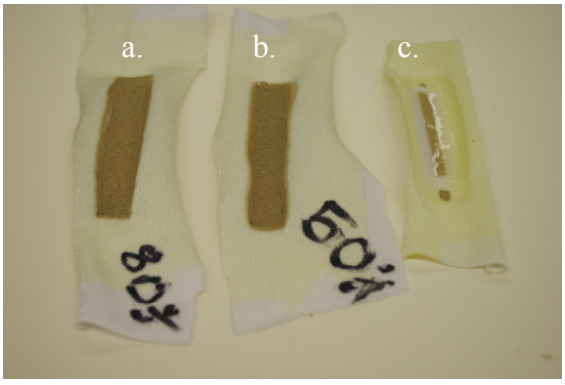

Figure 43. Silver powder and PDMS mixture with no chemical coupling agent: a. 50%, b. 80% and c. Silver paint between two layers of conductive silver paint.

The micrographs illustrate the segregation due to lack of a silane agent. The third strip on Figure 43 consisted of a layer of silver paint in between two layers of PDMS. This did not show good results either due to a lack of elasticity of the paint, which grew cracks with mild strain. This is illustrated in part b of Figure 44.

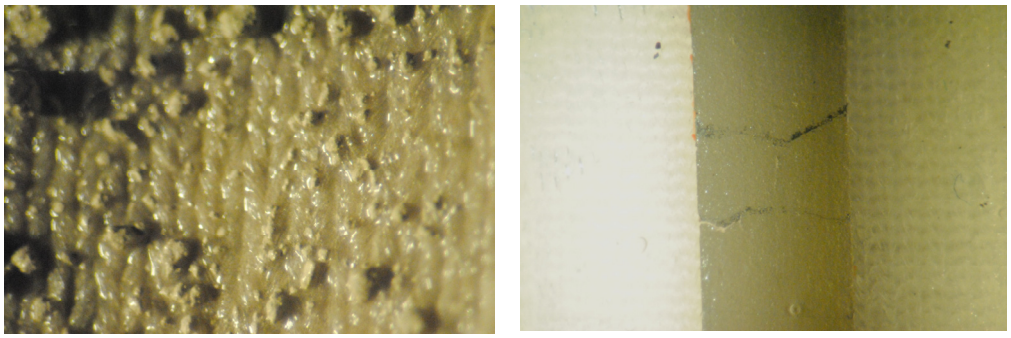

Figure 44. Micrographs of: a. silver powder in PDMS and b. silver paint sandwich.

Even concentration percentages predicted by [56] to be greater than 86% wt for good conductivity did not show good results. The conductive thread, with a composition of 87% C and 13% Ag had the compliance and good resistance characteristics for being implemented as a reasonably good connection line. Strands that were 13.5 cms in length had a resistance of 60 Ohms. Some micrographs of all the connection materials that were tested out are shown in Figure 45.

It can be noted from the previous figure that the paint adheres closely to the grooves of the fabric, causing the paint to quickly loose contact among the waves of the knit when stretched. As a result of this study, conductive thread will be adapted for the study of sensors embedded in socks.

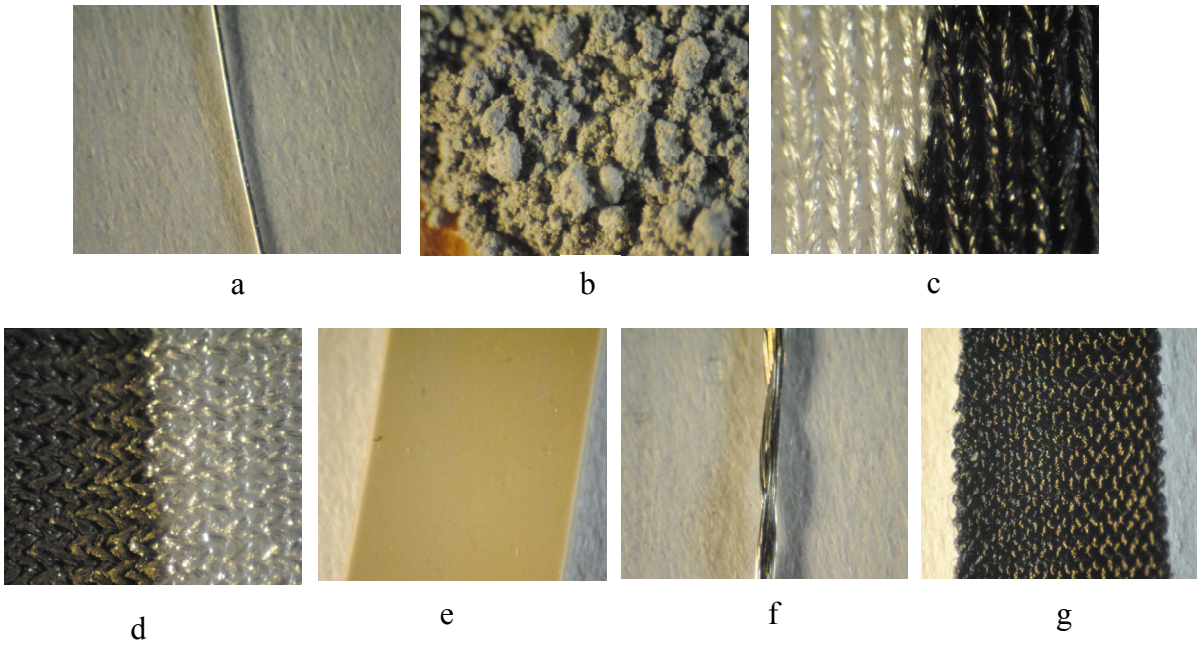

Figure 45. Connection materials micrographs: a. ultra thin wire, b. silver powder, c. carbon paint on nylon, d. silver paint on nylon, e. PDMS and silver powder in bulk form, f. conductive thread, g. Eeontex PI coated fabric.

Chapter 3. Experimental setup, Results and Discussion

3.1 Experimental Setup and Equipment

To understand the nature and sensor characteristics of coated fabrics with the polymer sensor, several sets of experiments were conducted. The variation in electrical resistance with the length of the coated sensor strip was measured. The gauge factor of a given coating applied to different substrates was determined in response to an initial change in length during different times following the application of strain. An electrodynamic shaker was also used in order to obtain the response of the sensor under different signals and signal frequencies. Following these experiments the sensor strip was placed in a rotating hinge with the purpose of obtaining a correlation of its output and the angle spanned by the wings of the hinge. Finally, a pilot study using these strips was applied to socks to detect foot motion. A wireless setup was used to transmit data from a carbon based sensor as well as a portable sock device using PI-coated sensors.

The experimental setups were built and customized to meet project requirements. They can be mainly grouped into three major set of experiments: first, the motor with sliding shaft for the gauge factor and pre-tension related experiments, second, the rotating hinge for the angle correlations including goniometers, and third, all the complementary setups such as the wooden foot models, microscope setups, and wireless setup.

Electric Circuit Setup

Three possible circuits were taken into consideration for the measurement of sensor resistance (Figure 46). Part a of this figure shows a direct measurement of resistance is possible with an Ohmmeter, however, it is not a practical approach for data acquisition since an additional hardware module for signal conditioning would be required. The Wheatstone bridge circuit is shown in part c, where any of the four resistors can be turned into the unknown resistor and one of the other three can be turned into a rheostat in order to balance the circuit (Vb=0). The output voltage Vb can be found when the circuit has not been balanced by using Equation 1.

$$Vb = (R1 * R3 - R2 * R4) * \mathrm{Vin}/((\mathrm{R1} + \mathrm{R2}) * (\mathrm{R3} + \mathrm{R4}))$$

Equation 1. Voltage output from Wheatstone bridge

This circuit can measure voltages more precisely since it measures differential voltages but is usually used for sensors which undergo very small changes in $\Delta R/R$. In the case of the carbon based polymer sensors, the relative changes in resistance are quite large. A voltage divider provided a good solution for measuring these large changes in resistance. Instead of working with voltage differentials, the voltage divider works with the actual voltage values being dropped across the resistive elements in the circuit. Therefore, this last approach was used in the data acquisition of sensor output (Figure 46b). The voltage output can be calculated using Equation 2.

$$Vout = Vin/(\frac{Rs}{R1} + 1)$$

Equation 2. Voltage output from voltage divider circuit.

In the voltage divider circuit (Figure 46b), an auxiliary resistor R1 (or series resistor R1) is used in series with the sensor Rs. The resistance of the auxiliary resistor was changed as needed to best match expected changes in the sensor resistance. In this scheme Vout corresponds to the voltage drop across R1 and Rs corresponds to the sensor resistance. In later graphs, Rs is plotted using the circuit formula shown in part c of the following figure.

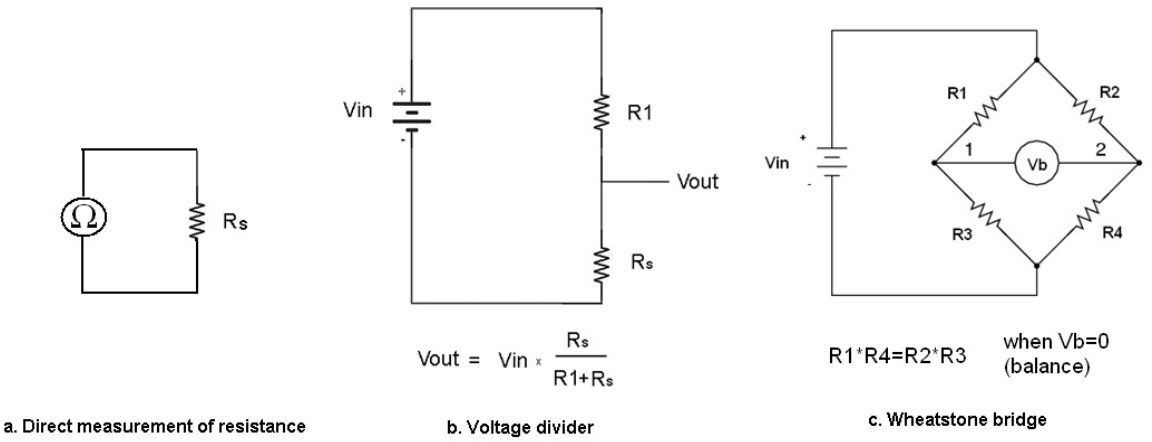

Figure 46. Circuits for resistance measurement: a. Direct measurement, b. Wheatstone Bridge, c. Voltage divider.

Sensor Resistance

A multimeter with two probes was used to measure resistance of the sensorized fabric as a function of the length of the sensor strip. One probe was held fixed and the other was displaced in increments of 1cm. The sample was placed on a flat surface without any strain before or during the test. The probe ends were held down with enough pressure for good contact with the conductive polymer. This direct measurement of resistance was performed on all the substrates.

Gauge Factor and other stretch related measurements

The experiments that involved stretch tests were performed using the motor setup shown in Figure 47. The section where the samples or sensor strips were placed is shown in Figure 48. A schematic which illustrates the whole setup can be seen in Figure 49.

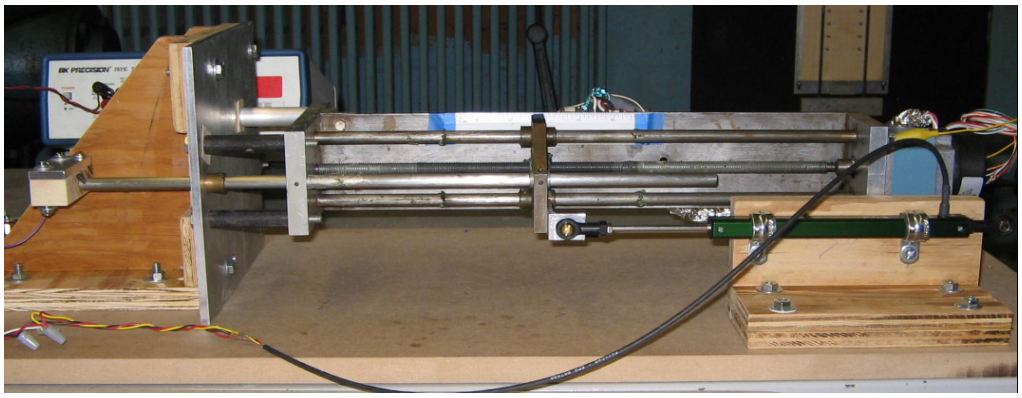

Figure 47. Stretch tests motor setup

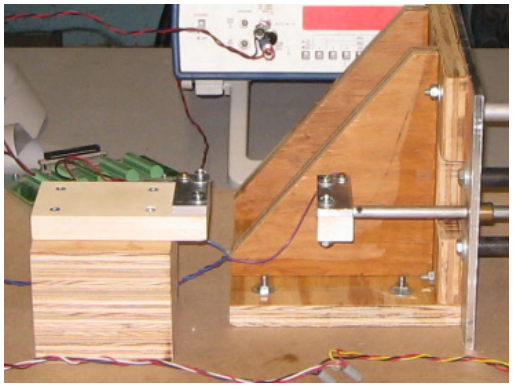

Figure 48. Section for placement of samples

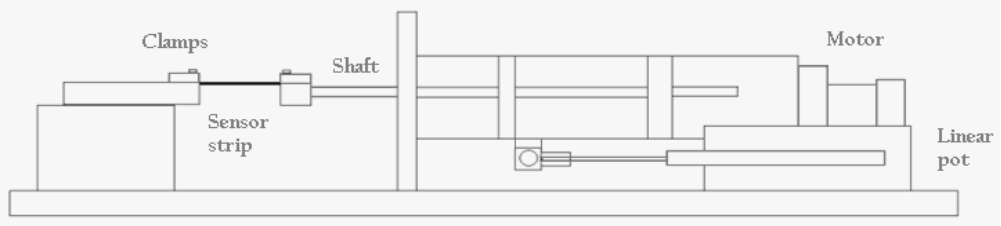

Figure 49. Motor setup schematic

The setup for taking gauge factor measurements consisted of a customized motor system, where the motor was controlled by a software program which gave predefined uniaxial displacements to one end of the sensor. This displacement was also monitored by a resistive linear pot that was attached to the displacing end for signal reference purposes. Each sample was carefully clamped between two conductive metallic electrodes, with a gauge length of 8cm and 0% pre-strain. One of the electrodes was attached to a mobile shaft. This is the distance across which the resistance values were taken. The sample was left with enough tension to get rid of any slack, which is a natural characteristic of unstretched fabrics and shows as wrinkles or non-uniformities. Then each sample was cycled three times at 30% strain, with a relaxation time of 5 minutes before taking the data. This was done with the purpose of 'breaking in' or stabilizing the resistance output of the conductive polymer sensor. Some samples sagged more than others after cycling, especially the ones containing cotton and rayon. The fabric growth was eliminated after cycling. The gauge factor test consisted of a continuous sequential set of stretches, where each stretch was held constant for 30 seconds. Samples were strained 5%, 10%, 15%, 20%, 25%, 30%, 35%, 40%, at a speed of 1 inch per second. All the samples were unstretched at a speed of 0.5 inch/s and then carefully loosened from the clamps.

The data taken for the calculation of the gauge factor consisted of taking three distinct resistance measurements for each value of strain. The first value of resistance was taken immediately after the stretch, the second value was taken after 10 seconds of the stretch and the third value was taken 25 seconds after the stretch. This test was repeated for the

three samples of each kind of substrate and the gauge factor was obtained and averaged for each substrate. For the gauge factor measurements, the data acquisition was composed of a National Instruments PCI-6024E card sampling at 200 Hz with a resolution of 12 bits. The computer board had a voltage range of +/- 5V. As was mentioned before, the voltage monitored corresponded to that of the voltage drop across the auxiliary resistor, which was transformed into a resistance change by a program written in Labview.

Electrodynamic Shaker

The samples were also submitted to electrodynamic shaker tests (Figure 50), where each sample would be stretched at a specific frequency determined by the shaker controller and through the amplifier. The amplifier used to power the shaker was a Hafler transnova P1500. The samples were stretched continuously at a frequency of 1Hz, a frequency that is representative of foot motion. Sinusoidal, square, and ramp signals were used to pull the strips, which were mounted with a gauge length of 2.5cm and were subjected to a cycling strain of 20%. The samples were clamped with metallic electrode plates on each end and the slack was eliminated, in preparation for the tests. One of the electrodes was fixed to a gauge and the other one fixed to the shaker.

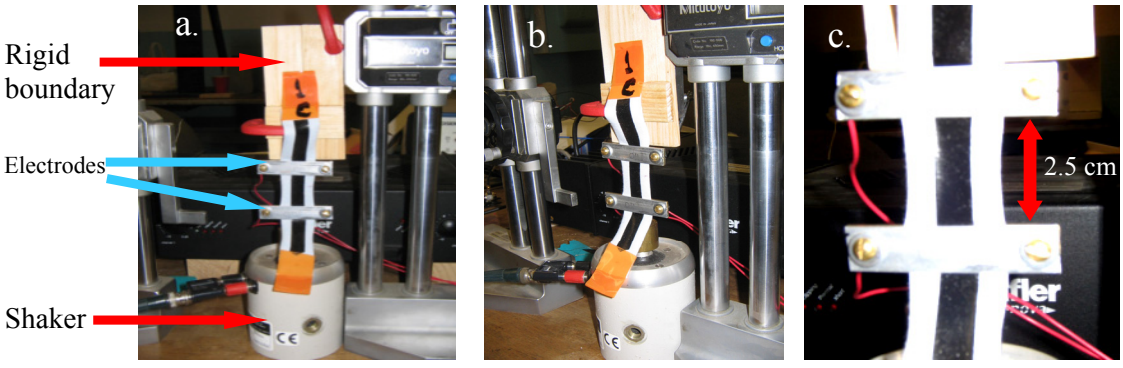

Figure 50. Electrodynamic Shaker setup: a. Shaker and fixed top end, b. Only part of sample is clamped, c. Gauge length between electrodes.

Pre-tension related measurements

The effects of sample pre-tension were analyzed with data taken on one substrate with different initial strain conditions. The gauge length was kept at 8 cm for all the cases. The first condition corresponded to a 5% slack or -5% strain in the sensor. The strain sequence applied in the previous section (5% to 40% in 5% increments) was introduced. After this test the clamps were removed and the sample was allowed to return to its original length with a relaxation time of 20 min. The second condition corresponded to a nominal 0% pre-strain which corresponded to just enough strain to get rid of natural slack. Sample was also allowed to relax for 20 min. The third condition consisted of a 5% pre-strain where the sample was clamped under tension.

The gauge-length effects on the gauge factor measurements were also measured. For this test one sample substrate was used. A gauge factor test was carried for gauge lengths of 2.5 cm, 5 cm and 8cm. The sample was allowed to have a relaxation time of 20 min between data takes. Repeatability features of the sensor responses for one substrate were also looked at.

The impact that the mounting has on the actual resistance measurements was heuristically evaluated by repeatedly mounting and un-mounting the same substrate sample in the clamps. The variation of resistance was in the vicinity of the same value, given the sample had already been cycled. Pressure on the clamps did not seem to affect the data takes if the sample was held tight enough for good contact.

A second repeatability characteristic was assessed by repeatedly stretching one sample substrate, with a gauge length of 8 cm. The sample was stretched six times (5 times effectively, as the first cycle was considered to be pre-cycling) and the strain was 20% for each of the repetitions. The sample was allowed to relax 15 minutes between takes. Motor velocity was 1 inch/s as in the previous section. The impact of stretching the fabric in the direction perpendicular to its long dimension was tested. For this purpose two samples were prepared on the same substrate used in this section, where the sensor strip would have its long direction forming 90 degrees and 45 degrees with the long direction of the fabric. Gauge factor measurements were carried with the same specifications of the previous section. Also, the long time drift curve of one sample, using the same substrate type, was observed during one hour.

Angle Correlation

For the angle correlation experiments using carbon polymer sensors, a hinge with a rotating wing was used (Figure 51). The data acquisition used corresponded to National Instruments PCI-6024E card sampling this time at 1000 Hz with a resolution of 12 bits, producing data files for 5 seconds for 5000 samples. The computer board had a voltage range of +/- 5V. The resistance measurements from the samples were also taken by means of an electric voltage divider where an auxiliary resistor was used in series with the sensor. The voltage values that will be analyzed in what follows for the angle correlation study correspond to the voltage across the auxiliary resistor of the divider, which is proportional to the voltage across the sensor and therefore to its resistance. The

voltage drop across the auxiliary resistor will be referred to as the sensor voltage for simplicity.

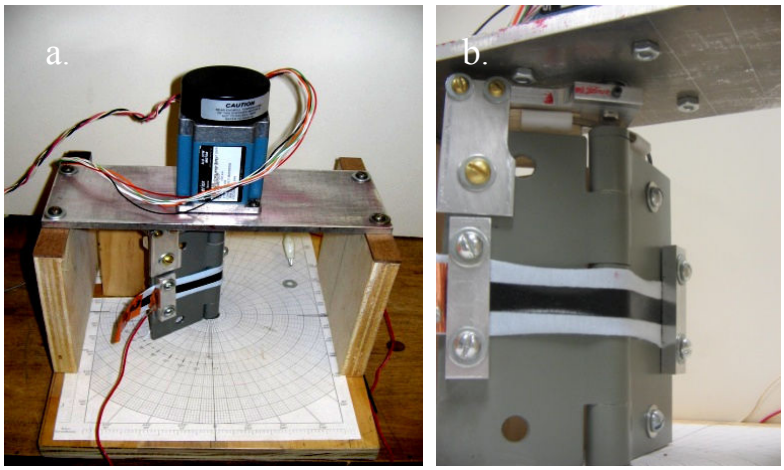

Figure 51. Hinge Setup: a Motor and hinge, b. hinge, electrogoniometer and sensor strip

A Biometrics F-32 electrogoniometer was used for obtaining the actual angles being swept by the hinge wing. The F-32 was accompanied by a customized amplification card, box and voltage source, as can be seen in Figure 52. A couple of mechanical goniometers were built as well, to be used in the same study. One of them is shown while being calibrated with graph polar paper in Figure 53.

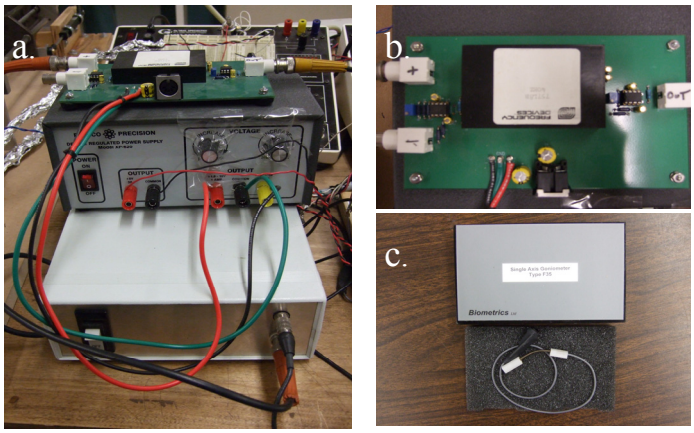

Figure 52. Electrogoniometer setup: a. complete setup, b. amplification card, c. electrogoniometer

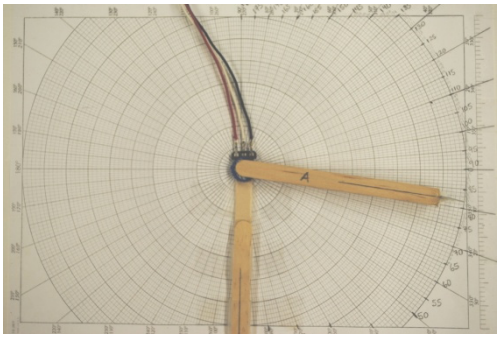

Figure 53. Mechanical goniometer

Pilot Sock Study

The sock study was aided as well by the construction of a foot solid model (Figure 54) in order to have a consistent way of measuring the impact of the location of the sensors on the sock. Models were built aiming male and female feet. Different clays were tested for potentially building both types of feet.

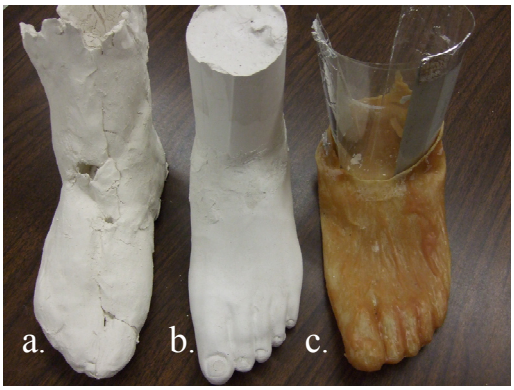

Figure 54. Foot model construction: a. Clay, b. Plaster, c. Plaster mold

The plaster model (Figure 54 part b) for example, was built using the plaster mold shown on part c of the same figure and it was made having male subjects in mind. The mold used to build the male plaster model was made of mold rubber. The mold rubber was coated on a real male prosthetic foot in order to obtain the mold shown in part c. The

resulting plaster model had a very smooth surface and was ready to be used as a sock coating mold. The prostetic foot was kindly provided by the Kinesiology Department at UMD.

A plaster mold with a different technique was also built for female subjects; it is shown in part a. of the figure being discussed. As a result of this different approach, its surface was very hard to even out and non suitable for the purpose for which it was built. A wooden carved model was also build for potential female subjects. This model was finally used as the mold for coating the socks. Figure 55 shows the finished version of the wooden model, which was the result of an intensive and onerous crafting procedure.

Figure 55. Wood carved foot solid model

Micrographs

The micrographs of the fabric textures were obtained by using a Bausch and Lomb microscope with 30x augment capability and a camera adaptor; these are shown in Figure 56. The cameras used for the micrographs were the Nikon SLR's D70 and D3000. The SEM images of the cross-sections of some of the sensors were taken with a JEOL 6500.

Figure 56. Optical microscope used for viewing the textures of the different fabrics: a. ocular and diopter, b. camera adaptor

Smaller initial setups were shown in section 2.1, as part of the illustration of the process which was followed to find the appropriate sensing material to be combined with fabrics for this study.

3.2 Experimental Results and Discussion

As discussed in Appendix A of this thesis, there are many ways to sensorize fabrics. The focus of the present study is to give fabrics electrical conductivity properties, so as to being able to apply an initial voltage and to retrieve information when the output voltage changes. This occurs when a fabric that has been coated with a conductive material undergoes strain, which enables the cloth to be used as a sensor. Coating stretchable fabrics with such a material -carbon-based polymer- is therefore the premise of the following set of experiments and discussion, and becomes the subject of the experimental setups presented in this section.

3.2.1 Resistance along length

The increase in resistance with length of all the substrates showed a linear behavior (Figure 57), with varying slopes for the different substrates. The smoothness of the curves depends on the uniformity of the coating. The curve corresponding to substrate 10 (diabetic sock), which is knitted of a noticeably thicker fiber, is noticeably smoother than the other curves, this could indicate that the hand coating produces a more homogenous coating on thicker fabrics, such as substrate 10 (Figure 40). This substrate also shows the lowest slope, indicating that the resistance had a less pronounced variation with length, or that the sensor was overall more conductive, i.e. had more coating material. The SEM image corresponding to substrate 10 (Figure 40) suggests the coarser and looser knit of substrate 10 produced more contact surface allowing more conductive composite to be deposited. Substrate 9, corresponding to the micro denier fiber fabric showed the highest slope of all the substrates, indicating that the conductive material had been absorbed in lesser proportion.

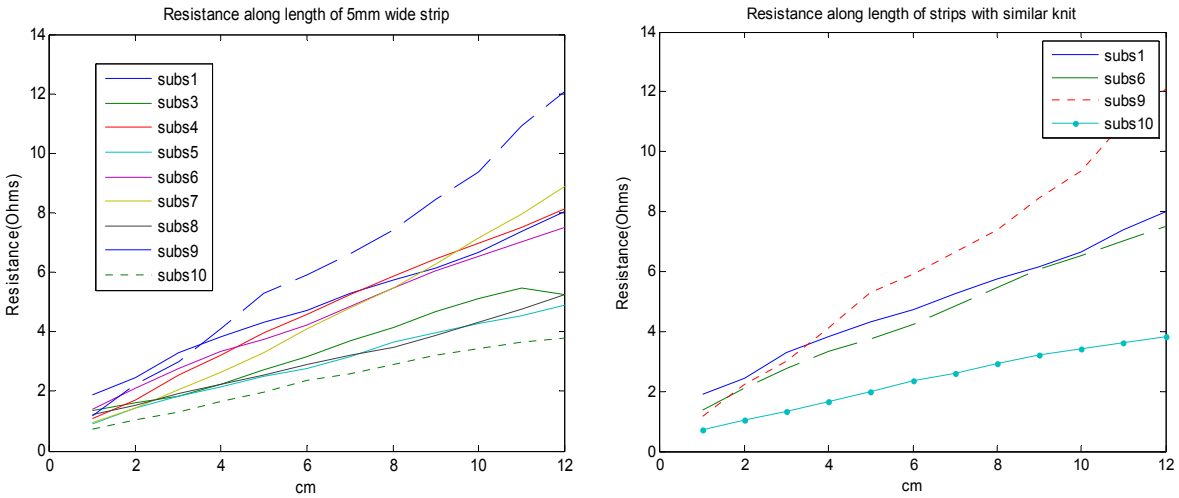

Figure 57. Resistance as a function of length for the different substrates: a. for all substrates, b. for substrates with similar knit

Resistance linear variation with increased sample length seemed not to be affected by the substrate composition. However, the rayon fabric seemed to have a moderate reaction to the coating, highlighting its natural crimp after the coating was put on. This substrate did not show the same smooth characteristics of the finished coating as shown by the other substrates.

3.2.2 Gauge factor measurements

For the gauge factor measurements, Figure 58 shows the sequential strains of 5% every 30 seconds. The resistance drift is noticeable in between stretch peaks; every increasing stretch produces an overall increment in the resistance and an overshoot. However, it is noticeable that the drift goes down faster at higher strains and that the resistance overshoots at each increment of strain increases as the strain percentage increases. This behavior was observed in all the substrates, plotted in the graphs shown in Figure 58.

Substrates 4,6,7,9, showed an overall higher resistance than the other substrates. The lowest resistance values were shown by substrates 2,5,10. The substrates with the higher resistance values had a tighter stitch than the ones with lower resistance values. Therefore, the tighter the knit stitch the less conductive coating gets deposited. Substrate 2 had coating problems and therefore it is possible that more conductive elastomer was deposited. All the substrates responded in a similar way to the strains applied and none showed any lag in response. All showed drift in resistance after the application of strain and all showed a similar drift rate for every value of strain, which may indicate that the drift does not depend on the substrate composition. A similar graph was obtained for changes in resistance over time. It shows that substrates 1, 6, and 8 had the overall larger

percent changes in resistance. While substrates 3,9 and 10, showed the lowest percent change in resistance.

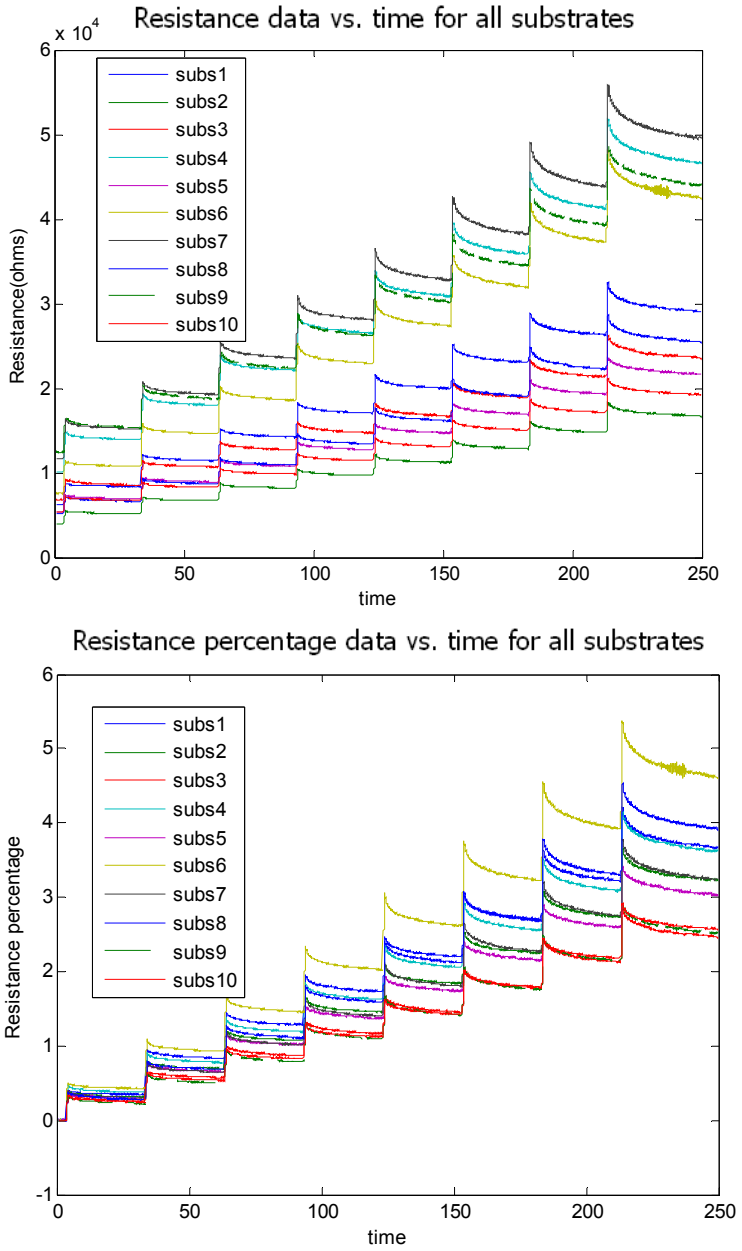

Figure 58. Resistance vs time and resistance percentage overall measurements for all substrates: a. Resistance values and b. Resistance percent change.

Percentage change in resistance measurements were graphed versus the strain applied in order to calculate the gauge factor. The three curves on Figure 59 correspond to resistance measurements taken at three different times after the application of the strain on substrate 1. The second graph of Figure 59 shows the percent change in resistance during the time of the test. A similar procedure was followed for all the substrates, and they all exhibited behaviors similar to that shown in Figure 59 for substrate 1.

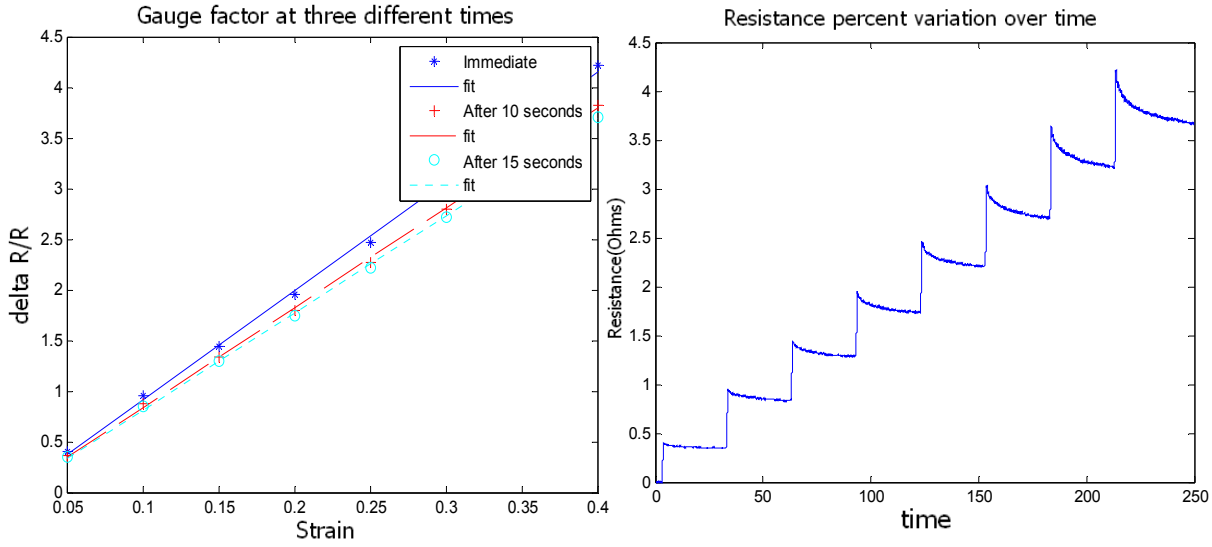

Figure 59. Resistance data taken for gauge factor test corresponding to substrate 1: a. Gauge factor at 3 different times and b. Resistance percent variation in time.

The gauge factor values were obtained for each of the three samples of each kind of substrate and then averaged for the same substrate. The values obtained are shown in Table 3. Gauge factor average values for all the substrates at three different times are shown in a histogram in Figure 60.

Table 3. Measured Gauge factors

Sample substrate	Av. gauge factor immediate	Av. gauge Factor 10s	Av. gauge Factor 25s
1	10.5	9.7	9.4
2	9.9	9.1	8.8
3	8.9	8.2	8.0
4	9.1	8.4	8.2
5	9.5	8.9	8.8
6	11.4	10.3	10.0
7	10.5	9.6	9.3
8	13.1	11.9	11.7
9	8.9	8.2	8.0
10	6.8	6.4	6.3

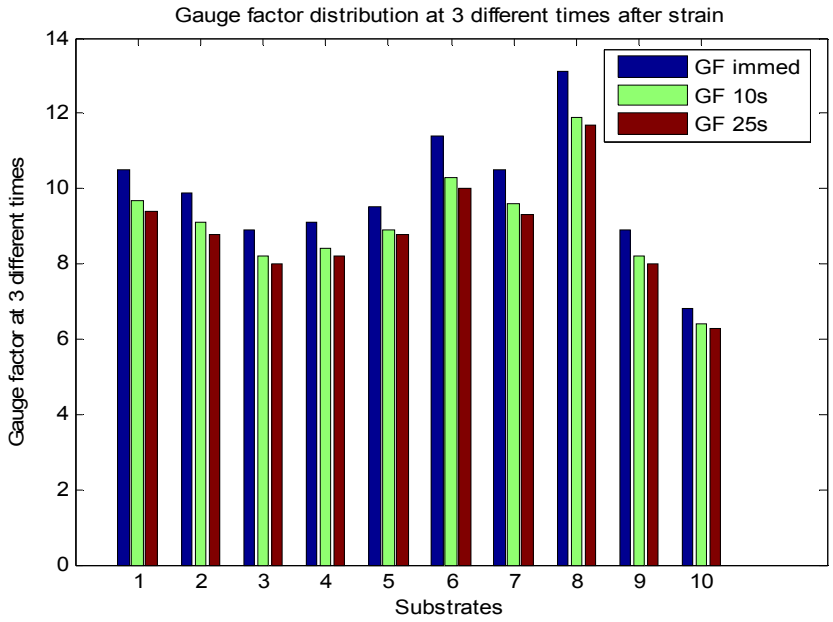

Figure 60. Gauge factor results at three different times for 10 substrates.

The obtained gauge factor values show that the gauge factor in all substrates has a tendency to decrease over time. This may indicate that the strip is very sensitive near the strain impulse and that it becomes less sensitive over time. The gauge factor values seem to have an overall variation with the substrate. This could be due to different factors

combined such as fiber thickness, fabric mechanical properties, density of substrate, wale and course count, etc... The lowest gauge factor values corresponded to those of the diabetic sock. This could be due to the presence of more conductive elastomer on the surface of the fabric substrate and an overall more conductive character. Substrate 9 had the highest linear change in resistance when unstretched, and it had one of the lowest gauge factors. More studies need to be conducted in this respect.

3.2.3 Other measurements

Pre-tension tests were carried on substrate 1, which corresponds to the cotton spandex blend. Three different pre-strains were applied and then a corresponding gauge factor test was applied to each one. Gauge length effects were also measured, a gauge factor test was performed on each of the strips of different lengths.

The results, summarized in Table 4, indicate that the gauge factor increases with increasing pre-strain. Sensor sensitivity increases with a positive pre-strain applied. The sample with -5% shows an unevenness in the first drift curve which is not observed in the other pre-strains. This result was expected, as the fabric may undergo shape irregularities when it is loose, affecting the resistance behavior of the sensor strip. For the gauge length effects (Table 5) it was observed that the gauge factor decreases with decreasing gauge length. Therefore the sensor becomes less sensitive as its length decreases.

Table 4. Pre-strain effects

Pre-strain	GF immed.	GF 10s	GF 25s
-5% pre-strain	7.7	7.1	6.9
0% pre strain	7.9	7.3	7.1
5% pre-strain	9.2	8.4	8.2

Table 5. Gauge length effects

Gauge-length	GF immed.	GF 10s	GF 25s
8cm	10.5	9.7	9.4
5 cm	8.2	7.5	7.4
2.5 cm	6.6	6.0	5.9

It was also noticeable that the drift became more uneven with decreasing gauge length and for each drift corresponding to each value of strain (Figure 61). This may be due to mounting end effects. The effect of the angle of the sensor strip with the long dimension of the fabric was not substantial. The samples of substrate 1 at 90 and 45 showed a similar gauge factor to that obtained from the test in the long direction (0 degrees). However, more tests will be conducted with more angles and more samples of the same

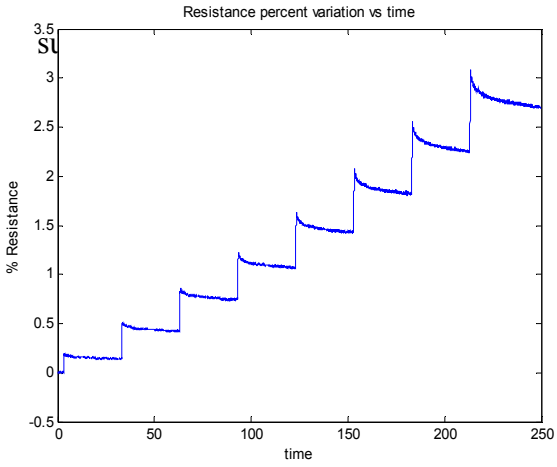

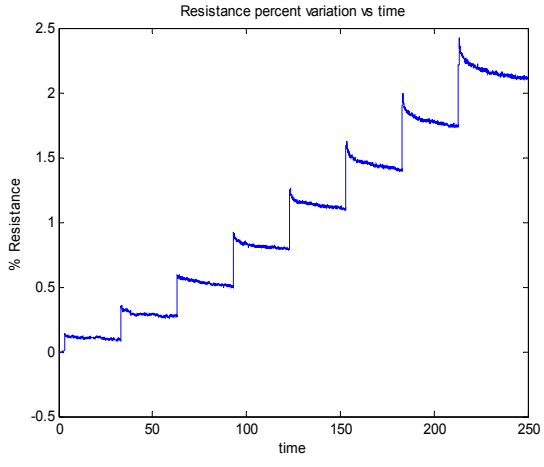

Figure 61. Resistance variation for gauge length of 5cm (left) and 2.5 cm (right).

Repeatability was observed in the shape of the sensor response (Figure 62). The relaxing time of 20 min, seemed not to be enough to bring the sensor to its original value and therefore did not produce the same values of resistance. After each repetition, a decreasing value of resistance was found. However, the resistance difference among the curves was in the only in the order of 200 ohms or less than 3 % of the nominal basal resistance values of 10kOhm.

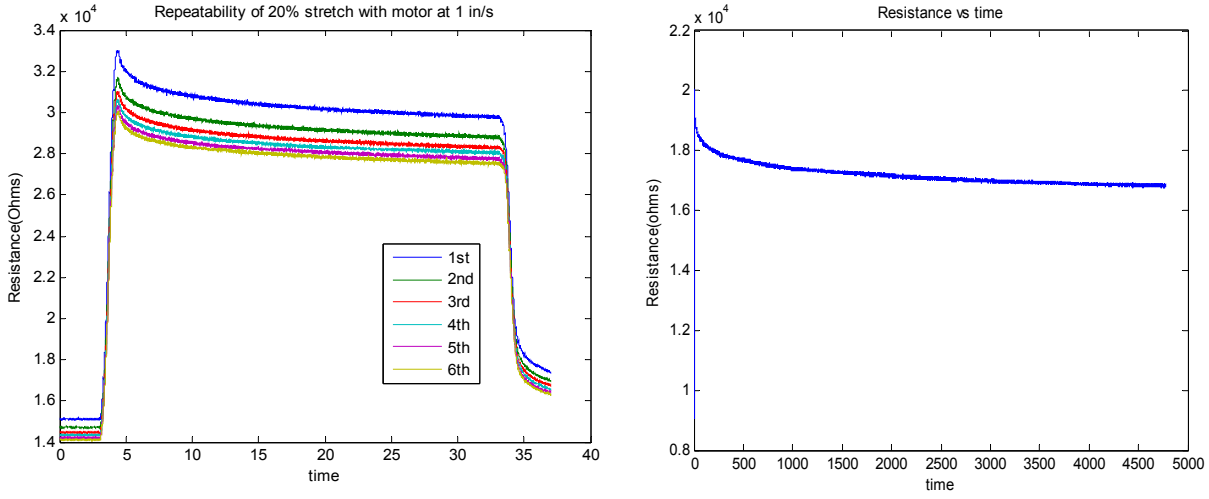

Figure 62. Repeatability test (left) and long time drift curve, on substrate 1.

A long time drift curve was obtained for substrate 1 for about 4700 seconds. The resistance drift rate seemed to have stalled around this time. This drift presents a challenge for the active usage of the conductive elastomer sensors.

3.2.4 Shaker results

Results of the shaker measurements with ramped, sinusoidal, and square wave excitation wave forms are shown in Figure 63 for substrate 1, and of sinusoidal excitation for substrates 4, 6 and 9 in Figure 63.

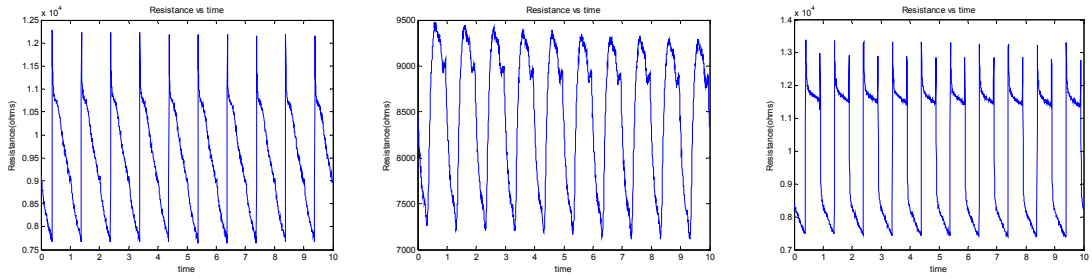

Ramp Sinusoidal Square

Figure 63. Ramp, sinusoidal and square signal responses of substrate 1 at gauge length of 2.5 cm.

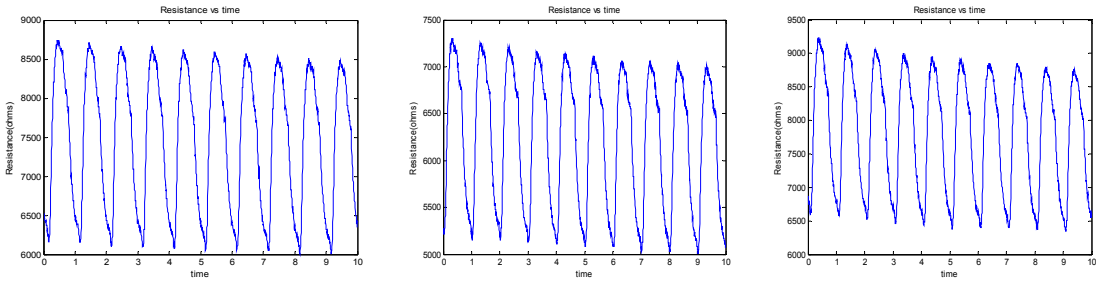

Substrate 4 (87% Nylon) Substrate 6 (Polyester blends) Substrate 9 (microdenier Nylon)

Figure 64. Sinusoidal signal responses of substrates of higher resilience at gauge length of 2.5 cm.

For these measurements it was found that all of the substrates gave output resistance behaviors similar to those shown by substrate 1. However, sinusoidal curves were smoother for substrates with fibers of higher intrinsic resilience, like nylon and polyester blends. Loose stitch knits, such as that of substrate 10, and fabrics with a higher

percentage of natural fibers presented additional peaks for the sinusoidal inputs, as seen in the sinusoid from Figure 64.

3.2.5 Angle correlation data processing

This section entails the data processing and angle correlation corresponding to the hinge setup. In this setup, the values of resistance from sensor substrate 1 (Substrates I) are correlated to the angle spanned by the hinge. The sensor strip was placed across the wings of the hinge so that any change in angle will reflect in a resistance change. Due to the fact that the sensor does not exhibit unique resistance values for unique angles, a differential approach was applied in order to back out angle information from the sensor. Shown below in Figure 65 is the sensor response for two different angular accelerations but the same angular deflections from 0° to 60°:

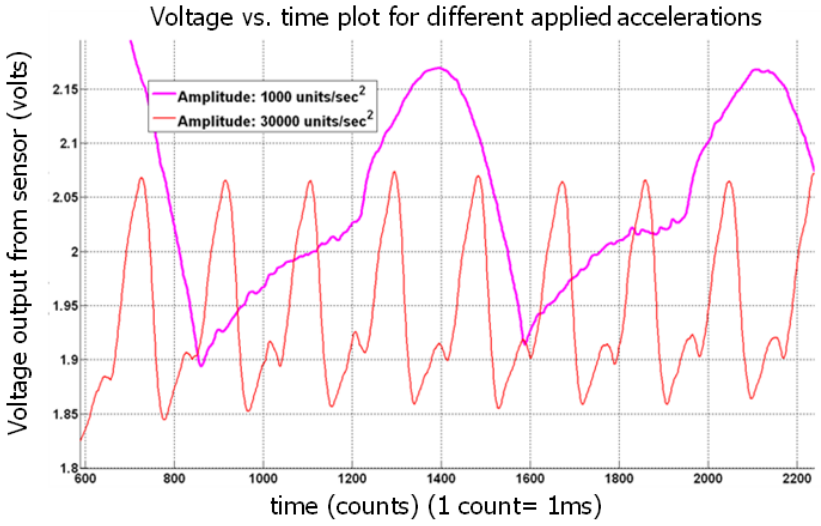

Figure 65. Voltage Variations for Peak Angular Accelerations as sensor is swept from 0° to 60°.

It can be observed that a unique voltage does not exist for a specific angle. It can also be observed that the voltage curve leading to a point is different from the voltage curve

leading away from it, indicative of elastic hysteresis. The process of determining a specific angle from a measured voltage therefore requires some information about the path of approach and rates of change. It was also observed that even though the absolute values of the voltages are different for different acceleration amplitudes, for a fixed span (say 60 ° as in the case above), the voltage waveform was repetitive or periodic for every curve, showing good repeatability. Also every curve follows a fixed trajectory, when approaching or receding a point. This information suggests that the rate of change of the angle spanned by the hinge is in some way related to the rate of change of voltage in a unique relation for a single value of acceleration. This indicates that if the rate of change of voltage could be determined, it could then be compared to some form of database in which already measured rates of change of voltage and corresponding rates of change of angles, for varying peak accelerations, are tabulated. This can be used to back out the rate of change of angle. For initial testing a database was created by sinusoidal accelerations with amplitudes ranging from 1000 °/sec^2 to 30000 °/sec^2, however only the portion of the database with accelerations 1000°/sec^2 to 4000°/sec^2 was used for the test with the random input signal. This was mainly due to a reduction in the file size and therefore computational time.

The angle acceleration values were selected keeping in mind the application to socks; however, in reality the foot can have accelerations of more than 30000 °/sec^2. According to data from ref [57], shown in Figure 66, the peak acceleration obtained during experimentation on a human foot was below 2500 rad/sec^2 which is over 140,000 °/sec^2 [57]. The experimental setup however limited the acceleration to 30,000° /sec^2. Also

from Figure 66 we see that angular displacement has a maximum range of about 35°. The maximum angle span for the experiment was expanded to 60° as a very safe limit to the maximum data range. In order to create this database, sensor voltage values for angles ranging from 0° to 60° were measured for each of these accelerations. An example of the raw and filtered data obtained from the sensor is shown below in Figure 67.

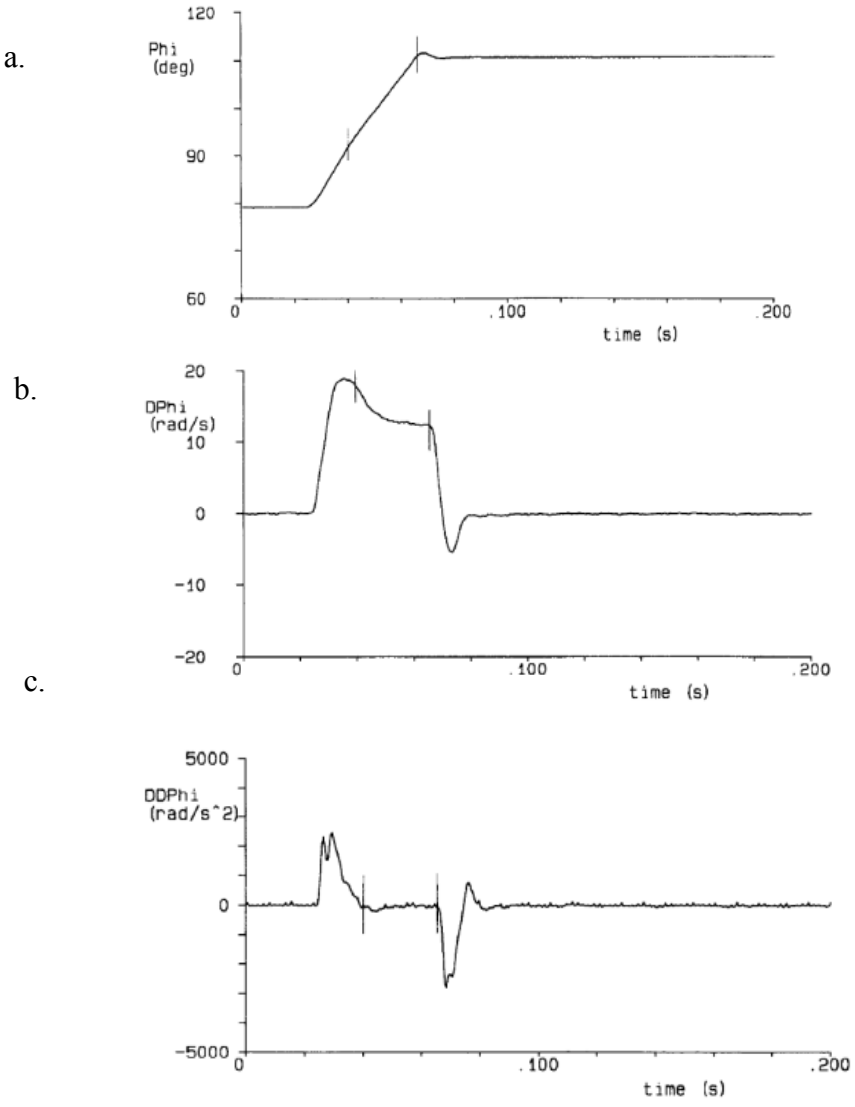

Figure 66.a. Rotation, b.Angular Velocity and c.Angular Acceleration of a Human Foot [57]

a.

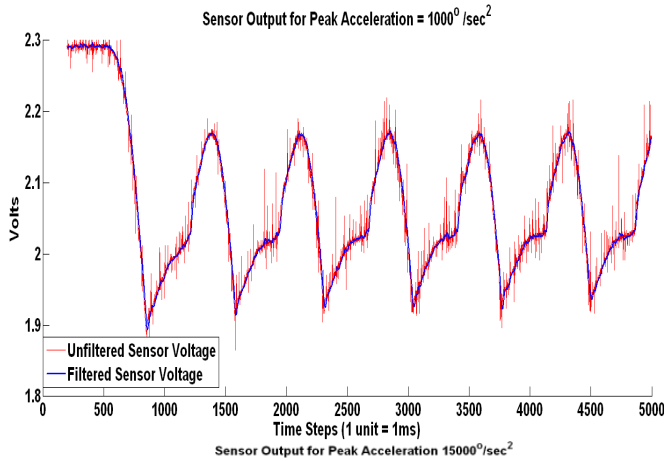

b.

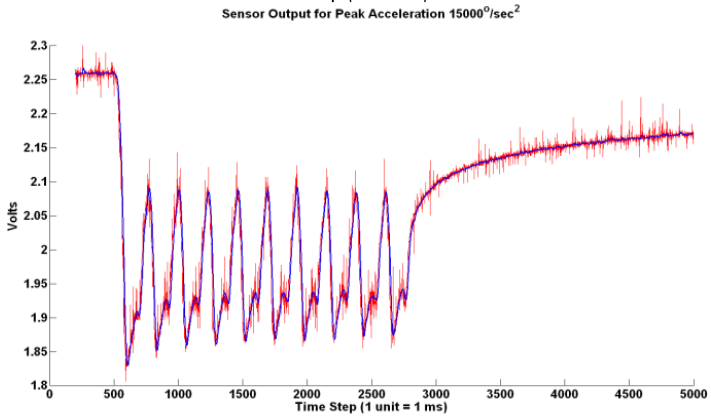

c.

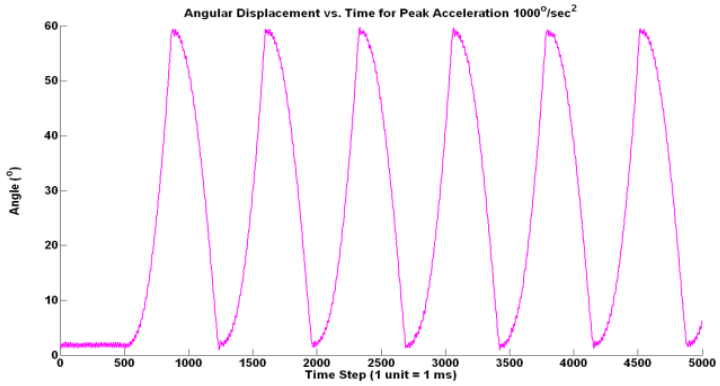

d.

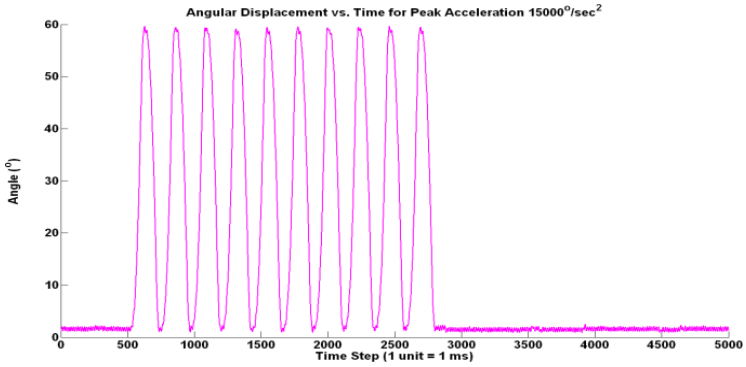

Figure 67. Sensor Voltage Variations for Angular Displacement: a. Sensor output for peak acceleration of 1000 deg/sec^2, b. Electrogoniometer output corresponding to (a), c. Sensor output with peak acceleration of 15000 deg/sec^2, d. Electrogoniometer output corresponding to (b)

The raw data obtained from the sensor was extremely noisy due to the crude nature of the apparatus used in testing (shown by the red curve in Figure 67). In order to obtain a cleaner signal a third order Butterworth low pass filter was used, with a sampling frequency of 1000 Hz with a maximum cut-off at 10 Hz (filtered signal shown in blue). Angular displacement was measured using the resistance based electrogoniometer. Since the quantity applied to each sensor in the considered application is a force/torque, these curves were all parameterized based on fixed peak angular acceleration. This data was then used to obtain rates of change for voltage, and corresponding rates of change of angle. The derivatives were calculated using the following numerical schemes (Equation 3):

First Point	Interior	End Point
$\frac{\delta Y}{\delta t} \cong \frac{(Y_2 - Y_1)}{\Delta t}$	$\frac{\delta Y_j}{\delta t} \cong \frac{1}{2\Delta t}(Y_{j+1} - Y_{j-1})$	$\frac{\delta Y_{end}}{\delta t} \cong \frac{(Y_{end} - Y_{end-1})}{\Delta t}$
First Order Accurate	Second Order Accurate	First Order Accurate
Taylor Error ≈ O (Δt)	Taylor Error ≈ O (Δt^2)	Taylor Error ≈ O (Δt)
Δt =1E-3 s	Δt^2 = 1E-6 s^2	Δt =1E-3 s

Equation 3. Numerical scheme for sensor output derivative: first point, interior points and end point equations.

Where Y is the quantity for which the derivative was calculated. For the lookup table, processed time rates of change for voltages with the corresponding angular time rates of change were stored for already quantified signals. It can be seen from Figure 67 that the

level of noise in the signal was much larger than error introduced due to the numerical approximation; therefore the approximation is reasonably accurate.

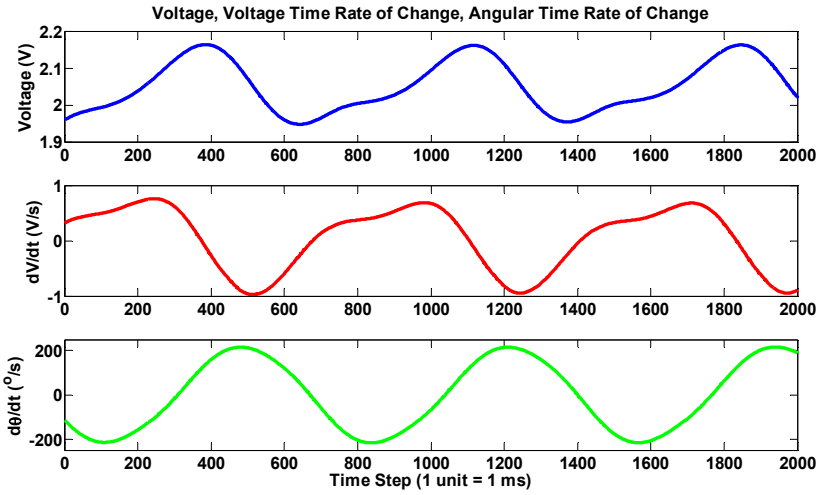

Figure 68. Voltage output (top) with corresponding time rate of change of voltage (center) and corresponding time rate of change of angle (right) from lookup table for 0-60 degree cyclic angular deflections at an acceleration rate of 1000 °/sec2.

Due to the small time step the minor variations present even in the filtered signal were greatly amplified and resulted in a large spread of data for calculated gradients, however the data was smoothed (Figure 68). This stresses the need of a setup involving smaller levels of noise and hence a smoother filtered output. For the first test case this data was smoothed using a local regression with weighted linear least squares and a 2^{nd} degree polynomial model, the method assigns zero weight to data outside six mean absolute deviations. After this smoothing process the derivative information for all the acceleration curves was stored in a lookup table. After building the lookup table random sensor signals could be compared in a recognition process to track the angular information. The recognition process involves reading in a specified signal. The underlying principle is that any input signal can be broken up into a number of discrete portions, which if taken to be small enough, can be modeled as segments of constant

acceleration. Rates of change along these localized curves can then be calculated and matched with already existing values of rates of change of voltage from the lookup table file. Once identified the corresponding rates of change of angles can be read directly from the file, and used to calculate the current position.

An input signal with a peak acceleration of 3000°/sec^2 was selected as the test case. Even though the acceleration was uniform the span was chosen from 0° to 30° which was half of that of the span for the data used to build the lookup table. This allowed for different rates of change at different absolute angle values than those already stored in the lookup table. Shown below in Figure 69 is the actual angular displacement as measured by the electrogoniometer along with corresponding voltage output across the sensor.

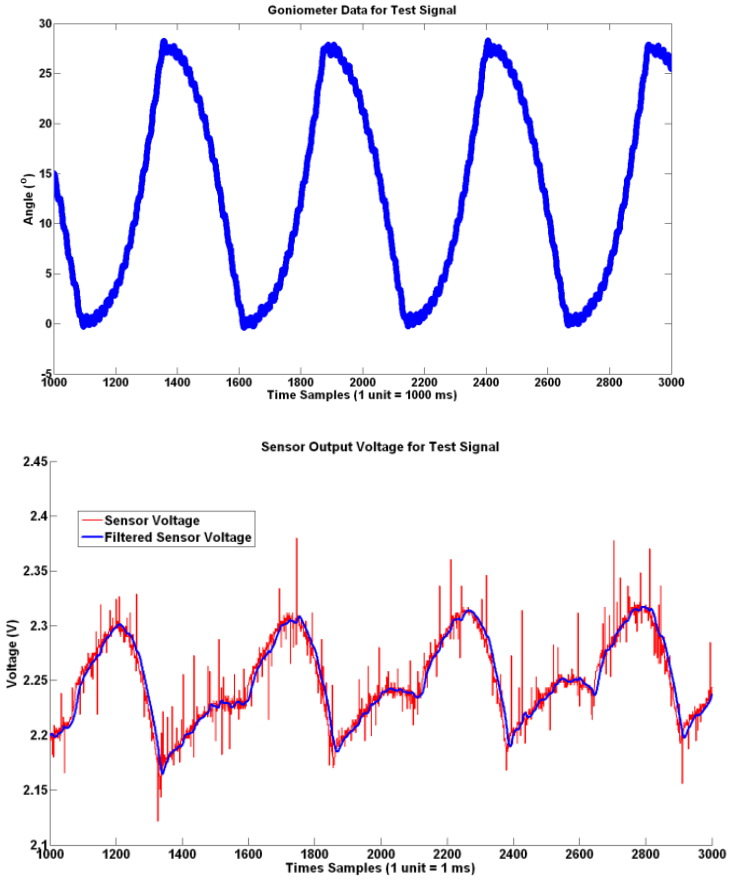

Figure 69. Goniometer Data with Corresponding Sensor Output Voltage-test signal.

Even after filtering there was too much fluctuation in the data obtained from the sensor due to noise associated with the actuating mechanism. The filtered signal was therefore conditioned using the same smoothing technique that was applied to the lookup table data before storage with a slight variation in the smoothing factor. This resulted in the curve along which the derivatives were much smoother.

The input voltage had to be smoothed not only because of the noise associated with it, but also because the very sharp change associated with the crests creates problems if there are minor fluctuations in the data available around that region. The calculated derivatives were smoothed for the same reason. As seen from Figure 70 there are several regions where values change sharply and small fluctuations in sensor voltage due to noise create very large errors in numerical approximations of the derivative.

The rate of change of voltage information was then compared through all the values available in the database, and the closest match was determined. Stored in the database along with rate of change of voltage is the corresponding rate of change of angle which was then read. By this method a complete time history for angular velocity is obtained, which is then again smoothed using the same algorithm with appropriate smoothing criteria. This criterion is again based on maximum limits of torque (angular acceleration) that the human foot can endure; this was implemented in the algorithm.

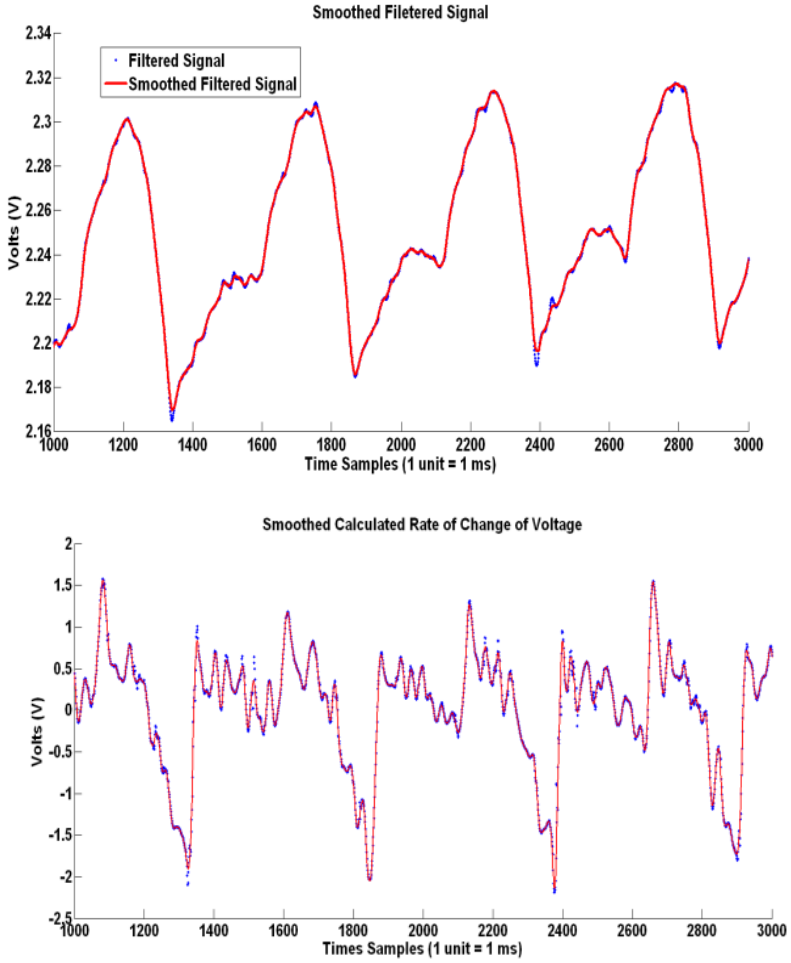

Figure 70. Smoothing of Input Voltage and Calculated Gradients.

Finally the smoother velocities can be integrated numerically using the simple algorithm (Equation 4):

$$d\theta_i = \frac{d\theta_i}{dt} * \Delta t \qquad \theta_{i+1} = \theta_i + d\theta_i$$

Equation 4. Algorithm for numerical integation of velocity.

The update in time for the angular displacement is calculated as the angular displacement at the previous state, plus the change in angle due to velocity (angular velocity). The contribution from the accelerative term is ignored in the displacement calculation due to the fact that it is 3 orders of magnitude smaller due to the scaling with Δt^2 and can be ignored for small acceleration values as those applied during this particular test. For the more general case a corrective term due to acceleration must be added resulting in the following update (Equation 5):

$$d\theta_i = \frac{d\theta_i}{dt} * \Delta t + \frac{1}{2}\frac{d^2\theta_i}{dt^2} * (\Delta t)^2$$

Equation 5. Acceleration update algorithm.

In order to use the above update, acceleration information for every time step must be computed using rates of change of velocities. One of the other reasons this term was omitted for the test case was that due to the nature of the available testing equipment, the data obtained was noisy; application of filters alleviated the problem to some extent, yet did not completely solve it. Due to this noise, calculation of higher order numerical derivatives was not meaningful since minor fluctuations due to noise are seen as very large changes in these higher order derivatives, due to the small time step used in calculation. However with the incorporation of filters before the digitization of the signal the motor-noise problem will be reduced to insignificant levels. It was also observed that the hinge would sometimes experience non-negligible amounts of coulomb friction against the floor due to imperfections in construction of the floor, and swelling of the polar scale paper which was used as a scale to calibrate the electrogoniometer. This

friction created ripples in an otherwise smooth displacement curve, and would appear as large fluctuations in the calculations of higher order derivatives.

The raw voltage data from the sensor is shown in Figure 71. The raw voltage was filtered and smoothed, this is shown in the same figure. The smoothed sensor voltage was then used to calculate the velocities (or first rates of change). These two smoothing procedures went through an iterative optimization of parameters to minimize the distance between the angle produced by the sensor voltage processing and the actual angle, measured by the electrogoniometer.

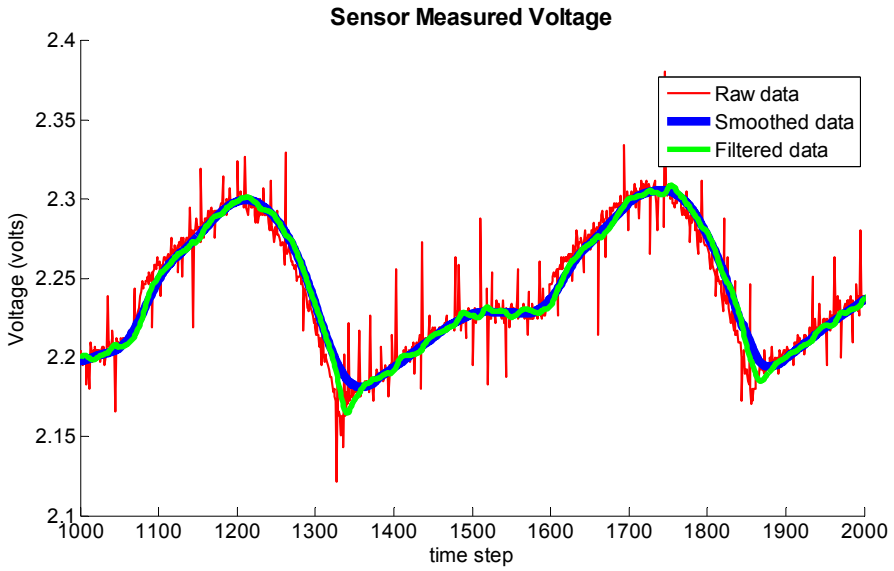

Figure 71. Raw, smoothed and filtered sensor voltage.

One of the iterations in the process of in tracking a 30° sinusoidal is shown in Figure 72 below. Another iteration of this process is shown in Figure 73.

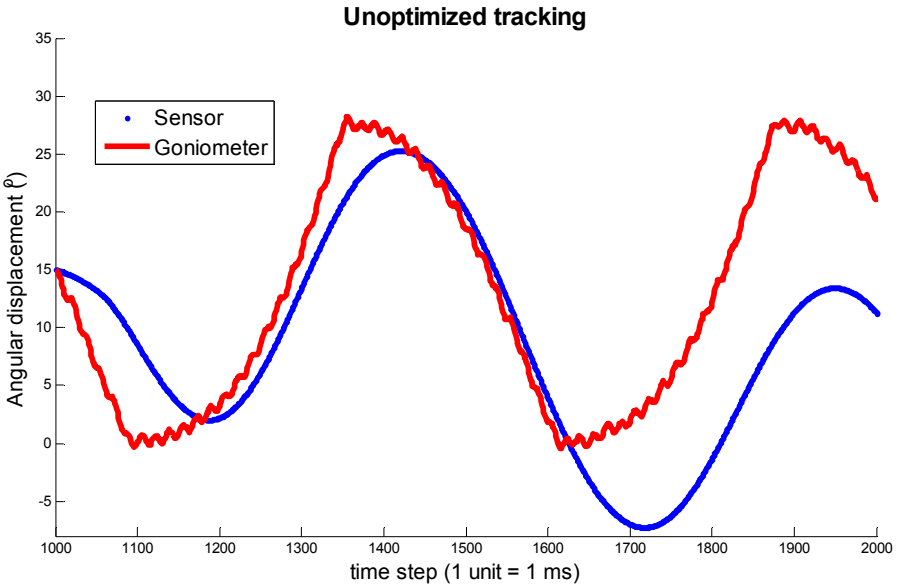

Figure 72. Unoptimized tracking of a 30° angle at 3000 °/sec2

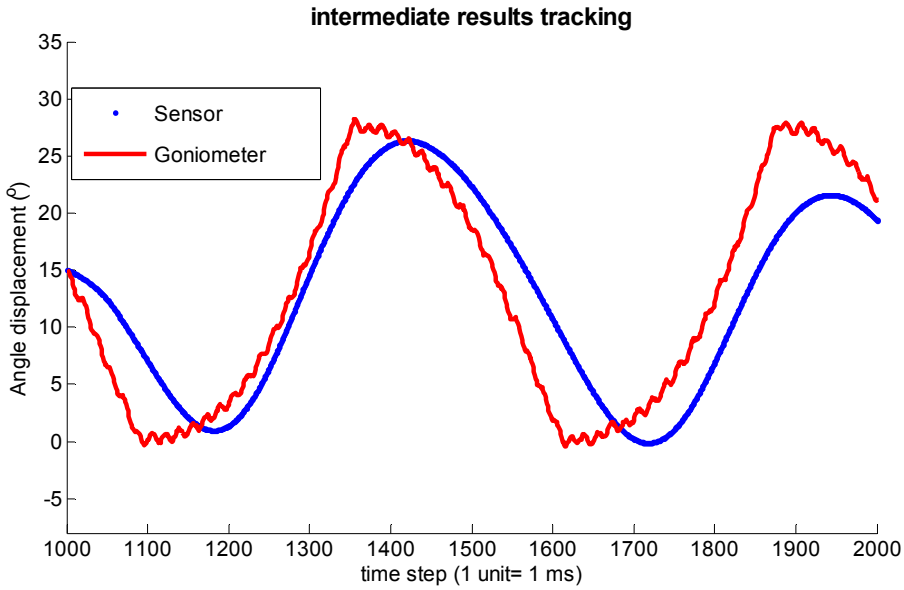

Figure 73. Intermediate tracking Results

An optimized angle tracking was obtained after several iterations of parameter modifications, the optimized angle is shown in Figure 74.

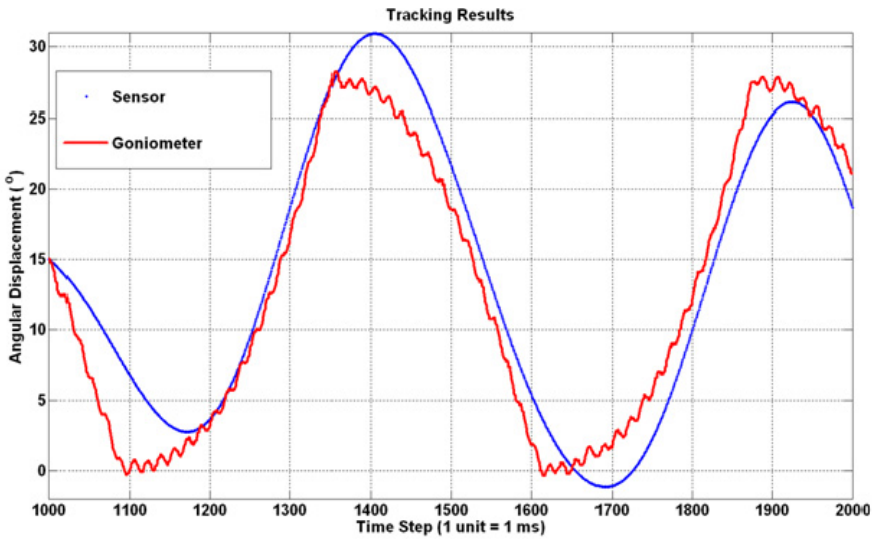

Figure 74. Optimized tracking

The suggested algorithm does a reasonable job of predicting angle changes in comparison to the electrogoniometer. The slight phase shift in the blue signal is an artifact of the processing algorithm. The signal is slightly displaced during the filtering process performed during data acquisition via Lab View. However since this method is dependent on the initial condition, and builds upon information from previous time steps, any errors quickly accumulate making the results inaccurate if the program is required to process over long periods of time. It is difficult to quantify what percent of the error in the results comes from the calculations, i.e. the numerical approximations and noise removal, making it hard to quantify the accuracy of the sensor. However on a quantitative basis it can be said that it is within 2-3° of the actual angle. Initially we see an over prediction in angle which quickly dampens out. Over the next cycle we see that the result is slightly under predicted. The over prediction that occurs during time steps n = 1000-1200 is partially because of the lag introduced during filtering. The results then follow the actual curve fairly closely up until time step n = 1325 where they overshoot the actual displacement by about 1° at n = 1400. From there on up until n = 1650 the results are

within 1-2° of the actual angles. The error during this part of the cycle appears to be more due to phase shift in the signal due to filtering. Same is true for n = 1650 to n = 1850. After this point the error in prediction occurs mainly due to accumulation of numerical error in calculation of derivatives. At n = 1900 the peak is under predicted by about 4°.

3.2.6 Real-Time Monitoring and Algorithm Improvement

The data shown in the above figures in section 3.2.5 was acquired using NI Lab View. Acquired data was then filtered and processed using MATLAB. The runtimes associated with the acquisition and initial filtering are on the order of less than 1 ms and therefore can be ignored. The CPU runtime for the entire algorithm (processing code) is about 500 milliseconds, for a total of 501 total runtime. The integration of the MATLAB code in Lab View will reduce this runtime, since it needs only to be compiled once. This will further reduce the runtime down to a few milliseconds (< 20) and hence any signal can be monitored with a delay less than 20 milliseconds. At the frequencies of motion this introduces a negligible phase delay.

The other major consideration is the improvement of the recognition technique. Right now the program is designed to calculate rates of change of voltage and compare them to existing ones and then looking for the "best" match and the corresponding angular velocity. For reasons mentioned earlier the algorithm is currently designed to work with low values of accelerations. One major improvement would be to establish uniqueness to values in the table and the incorporation of the accelerative term in determining the angle

update. Although this not a computational challenge the task is not simple and requires a setup that has much smaller levels of signal noise. This will require isolation or at least distancing of the actuating motor from the sensor itself. A mechanical solution is one of the possibilities and currently the use of a mechanical extension of length greater than 1 m is being investigated. This will put the actuator at a much greater distance from the setup than it already is. Also the implementation of an analog filter between the sensor and the acquisition system is being considered, the major consideration here would be the shifting effects of such electronics being used to perform the filtering.

Apart from the addition of the acceleration term there are several methods of improving this algorithm, some of which are being currently investigated. For instance, each of the smoothing processes had parameters that were tuned to this particular problem. This tuning had to be performed manually. Work is being done on developing an algorithm that is capable of automatically tuning these parameters by performing a minimization of difference residuals based on pre-existing data which will be added to the lookup table. Although this imparts more flexibility and robustness to the system it also increases run-time and therefore the actual implementation of such a program for real-time monitoring and integration with a controller is still questionable, in case an actuation mechanism needed to be incorporated. Another major improvement underway is the addition of the ability to interpolate between lookup table data points. That way instead of using the closest match the program will be able to take the two closest data points and interpolate for the required solution between those points. The actual model in which this interpolation will be based is yet to be determined. Based on the accuracy of the

interpolation model the lookup table file size may be considerably reduced. As of now the file is a few hundred kilobytes, which is not too large. However a smaller file will allow for quicker run-times. The addition of the interpolation feature will cause an increase in run-time. A trade study in order to determine the exact trade-off is also underway.

A different methodology for determining the "best" match rate of change will also be considered. Instead of simply comparing values for rates of change, the algorithm will be designed so that it first determines the best matching curves based on the acceleration the hinge is undergoing. It will then look for the closest points based on rate of change of voltage and interpolate between them. The corresponding angular information will then be calculated for the new result. The structure for the proposed algorithm is shown below in the flow diagram (Figure 75).

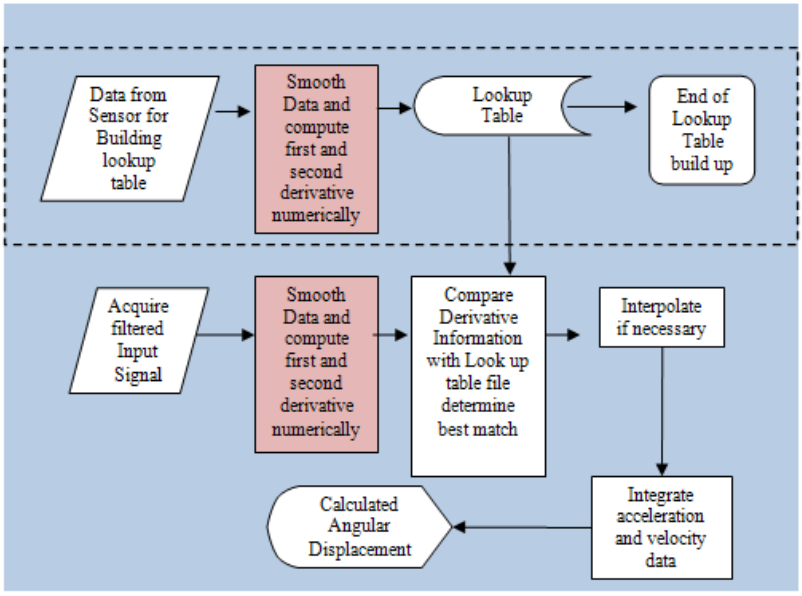

Figure 75. Flow Diagram for Proposed Algorithm for Voltage and Angle (Lookup table generation cycle is marked with a dotted box).

3.2.7 Sensorized socks- A pilot study

A pilot study to assess the potential for using this sensing fabric in quantifying foot motion using socks was conducted. Each sock was fitted to a mold and then the masking procedure took place. The locations of the sensors were different from one sock to the other and were printed on anatomic areas estimated to undergo larger strains. These locations were found to be around the main foot joints (metatarsophalangeal and ankle) and other key locations. Commercially available socks were chosen for printing on the conductive elastomer sensors. The substrates were chosen on the basis of signal smoothness and best fit to the foot and therefore better compliance. The right sock of each pair was used. The first sock was made of substrate 9 material and the second sock was made of substrate 5 material (Figure 76). These were selected because they were based on substrates of high resilience (Nylon) enabling better sensor output characteristics. These substrates also had the smallest fibers and were therefore much more comfortable for the human subject. A 3D mold for the sock was used to emulate the pre-strain that a foot would generate in the stretchable fabric in order to print on the sensors.

The sensors were connected to the electrical leads by using conductive thread which had a resistance of about 82 ohms/ft and a composition of 87% C and 13% Ag. The effects of salt and water were observed by placing the thread in different concentrations of salt over a period of two days. The resistance of the thread showed to be in the vicinity of 0.5 MΩ for concentrations of 15% and up over a length of 6cm. The thread was sown into the

sock as a conductive path which ended on the sock cuff. From this point the threads were interfaced with leads (Figure 77) which took the data to the voltage divider circuit, then to the data acquisition and into the computer program. The sensors were set in a basic configuration of one channel per sensor for maximum resolution.

Figure 76. Sensorized socks made from substrates 9 (white) and 5 (dark)

Figure 77. Acquisition setup for sensorized sock.

The following graphs correspond to the response of substrate 5 (96% Tactel nylon) which has three sensors: one on the foot joint (heel), one on the metatarsophalangeal joint and

one on the ankle joint. Figure 78 part a. shows the time domain response during dorsiflexion of the foot, and part b. of the same figure shows the frequency domain of this type of motion. It was possible to extract the frequency at which the foot was being dorsiflexed using the resistance signals given by the prototype sensorized socks.

a.

b.

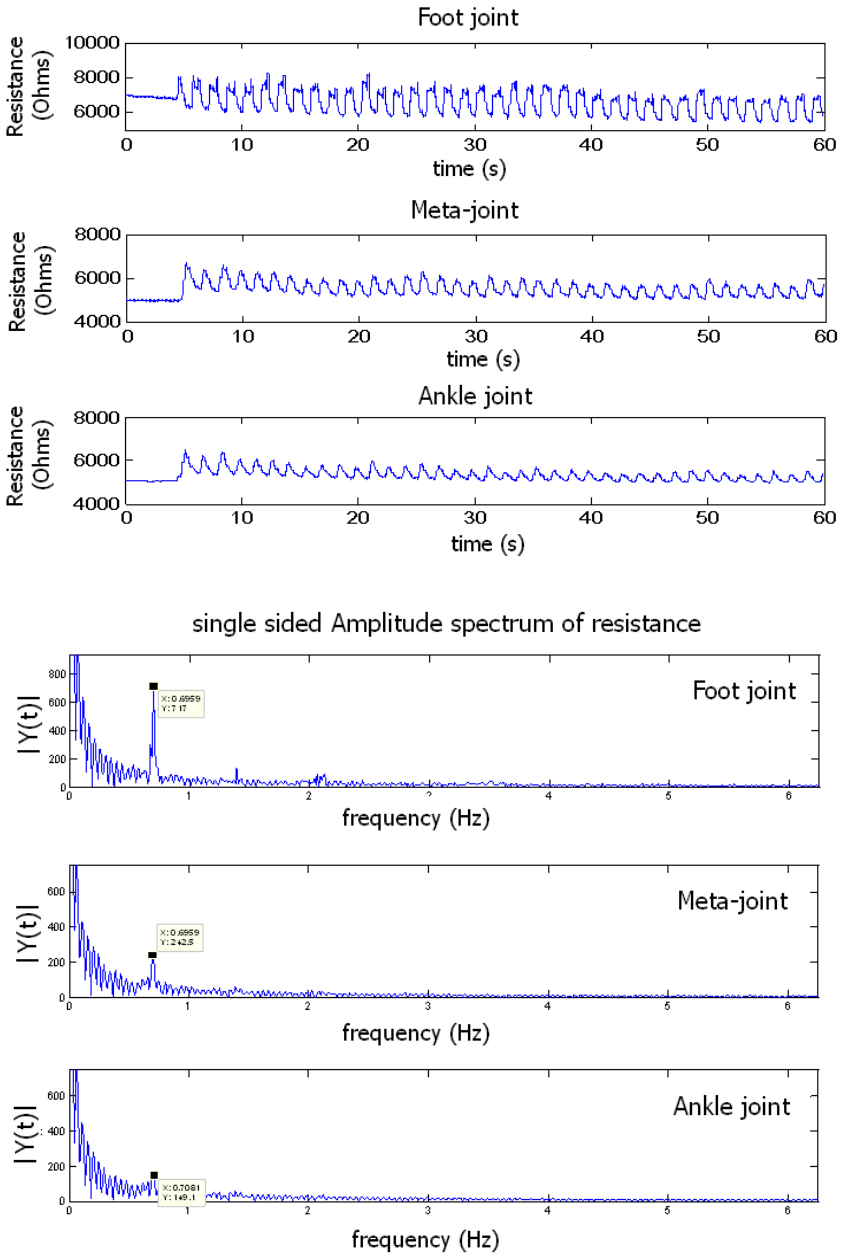

Figure 78. Data from pilot sock sensors: a. Resistance vs time and b. Frequency domain

Other sock prototypes with slightly larger amounts of sensor material (to reduce value of resistance) were built on other Nylon based substrates. However, it was found that the stiffness of the sensors increased to the extent that the fabric substrate no longer produced enough strain to cause measurable changes in resistance. This stiffening effect was also fostered by an extended exposure to heat, which was used to cure an additional amount of sensor material placed on the edges to join the thread with the sensor. Therefore there is a tradeoff between high resistance values and sensitivity to strain.

Another sock prototype was built using polypyrrole based sensors or PI conjugated sensors (12). With this material, the resistance was linear and did not present drift. Three sensors were glued onto the heel (center, left and right) on the external side, never in contact with the skin. Similarly, the conduction lines consisted of sewn conductive thread. The thread which remained un-sewn was insulated by fabric tubes, ending in a lead. The leads were then connected to the data acquisition. This sock can be seen in Figure 79.

Figure 79. PI-coated fabric sensors on sock

A calibration file was collected by flexing the foot in the saggital plane repeatedly at different angles and speeds. Angular data was simultaneously acquired using a mechanical goniometer. The calibration file consisted then of four sets of data in time; three sensors and the saggital angle, in this case the angle between the two foot segments according to the simplest foot model. A test run file was collected and a different algorithm was used to correlate sensor output to angles (Figure 80). Each run point was compared to each calibration point by calculating the differences between them which were used to retrieve the previously calibrated angular data. The values from the three sensors were averaged to find the angles at each time step.

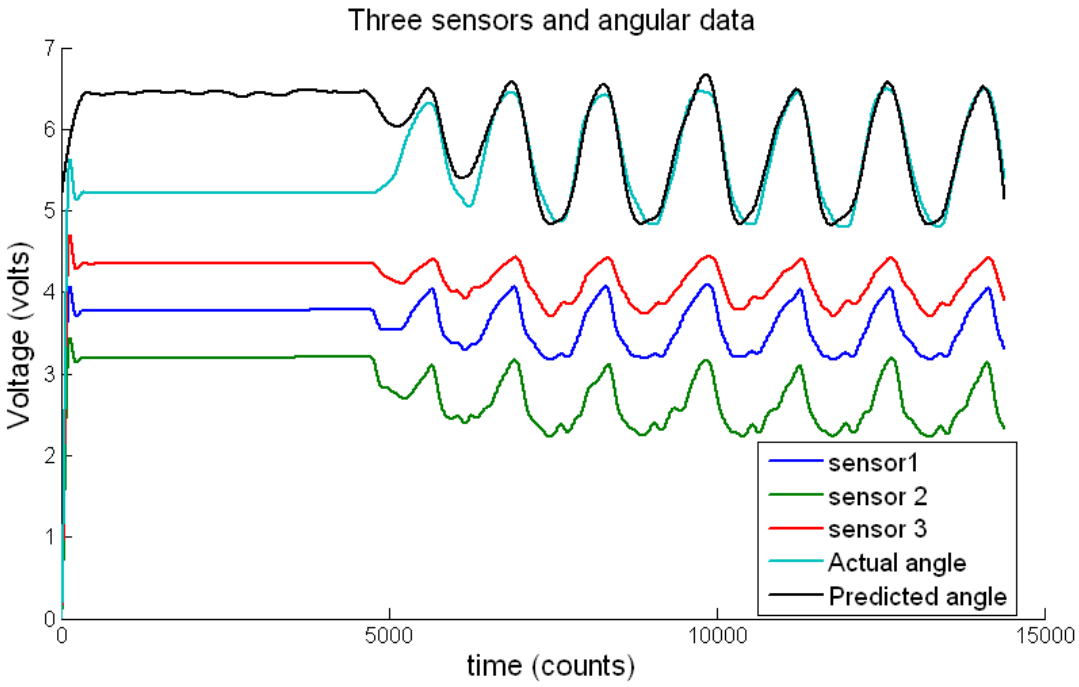

Figure 80. Pi-coated fabric three sensor output and relative angle, when foot is dorsiflexed cyclically

In Figure 80, the green curve represents the actual angle and the black one represents the angle estimation derived through sensor values with the new algorithm. It can be seen that the algorithm was able to give a close estimate to the actual angle.

3.2.8 Wireless Integration and Real Time Processing

The ultimate goal of this study is to integrate these sensors for foot posture monitoring applications. The integration of a wireless transmitter allows minimum intrusion while making measurements. Conventional techniques include attaching several long leads to power the sensor and read data from but the method becomes very intrusive and the movement of the foot could possibly be affected by the presence of all the wired connectors. It was therefore required that there be some method of wireless data transmission. Also, the main purpose of using these types of fabric based sensors is to "transform" certain sections of the fabric into sensors, allowing a conventional garment to become a functional sensor data transmitter. The wireless transmitter is mounted on a board of nearly its size that contains a power voltage regulator. Powering the sensor and the wireless transmitter was achieved using a small battery. This was not an issue since powerful compact batteries are abundant and cheap. The requirements on the wireless radio were however a bit more challenging. The radio had to be small enough to be comfortably attached to the leg, while powerful enough to transmit several streams of data in real-time with minimal lag and a per channel frequency of at least 40 Hz (5 to 10 times above the Nyquist frequency associated with digital sampling of human locomotion). The radios also had to have minimal power consumption since they would be operating of a small battery. The method also had to be cost effective to fit the budget restrictions imposed on the project.

The solution was found in the form of 2.4 GHz X-Bee commercial digital radios manufactured by Digi (Figure 81). The radios have a power consumption of 100 mW when operating and transmitting on all channels, with a line of sight transmission maximum of 1600 m. They allow for simultaneous transmission of four channels to a maximum of 1000 Hz, hence allowing a transmission rate of 250 samples per second per channel. Although this is a little less than what it would be required to over sample a 40 Hz load, it was sufficiently above the Nyquist criteria for good time domain representation. Two radios would easily allow for the required sample rate (2 sensors per radio) and would not be hard to accommodate given the small size of the devices. Shown below in the image are the transmitter and receiver with dimensions.

The transmitter unit is 28 mm x 28 mm x 5 mm and can comfortably be tied across any portion of the lower leg above the foot. The device weighs less than 3 grams so weight is not an issue at all. The receiving unit can talk to 16 transmitters simultaneously allowing for simultaneous communications from 64 sensors. For the specific application only four sensors are required. Although resolution is not an issue, it is on the order of 1mV, there are problems associated with the implementation of this wireless device. The biggest one is the fact that the line of data shown above requires parsing (separating signal information from other frame data). This parsing is separate from the filtering process and not only complicates the filtering process but also creates a delay since there is CPU time associated with it. The reason it complicates the filtering process is that a continuous filter expects data at fixed sampling rate.

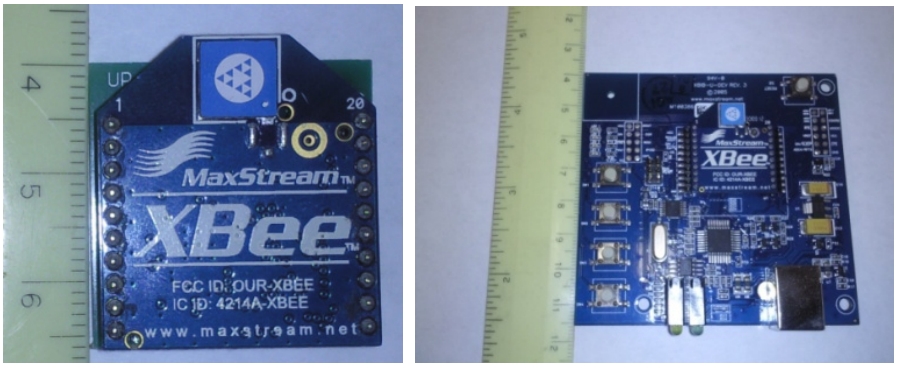

Figure 81. Wireless Transmitter and Receiving Unit.

The processing program is setup entirely in Lab View and involves a loop which reads the serial port continuously at intervals that are determined by the overall processing time. After the first scan the obtained data is sent for processing and once the processing is complete the voltage value is stored in a buffer, after which the second scan is initiated. Due to the time consumed by processing there is a delay between scans dependant on the processing time involved. Therefore at the second scan the read program may, or may not find any data dependant on whether or not the processing time was long enough to allow enough time between runs to acquire data being received at the transmission frequency. On the other hand if the processing time is too high chances are that data will be missed. Currently it is small enough that no data is missed, however with the implementation of more complicated algorithms this might increase significantly. However at present there are intervals in which no data is received and the program has to throw such samples out. Real-time filtering thus becomes complicated since the true sampling frequency is determined by how long it takes the computer to process the data before it can be filtered. In order to get around this problem data is stored in a buffer and filtered in samples of 5000, which creates a 5 second lag between measurement and display. The solution to

this problem is parallelizing the two branches of the program such that the acquisition process runs in parallel to the data processing loop. This will not only guarantee a time accurate spacing of samples, but will also be useful in the future when a complicated more time consuming algorithm is used. The following graph (Figure 82) shows sensor data acquired wirelessly at 1000 Hz for a hinge wing gyrating 75 degrees at a constant velocity of 100 °/sec for demonstration purposes to avoid any data loss from the possible ones mentioned before. The filtering and smoothing curves are shown. The filtering shows an induced lag, however, the smoothed curve cannot be implemented in a straightforward manner in real-time. Work in this area will continue to be done to enhance the data transmission characteristics.

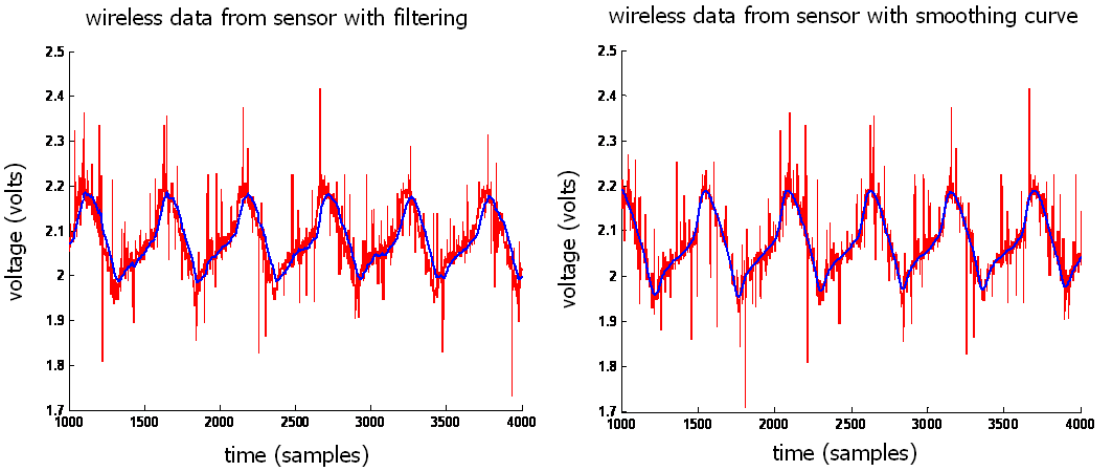

Figure 82. Filtered (left) and smoothed (right) data from sensor flexed by motor-hinge wing and acquired with wireless sensor.

Finally, the transmission of wireless data using fabric sensors on sock was achieved using the PI-conjugated fabric sensors and a transmitter strapped to the leg. The system was completely portable, comfortable and unobtrusive. Figure 83 shows the sock and portable case which contains a small circuit, board, battery and wireless transmitter. The results from a trial run corresponding to walking motion can be seen in Figure 84. The noise was

substantially reduced compared to the hinge experiment due to the absence of the motor. A lowpass filter was implemented in Labview and was applied to the acquisition of these signals. Figure 84 also shows that every sensor produces a regular repetitive pattern, with a different signal shape. These characteristics enable this system not only to obtain angles, but also to characterize human motion.

Figure 83. Wireless sensorized sock with PI-coated sensors

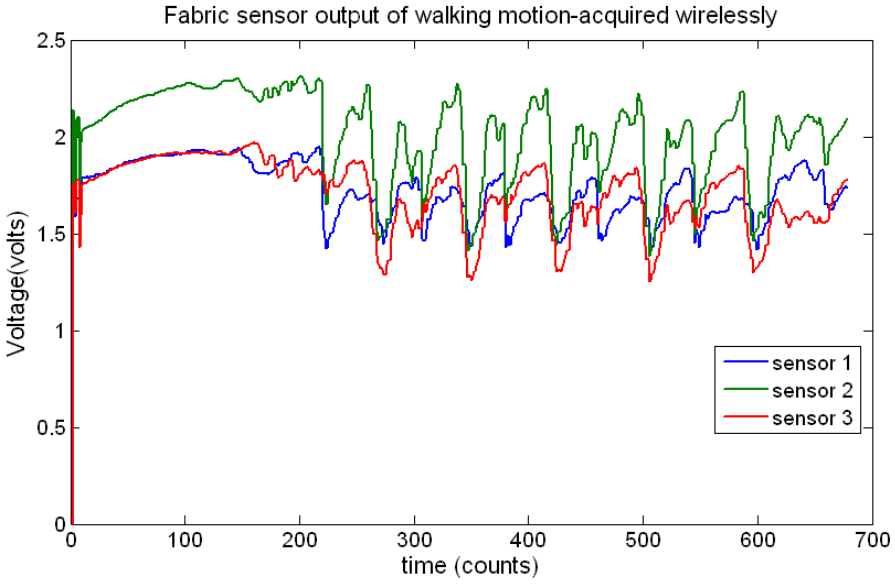

Figure 84. Wireless sock data corresponding to three fabric sensors during walking motion.

Chapter 4: Summary and Conclusions

This thesis presents an investigation into strategies for sensorizing fabrics for potential uses in monitoring of foot motion. The first chapter of this thesis presents a review of the state of the art in e-textiles and gait analysis. Chapter 2 then presents the process which was followed to find the sensor material as well as a study of different substrates and connection materials. From those studies, the carbon based polymer was identified as being most suitable for the intended application. A set of experiments were then conducted with this sensor material and are presented with their corresponding results in Chapter 3. These experiments include; estimating sensor gauge factors of carbon-based polymer on different substrates, finding an angle correlation based on the sensor output, and integrating the sensors into an actual sock. Wireless transmission of the signals produced by the carbon based and PI-coated sensors was achieved. Finally, a fully portable sensorized sock was built and tested, demonstrating the ability to capture foot position and becoming a new tool for gait analysis.

Specific findings of this thesis include:

- Linear dependence of resistance with length of sensor.
- Gauge factors are affected by substrate choice.
- Gauge factor decreases with time for every substrate.
- Gauge factor decreases with length of sensor.
- Pre-strained sensors produce increased sensor sensitivity.
- Sensor drift was present regardless of substrate.
- Nylon and Polyester fabrics showed best response to sinusoidal inputs.
- Fabric paints and glues, non-conductive fabric, silicones, are useful for insulation.

- Conductive thread, conductive fabric, inks, paints and polymers can be used as conduction lines or conductive connections.
- Substrate characteristics such as tightness of stitch, fiber resilience, and yarn twist affect the sensor characteristics.
- A first sock prototype using carbon-based sensors showed ability to track foot flexing frequency and enabling the tracking of angles.
- A database or lookup table of numerical derivatives of associated sensor voltage allowed angle correlation using a carbon-based sensor strip on a hinge mechanism.
- A PI-coated sensor sock prototype showed the ability to track the foot ankle angle on the saggital plane.
- An averaging algorithm based on smallest differences between calibrated and test voltages allowed to find foot angles using the PI-coated sock.
- A wireless sensorized sock was able to transmit walking motion with good signal characteristics and low noise.

The carbon conductive polymer was applied to 10 different substrates. Resistance linearity with length was insensitive to substrate. The gauge factor was obtained for all the substrates at 3 different times after the strain was applied. It was observed that the gauge factor decreases with time regardless of substrate. The substrate has an impact over the gauge factor. Gauge factors were measured as a function of sample length and pre-strain. It was found that shorter sensors had a lower gauge factor. Pre-strained sensors produced larger gauge factors. The carbon based sensors present a resistance drift behavior which does not seem to be affected by the substrates they are applied on, it was present in all the substrates. Nylon and polyester fabrics showed a better response to sinusoidal inputs. These fibers have added intrinsic resilience which causes smoother sinusoidal reproducibility. Thinner and denser fibers produced a higher linear resistance

and lower gauge factors. Thicker and coarser fiber fabrics allowed more conductive material to be adhered and therefore showed a lower linear resistance; that is, they were overall more conductive, though they had lower gauge factors. Higher gauge factors were obtained in fabrics with a bulky consistency.

A stretch-bend test was conducted on a polymer coated fabric sensor strip for the possible correlation of angles and sensor output. Sensor output is sensitive to the acceleration of the hinge wing that stretches the sensor. After the sensor voltage output was smoothed and filtered a scheme for data processing was implemented and tested. Numerical derivatives of the sensor output voltages were calculated as well as for the angular displacement measured by an electrogoniometer. A database was built by storing the time rates of change of angle and sensor voltage. This database serves as a lookup table for the identification or recognition of angles associated to random sensor voltage inputs. The look up table collected for a test case consisted of data collected for accelerations from 1000 to 3000 °/sec^2 and for an angle range of 0 to 60 degrees. The test case was an input signal with angle range 0 to 30 degrees and an acceleration of 3000 °/sec^2. After applying the smoothing schemes, the sensor output was compared to the lookup table, which outputs rates of change of voltage and then by integrating the angle was obtained.

The algorithm that was used showed good tracking ability of the original angle of 30 degrees. Since the overall purpose of this project was to implement this processing scheme to sensors on a sock, wireless capabilities were implemented for ease of data take and reduction of motion hindrance. Wireless transmission of sensor data from the hinge

sensor was achieved, and it presents approachable challenges to be completely implemented in real time due to delays in all the data interfaces. The hinge test as an emulation of an ankle joint showed that these sensors can be used to track human joint angles with the algorithm described above, with the advantage of having executable real time processing algorithms.

A proof of concept implementation of the carbon-based fabric sensors for distinguishing motion during dorsiflexion was showed. The foot flexing frequency was obtained from the signals using an FFT. Another sock was sensorized using PI-coated fabric. It showed to have linear output properties and almost no drift. It was calibrated using a mechanical goniometer and it was able to predict the saggital ankle angles spanned by the foot. A completely wireless sensorized sock was implemented using PI-coated sensors, therefore producing a portable foot monitoring system. Wireless transmission of data from a sensorized sock was achieved for a walking motion test run. The test showed desirable signal characteristics for good processing results. Many studies of human motion can be performed with these portable smart fabric sensors, including that of obtaining foot angles (out of plane motion), and human gait characterization.

Future work

Many improvements can be made with respect to the different aspects of the smart fabric sensors. One of them is to implement the post-processing algorithms of signals in real time. For the sock with carbon polymer sensors, the real time processing would be more involved than the one for the PI-coated sock. This is due to the drift present in the carbon

sensing material. However, the polymer can be considered to have an advantage in terms of the fabric integration properties. Another aspect entails modifying or enhancing sensing materials and substrates. One could investigate the possible dependency of sensor response with several fabric parameters and/or possibly optimize the coating. The electrical connections could also be modified, such as adapting them to be less fragile. In terms of the wireless features, a smaller transmitter would be desirable to enhance portability and robustness. Optimization of the number of sensors and the sensor locations on the foot would constitute another improvement. More types of foot motion could be analyzed and characterized with the sensorized sock, as well as a full gait study, i.e. walking, striding, and running under different gait paramenters such as speed, stride length, etc., and anthropometric data. Specialized software should also be developed for the interpretation and processing of the resistance signals from the sensors.

Other issues need to be addressed as well in future studies; the effects of the environment, including moisture and salt on the sensor strip, washability, wear and tear effects, fabric water absorption, individual sensor calibration, insulation of the conductive thread connections, localized pressure detection and shoe effects.

In terms of future associated studies, there are many paths that could be explored to enhance or expand the current study. For instance, a study could be conducted on new sensor materials which would enable less computationally expensive real-time algorithms. The fabric could also be intrinsically modified by introducing new fibers to adjust or change targeted properties. More compact and flexible elements could be

developed or adapted; compact transmitters, flexible electronic boards and circuits, and better insulated conduction lines. More flexible electronics technologies could also be implemented in the socks enhancing the robustness of the system. Other associated research paths may include: enhanced signals processing schemes for biomechanical data from fabric sensors, pattern recognition algorithms applied to the signals coming from the sensors, and neural networks schemes, in the case of a study with an increased number of sensors.

Appendices

Appendix A. Smart Fabrics and e-textiles

A.1 E-textiles: Available technologies to make fabrics smart (state of the art)

This section intends to provide a broad view of the field, and within this framework indicate current benchmarks, textile techniques for circuitry and a few new technologies which could be incorporated or which can complement smart fabrics.

The field of smart fabrics is very broad and can be categorized in levels of sensor element integration with the fabrics. Fabric sensors may be made of conventional electronic materials or they can be made of adapted fabric constitutive components acting as electronic components, giving birth to intrinsically functional technologies. It is also important to mention that these technologies do not intend to replace the mainstream hard electronics, but to expand the functionality of fabrics as sensors and to provide a new environment of human-technology interaction. Electronic textiles are not expected to compete with high density- high performance electronic systems typified by current computer or telecommunications products. Rather, they are expected to have unique applications given their advantages of being flexible and being useful over large surface areas. They could demonstrate a significant cost improvement over other more conventional approaches. In general, smart fabrics should be regarded as complimentary in expanding interaction environments and in enabling technology features that could not

be carried in any other way. We will start an e-textiles overview at the lowest level of integration, i.e. adapted electronic components to fabrics.

A1.1E-textiles

This category is at the most superficial level of fabric-sensor integration. Most of the current applications of e-textiles intend to permeate daily human life with already available technology. Small electronic components are being customized in order to make them as portable and small as possible. They have become the next target in the race for complete human-technology integration. Current computer technologies are still far from being integrated naturally into man's life; a laptop though mobile, lacks flexibility in the way it interacts with the human being. The goal is to have a computer integrated into every aspect of life providing useful information and useful tools without hindering motion or interrupting normal activities.

Electronic textiles (e-textiles) are fabrics that have electronics and interconnections woven into them or superficially attached to them. They deal with all the electronic and computational technology that may be integrated into fabrics to give them special enabling characteristics. For example, a conventional resistor or diode can be sewn or attached to a fabric with special connections. This incorporation makes the electronic components less visible, more robustly integrated into the textile and less susceptible to the environment [58], producing not only an aesthetic compactness but a very functional portability. The rising interest in this technology stems in the physical flexibility and

large size characteristics of the e-textiles, which would be unachievable with conventional electronics fabrication methods. These characteristics and the ever evolving consumer needs of modern-life-demands have resulted in very creative and practical e-textiles solutions that continue to expand conceptually and technologically.

Electronic textiles evolved from the concept of wearable electronics and have also become an enabling technology for this field. As the electronics industry began to reduce the electrical components in size, the idea of wearing the computers themselves was progressively growing in feasibility. The size of the components also determined to what extent they could be mixed with fabrics. As within the broader field of Smart Fabrics, there are different levels of integration within the field of e-textiles and they depend on how fundamentally the electronic components are integrated with the fabric components. Therefore, a way to categorize the levels of integration depends on the structure of the fabrics themselves. Small textile components such as fibers are used to build large surface textiles, such as in wovens and knits. In these cases, fibers of different origins and compositions are mechanically tied in different patterns to build larger fibers called yarns, and these yarns are mechanically tied in different patterns and configurations as well to build fabrics.

E-textiles range from very superficially attached electronic components to substitution of fibers and yarns with sensing properties inserted into the normal fabric. These are reviewed in the following section.

A.1.2 E-textile applications on degree of fabric integration

The levels of sensing element integration are shown schematically in Figure 3. In this figure, wearable computers are at the lowest level of integration [59]. Any electronic portable device such as an iPod belong to this category. One good development in this area is the Zypad [60] (Figure 85), developed by Arcom Control Systems. It is a wrist computer with GPS, Wi-Fi and integrated PAN or bluetooth. It has a user friendly operating system; it can run on Windows or Linux. It has its main applications in logistics, emergency services, security, defense, healthcare, maintenance and any area that would benefit from large amounts of data when hands free are necessary. It has a total weight of 290 grams and a processor PXA270 processor at 400 MHz, a USB port, a color display with 128 MB ram. It can track whether the user has been motionless for a specified amount of time and has a tilt and reckoning system which detects the position of the user's arm. Other developments, shown in, include the famous wrist PDA's and the Timex Data Link [61] from the Timex Corporation which enables data transfer through a link with a computer. It has been certified by NASA for space travel and has been used already by astronauts in space missions. Golden-i, by the Kopin Corporation [19], is a Bluetooth headset that provides a 15-inch virtual display with a hands free, natural-speech-recognition interface for wireless remote control over a range of devices including mobile phones, PCs, company networks and wireless systems. It also includes a thumb optical mouse, a speaker and dual DSP noise cancelling microphones. The user can visualize the computer screen through the virtual eye display and can manipulate the cursor with the thumb mouse.

Zypad **Timex data link** **Golden-i**

Figure 85.Wearable Computers: a. Zypad [60], b. Timex data link [61], c. Golden-I [19]

However, these devices are still not incorporated into clothing. The next level of integration consists of electronic components surface mounted on clothing, forming a hybrid. This concept is illustrated in Figure 86 by the MIT Mithril project [20], which is a research platform that investigates the possible new-techniques of human-computer interaction for body-worn applications. It combines body-worn computation, sensing, and networking in a clothing integrated design. It uses one or more low-power computing cores; the Linux cores provide substantial on-body computation, signal processing and classification and networking resources to the user. They communicate with each other and the outside world through an Ethernet interface which is connected to a wireless bridge. It also includes a microcontroller-based data acquisition platform suitable for a wide range or low-bandwidth biomedical and environmental user sensing applications. Full VGA head-mount display, CCD cameras and other audio input/output devices can be connected through USB ports. Other sensors incorporated are a 3-axis accelerometer, an IR tag reader, a microphone, and a headphone driver. This approach though technologically appealing still has bulky and somewhat heavy components.

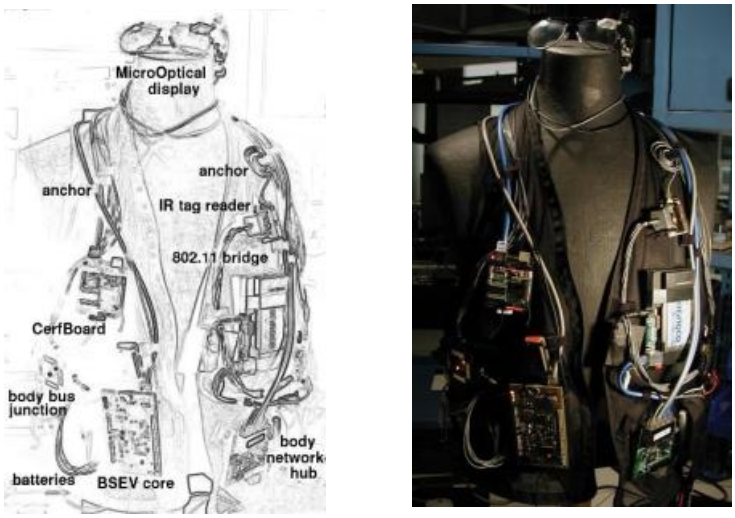

Figure 86. Surface Mounted electronics-'The MIThril project': a. Schematic, b. Prototype[20]

Electronic clothing hybrids are the following step in electronics integration into textiles and this is where the concept 'e-textiles' is born; all the electronic and textile technologies with equal or greater level of integration are usually considered e-textiles. In this category, the electronic elements are smaller, more portable and new technologies for circuitry realization appear. The major motivators for the development of e-textiles are; the leisure industry (civilian applications), army developments (aggregated values for defense applications) and research developments (mainly in the medical field). The LED shirt (Figure 87) is one clothing hybrid inspired by leisure applications [12]; a PDA remotely controls the display on the shirt so it displays messages at varying speeds. It consists of an array of LED components, each with fabric pads soldered to their leads and then sewn onto the cloth with conductive thread. All the interconnections are achieved using conductive thread. 'Communicating shirts' is also another implementation of this concept. IR transceivers on each shirt allow communication between the two shirts. Temperature sensors can also be sewn to create temperature responsive garments.

Figure 87. Electronic Clothing Hybrids: LED shirt [12]

Other leisure developments promise to permeate modern life. The row and column fabric keyboard (Figure 88) is a fabric switch matrix sewn from conducting and non-conducting fabric. The keyboard consists of two layers of highly conductive metallic organza (another level of integration) with a resistance of approximately 10 Ohm/meter and non-conducting rows separated but an insulating layer of nylon netting (also known as tulle). When pressed at the right point the two conducting layers make contact through spaces in the nylon netting and current flows from a row electrode to a column electrode. Gripper snaps are used to connect wires from the microcontroller to the organza. This is one of the new connection techniques that appear as a consequence of the needs of this new technology. The keyboard can be rolled up, and washed without affecting its electrical properties. The microcontroller is programmed to generate standard MIDI control information, allowing triggering of different notes at one strike. However, it is not pressure sensitive.

Another leisure application of interest is the musical Jacket (Figure 88) with an embroidered keypad. The musical jacket is an actual instrument that allows playing notes, chords, rhythms and accompaniment using any instrument in MIDI format. A fabric

keypad is embroidered into the jacket, amplifier speakers and batteries are also embedded. It uses a PIC microcontroller to perform capacitive measurements of connections to sewn electrodes on the denim surface. In this case, the measurement was implemented almost entirely in software as an exercise in developing electric field sensors with a minimum hardware. The electrode array is sewn in the pattern of a telephone keypad, with traces leading from the symbols to an array of connection pads intended to meet a conventional circuit board. Each electrode is sewn from a single continuous thread that crosses itself many times, leading to a multiplicity of intersections that create parallel resistances and increase the overall conductivity of the sewn circuit. The embroidered keypad uses capacitive sensing; the measured capacitance is compared to a threshold to distinguish contact events. This measurement is implemented using a single bidirectional digital I/O (input/output) pin per electrode and a large leakage resistor, which can be sewn in highly resistive yarn. Key contact events are outputted as a serial data stream by the microcontroller .The circuit board makes contact with the electrodes at the circular pad only at the bottom of the electrode pattern. This jacket can be also used for educational purposes.

The education field, though not a big leader in e-textiles but definitely a receiver of all the possible benefits of sensorized garments, awaits more smart fabric developments. One of the major efforts in this field comprises the introduction of electronic circuits at early ages [21]. These circuits are all fabric based and intend to enable novices to build their own computational devices by sewing stitchable components such as

microcontrollers, sensors, and actuators with conductive thread to fabric surfaces. It intends to engage different audiences in programming and electronics.

Fabric Keyboard **MIDI Jacket with capacitive fabric keyboard**

Figure 88. Electronic Hybrids: a. Fabric Keyboard, b. MIDI Jacket [12]

Electronic textile kits [15] provide an educational yet reachable strategy to introduce knowledge in technology and electronic circuit concepts without an apparent academic effort.

One of the educational applications is the electronic table cloth is a sensor surface that allows users to interact with a computer and with each other in the context of a social function. Attendees identified themselves to the system by setting their assigned ‘coaster tags’ on a swirling pattern (Figure 89). The coaster is in turn a capacitively coupled radio frequency identification (RFID) tag and is read by the tag reader in the table cloth when the user sets it on the swirling pattern and touches the fabric electrode on top of the coaster. The computer enters then into a dialog with the user through the appropriate fluorescent display. Therefore, an ordinary table is turned into a piece of interactive furniture in everyday life or in an educational environment. Wall dimmers have recently

entered the market and are a proposal for a new perception of the environment. They can be made of wool felt, conductive yarn, neoprene and acrylic.

Interactive table cloth **Wall dimmers**

Figure 89. E-textiles applications: a. Interactive table cloth, b. Wall dimmers [5].

The next level of integration of sensor capabilities into fabrics is the one that manages to incorporate conductive thread and non conductive thread in the intrinsic construction of the fiber or yarn. That is, not as an external conductive thread conduction line but one that is already intertwined into the bulk of the fabric. Silk organza, as was mentioned before provides a natural way of having conduction lines without having to sew them specifically for this purpose. In this case a silk thread is woven with a conductive thread [5], this fabric is known as metallic organza (Figure 90). In its primary form, it is a finely woven silk fabric with a thin gold helix wrapped around each thread that runs along the weft (fibers running horizontally) of the fabric. The warp (fibers running vertically) of this fabric consists of parallel silk threads. Through this warp, the weft is woven with a silk thread that has been wrapped in a metal foil helix. The metallic thread is prepared just like cloth-core telephone wire and is highly conductive, about 0.1 Ohm/cm. The fabric is anisotropically conductive because the conductors only run in one direction. The spacing between them also permits them to be individually addressed so that one single

strip can function as a ribbon cable. It is resistant to shear because the square cells turn into parallelograms when sheared, allowing the conductive lines to be parallel and separated at all times. The silk fiber core has a high tensile strength and can withstand high temperatures.

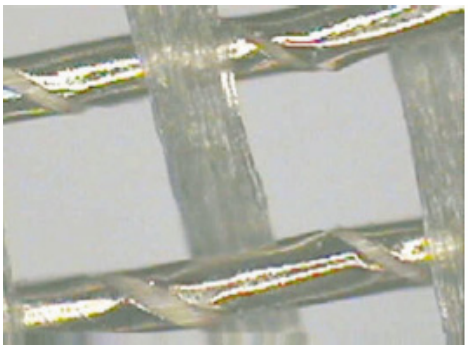

Figure 90. Metallic organza [5]

Finally, fabricating the actual components with the basic fabric constituents is at the deepest level of integration. This is found for example in photovoltaic fabric cells [8]. Konarka technologies performed a series of experiments that proved the feasibility of building a photovoltaic cell (Figure 91) using dye-sensitized titanium and electrolyte on a metal wire core. The approach taken was based on the sequential coating processes used in making fiber optics namely a fiber core or wire as the primary electrode, which is passed through a series of vertically aligned coating cups. Each of the cups contains a coating fluid that has a specific function in the photocell. A second wire, used as the counter electrode, is brought into the process prior to entering the final coating cup. This final cup has a photoploymerizable, transparent cladding which hardens when passed through a UV chamber. Upon exiting the UV chamber, the finished PV fiber is spooled.

When the fiber is exposed to visible radiation, it generates electrical power. Their efficiency is around 6% with an average value of 4 to 5%.

Other developments in this area use the same concept of dye sensitized solar cells (DSSC's) but using different dyes such as a photosensitized nanomatrix material [62]. In this case, the fiber core includes a flexible polymeric material e.g. polyethylene therepthalate, and flax, cotton, wool silk, nylon and/or combinations of these. The photosensitized nanomaterial includes nanoparticles or a heterojunction composite material. The photosensitizing agent may be a dye or an organic molecule such as xanthine, cyanine, merocyanine, pthalocyanine, or pyrrole. In this configuration, the photovoltaic material includes a fiber core with an outer surface, a photoconversion material (nanomatrix material) disposed on the outer surface and an electrical conductor circumferentially covering the photoconversion material.

Another approach, with less in-situ construction, consists of sewing an optoelectronically active optical fiber into the fabric [8]. This fiber consists of dye sensitized solar cell deposited on a claddingless optical fiber. Silica and plastic optical fibers are used as a substrate. This fiber converts the light modes that propagate in the modified cladding into electrical signals. This concept though might be classified as one notch less in fabric integration due to the presence of the optical fiber materials. However, it belongs to the ultimate integration category since it is really a fiber; its diameter is only about one or two millimeters and can be of extensive length.

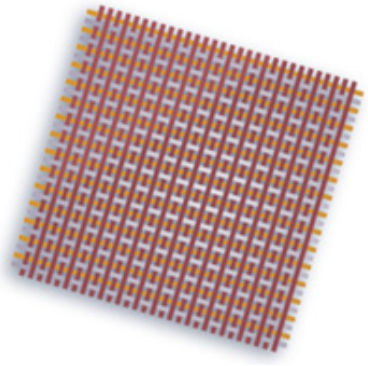

Figure 91. Photovoltaic array of fibers[8]

A.1.3 Major development motivators

The field of e-textiles finds great motivation for development mainly in these three areas: civilian, biomedical, military developments and research investigations, as mentioned in section 1.2. This is also true for smart fabrics in general.

Leisure, civilian and apparel applications entail commercial applications of e-textiles. This is due to the ubiquitous character and the easiness in adaptability of this technology. There are numerous applications being developed for an ultimate integration into daily life. For the apparel industry, the term 'techno-fashion' [63] refers to the introduction of electrical elements and devices with functional applications into garments. This intends to redefine the human machine interaction, trying to provide a more pragmatic, expressive and productive lifestyle. The industry is slowly producing consumer goods that introduce this technology, such as the wall dimmer, smart jackets, fabric keyboard, etc… that were mentioned above. Other smart fabric related commercial applications include outerwear and backpacks such as that of voltaic solar bags [64], where the consumer can recharge

their handheld electronics at any time using solar cell energy. The 'Scottevest Solar Jacket' also makes use of solar panels attached to clothes; this is shown in Figure 92. The panels charge a small battery which powers the device almost immediately after the solar panels are exposed to sunlight. Once the battery is fully charged the panels can be removed and portable electronic devices such as iPods or cellphones can be connected to use the stored power [65].

Figure 92. E-textiles commercial applications: a. Scottevest Solar Jacket [65] and b. O'Neill-Infineon media Jacket [66].

Other less integrated e-textile bags are the ones that have iPod remotes built into the straps, built in speakers and built in Bluetooth capabilities to synchronize the electronic devices the person is carrying. Such is the case for the bluetooth mp3 snowboarding jacket by Infineon-O'Neill technologies [66]. In this device, the microphone and cellphone are integrated into the jacket; the cellphone is controlled via bluetooth to enable a hands free operation. There are also other developments such as that of light emitting fabrics like GlowSkin (by Safelites), which features thin, flexible, durable electroluminescent polymer film strips that are easily applied on fabrics [67]. Being a major spin-off of the plastic electronics industry it is rapidly being integrated as part of textile systems. Another company that has developed products that incorporate

electroluminescent materials is Canesis, a textile research and development company, and AWI. A safety vest that incorporates this technology is shown in Figure 93. Canesis has also developed a heating system that is completely based on textile materials. This heating system is durable and washable and is being currently incorporated in commercial products such as upholstery and blankets. A sock with this thermally active material is shown in Figure 94.

Figure 93. Canesis Electroluminescent (EL) safety garment: a. Garment with EL display off, b. with display on [68].

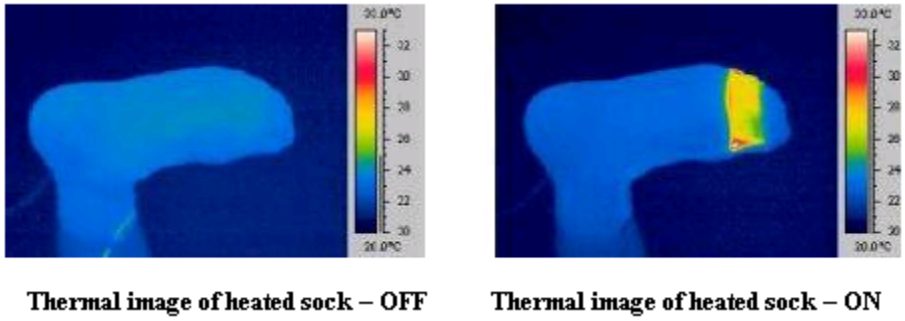

Figure 94. Thermally heated sock (Canesis) [68]: a. Thermal image off, b. Thermal image on.

Companies and brand manufacturers that are incorporating e-textiles technologies into their products usually have to develop the product first, as a prototype idea and then commercialize it. This is the case of Adidas Footscan [69], which uses smart fabrics technology customized by its developers. In general, smart fabrics applications so far have to be individually developed for each particular application, unlike the electronics industry itself where the components are commercially available and they just need to be assembled to get a prototype. To this extent, new companies are being born in the need for a developer interface that will help in the research and development of new ways to integrate fabric technologies into a company's series of products or as new marketable products. One of these new trend companies is R&D Cetemmsa [70], which besides providing consulting for development of new products also carries scientific investigations such as a study of inkjet printed organic RF Structures.

Health and sport applications are numerous. Monitoring heart rate or jogging speed has become an association of healthiness and wellbeing. Some developments include: The Heat blanket, the NuMetrex heart sensing cardio shirt by Textronics [71] (Figure 95), the Adidas Footscan system, iPod pedometer [72], among others. The Smartex project also intends to get ECG signals (electrocardiograms) by means of a conductive thread that is interwoven in non conductive fabric.

BioHarness by Zephyr (Figure 96) is another one of the advanced products that emerged from smart textiles developments. It measures the heart rate and rhythm and can monitor the expansion and contraction of the chest. With a series of solid state sensors, three

accelerometers and a thermometer, the device transmits data wirelessly through an ISM link, being GPRS enabled as well [73].

Figure 95.Textronics conductive elastic fabric used for ECG chest straps [15]: a. Close up of fabric sensor, b. Chest strap.

It can provide among others; ECG, respiration trends, posture, activity and skin temperature. NASA is using this device to study sleep deprivation in preparation for future manned space missions. Stanford University and other universities are also using this device as an alternative to bedside monitoring units.

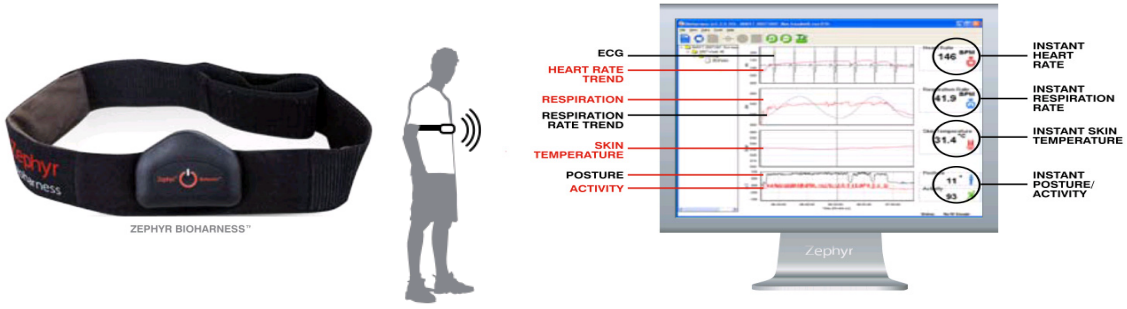

Figure 96. Zephyr Bioharness [73]: a. Chest strap, b. Transmitter and c. User interface

Zephyr also launched the ShoePod (Figure 97), which is a smart fabric insole. The insole consists of small pressure sensors made from smart fabrics embedded in a specialized foam rubber. It measures the pressure applied to different parts of the foot in minute detail by first statistically sampling the pressures over eight locations on each foot. The

device measures the compression of the foam 800 times per second, taking about 125 measurements during footfall. The ShoePod [74] can point out at which instance the way an athlete is using his feet changes enough to produce a decrease in efficiency, determining this way which exercise regimes are needed for building specific muscle sets. A prototype for diabetics is also being developed by the same company; here a profile of pressures and temperatures is used to detect the early symptoms of DPN (Diabetic peripheral neuropathy) which is preceded by calluses and inflammation.

Figure 97. ShoePod [74]: a. smart fabric insole, b. receiver and c. graphic interface

Other developments for foot monitoring have been implemented devices such as Gebiom (Figure 98) [75], which can generate plantar pressure profiles. The soles have several sensors that transmit the information wirelessly and which acquire data at about 200Hz. This device also intends to provide useful monitoring data for the diabetic foot. FSR tactile sensors are also used for the pressure sensing task. For example, PPS tactile sensors which are capacitive based can be used as insoles or can be used to measure finger pressures of the hand (Figure 99) [76]. Other similar plantar pressure measurement systems include *tekscan*, and *pedar*.

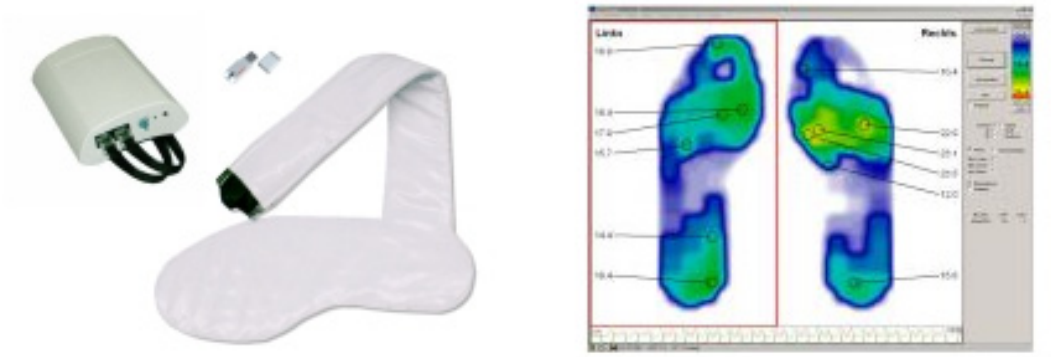

Figure 98. Gebiom plantar pressure system [75]: a. insole and b. GUI

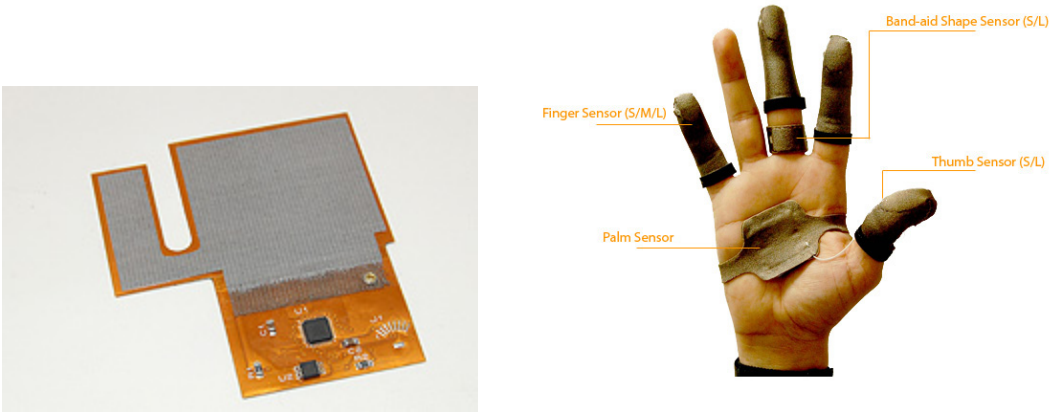

a. PPS digitacts b. TPS-human tactile system

Figure 99. PPS digitacts and TPS-pressure measurement system for human [76]

Army and defense [14] is another major motivator for e-textiles. In the race for better battle equipment, any additional value will contribute to a better performance. The feasibility and increased practicality of electronic textiles have raised many potential applications in this field. Army developments may involve all the possible levels of integration of smart textiles. This all has the purpose of being of aid to the soldier in the battle or mission field. Future warrior systems will be equipped with head-up displays,

wireless weapons, GPS applications, chemical and biological threat detectors, harvested energy battery power, personal physiological status sensors, combat ID sensors and all of these should be linked to the soldier's personal computer to assist him in situational awareness and strategy understanding and deployment. Some of the previous soldier aids may be realizable with the aid of e-textiles. That is, i.e. textile antennas, self decontaminating fabrics and novel textile conductive cables (Figure 100) for reduced overall weight are some of the smart fabrics implementations in this field. Nanotechnology is another one of the new science fields that will play a major role in the development of the new generation of the Army uniforms and equipment. Chemically protective over-garments can be produced with the aid of nanotechnology, shielding the soldier from deadly microorganisms or deadly chemicals.

Figure 100. E-textiles applications in defense: a. Soldier portable computer [14], b. textile information cable .

Finally, the last motivator of electronic textiles expansion is academic research with biomedical purposes or purely academic purposes. One of the biomedical applications focuses on monitoring the entirety of human vital signals and some dynamics of motion. A complete measurement of body variables can be achieved by a suit with several wired measurement devices, called the "Hokie Suit", shown in Figure 101. This extremely

compliant and lightweight garment intends to eventually monitor body motion and vital signs for health monitoring and prevention of falls in the elderly people. The pants of the suit will be able to measure the walking gait for aiding in the monitoring of progressive diseases such as Parkinson's in which patients develop distinctive gait patterns, as was mentioned above. The suit has accelerometers, piezoelectric films and microcontrollers and it can calculate the stride length. It has also developed a technique to compensate for the foot changing direction at each stride. The shirt of the suit should be able to measure heart rate, temperature and blood pressure [17].

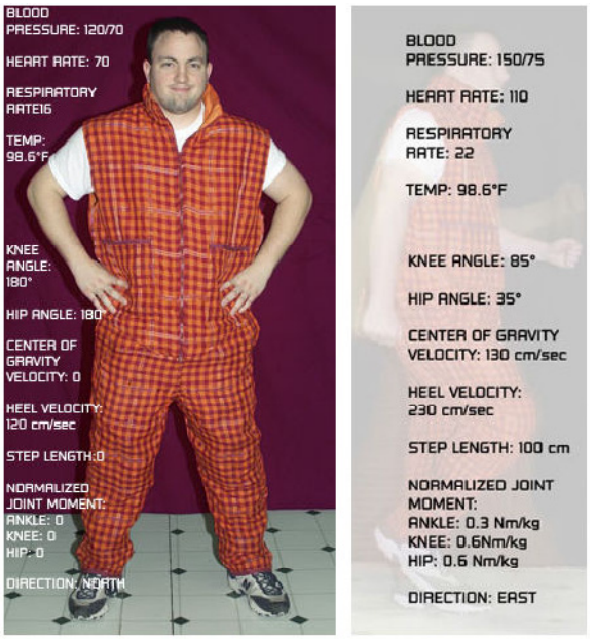

Figure 101. E-textiles application in research: Virginia Tech's Hokie Suit [17]

In the perspective of all these development motivations and resulting devices, it can be noted that there is not a single procedure or technique to follow A wide variety of issues need to be considered in order to design and develop a smart textiles product. A successful design takes the expertise of multidisciplinary professionals, including textile

scientists, polymer chemists, physicists, bioengineers, software engineers, and mechatronics engineers, among others.

A.2 Fabrication and connection techniques for e-textiles

New techniques have to be used in order to obtain good circuit integration into the fabrics. The new mechanical requirements have lead to a series of novel fabrication methods. Electronic components need to be smaller in size, compact, conformable or at least easily encapsulated. The interconnections also present a challenge. Conductive threads of different kinds, conductive inks and conductive fabric itself may all be used as compliant interconnects. All these components may have different techniques of encapsulation, printing and joint connection. This will be addressed in this section.

A.2.1 Textile circuitry

A first step in manufacturing textile circuitry is to find textiles and yarns that are suitable for use in fabric circuitry and then the methods for circuit patterning. One primary method is called *e-broidery* [5], which consists of numerically controlled embroidery using conductive thread (Figure 102). This is used to stitch patterns that define circuit traces, component connection pads or sensing surfaces. The design of such design layouts and stitch patterns can be done using CAD. The yarns used have to be strong and flexible enough to be sewn at high speeds without breaks in the threads which would cause an electrical break. The threads also must keep their electrical properties when washed; dry cleaning is preferred and other environmental agents such as water, alcohol and sweat are considered as an everyday occurrence.

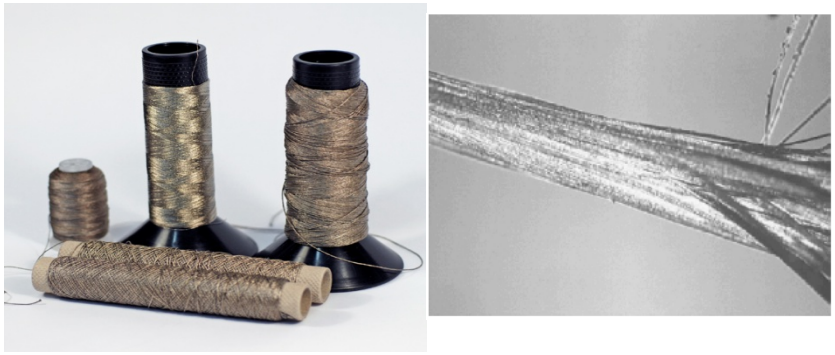

Figure 102. a. Conductive thread-silver plated nylon and b. 100% stainless steel fiber bundle [78]

Yarns of different electrical resistances can be used to replace standard capacitors, resistors, and inductors. The circuit on fabric is designed as one being of low power consumption and high input impedance, which is opposite to the conventional requirement of low impedance for component interconnections. Several available yarns can be used for connections and circuit elements, these include silverized conductive thread [77], stainless steel (stainless 316L, stainless 302 steel) thread [78] (which originates from filters to process fine powders) and nylon or polyester silverized thread. Other materials that can be used are NiCr, FeCr alloys, titanium, gold or tin. An ideal yarn or textile for fabric would have completely adjustable electrical properties and would maintain those properties while being sewn, flexed, and worn. The stainless steel thread presents some advantages since it is biologically inert and not sensitive to washing or sweat (resistant to corrosion) and has a low cost. They vary in composition from 100 percent continuous conductive steel fibers to feltings or composites of polyester [4]. Different resistivities are achieved by varying the proportion of the two constituent fibers. The conductivity is limited though by the manufacturing process in producing them. Also, the more steel they have, the less their elasticity; therefore, the less capability of

being machine sewn. These fibers are available in diameters from 12 microns to 100 microns or even 2 microns.

Another technique consists of 'ironing on' the circuits on to the fabric [28]. This is done by first attaching a heat activated adhesive to a conductive fabric (Sn/Cu coated [79]). Then, a laser cutter is used to draw the circuit pattern into the conductive fabric, cutting the paper backing in the process. Then the paper backing corresponding to the circuit is peeled off leaving the conductive fabric exposed. Then the circuit is ironed onto a piece of non conducting fabric. Only the parts of the conductive fabric where the paper was removed adhere to the non-conductive piece of cloth. As a final step, the conductive fabric that is not part of the circuit is peeled away. Once the circuit is attached to its backing cloth, it can be soldered like a traditional PCB. This process is shown in Figure 103.

Other alternatives for textile circuitry include conductive inks that are painted on the fabric to create the conductive patterns, such as the process of ink-jet printing [80, 81]. Others simply use the regular type of wire that would be used in a conventional circuit but try to pre-shape it so that when bent it won't restraint the motion of the fabric or the wearer. This approach though is not the ideal scenario because the wire itself is not compliant enough.

Steps to building a fabric PCB:

a. The circuit (adhesive on fabric) is cut by a laser
b. The cut circuit and its backing fabric
c. The paper underneath the circuit is removed
d. The circuit is ironed onto its backing fabric
e. The conductive fabric that is not part of the circuit is removed
f. This is the completed circuit

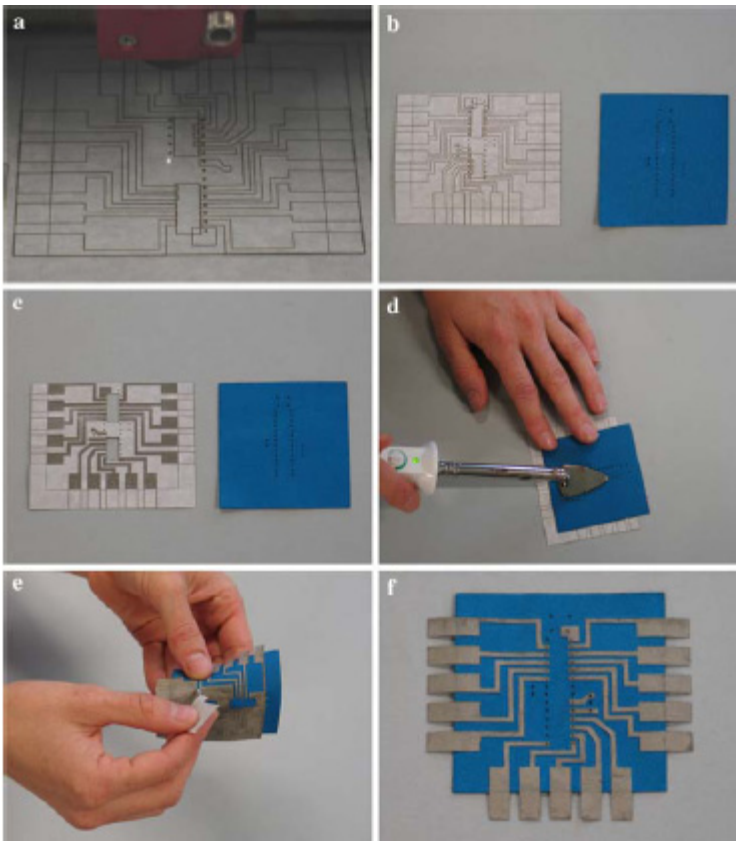

Figure 103. Steps to building a fabric PCB [28]

A.2.2 Interface between components and circuitry

The joining of the component leads and the circuitry conductive lines has to be one that can withstand the flexing and stretching that clothing and textiles usually experience. One method is to solder the leads of the components directly to the conductive thread of the fabric such as in the metallic organza. A PIC16C84 microcontroller and its supporting components are soldered directly onto a patch of metallic organza. This circuit uses bidirectional I/O pins on the PIC to control LEDs and to sense touch along the length of the fabric and uses audible feedback through a piezoelectric speaker to reinforce the sense of interaction. All of the components are soldered directly onto the surface of the

metallic organza weave except for the microcontroller, which sits on a socket soldered to the organza; this is shown in Figure 104.

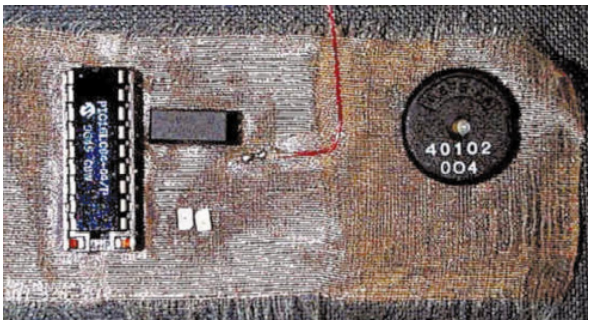

Figure 104. Electronic components soldered on Metallic organza [5]

Another type of connection is made by simply sewing the components to the conductive lines on the fabric. Stitchable batteries (coin cell batteries) shown in (Figure 105). , are placed in a fabric holder that can be sewn into the fabric. Then the holder leads are soldered to a piece of fabric PCB. Components are then easy to sew into the e-textile; this is done by the use of conductive thread. The same technique can be applied to microcontrollers and other electronic elements. The resistance across a typical fabric tab to stitching joint is less than 1 Ohm. Fabric switches are another way of connecting the electronic elements and can be made by putting two pieces of conductive fabric together but separated by a piece of felt with a hole in it. When the switch is pressed the two pieces of conductive fabric contact one another through the hole. A good complementary implementation of this approach is to use gripper snaps. Another alternative which is similar to stitching the components is to staple them under pressure, this allows motion while still in contact, but restraints motion.

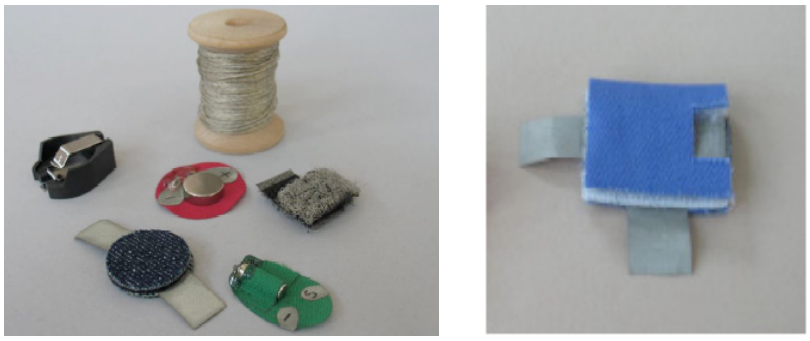

Figure 105. a. Stitchable batteries and b. fabric switch [28]

Finally, electronic components may also be bonded to a conductive substrate by using conductive adhesives.

A.2.3 Encapsulation and insulation

Microcontroller fabric-soldered joints are created by soldering the leads of the microcontroller to a fabric PCB, and then both the solder joints and the microcontroller are encapsulated in epoxy as shown in (Figure 106) [28].

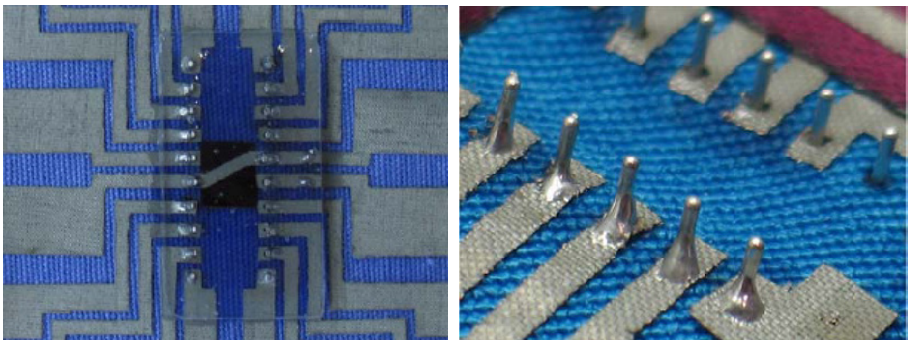

Figure 106. a. Encapsulation of solder-conductive fabric joints and b. solder joints before encapsulation [28].

Electronic components can be insulated by placing them into a Plastic Threaded Chip Carrier [5], which is different from a Plastic Leadless Chip Carrier, a common technique

for surface mount integrated circuit packaging and is designed to be soldered onto printed copper circuit traces on a rigid or semi-rigid circuit board. The PTCC (Figure 107) is designed to be stitched or woven into a fabric circuit and therefore has long and flexible conducting leads which connect to the threads. The threads may be attached to the substrate by covering stitches that are in electrical connection to the rest of the circuitry made also by e-broidering. The threads that leave the package are bundles of approximately 100 continuous steel fibers which are micro-spot welded to the lead frame stubs (connection between the inside and outside of the plastic carrier) and then the entire structure is sealed in a plastic carrier. These packages can be washed without harm to either their internal electrical properties or their connections to the substrate and other components.

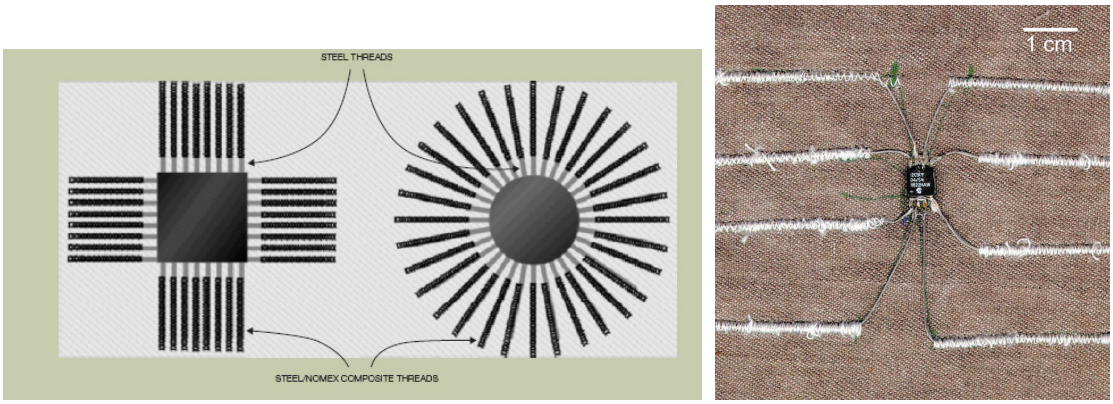

Figure 107. a. Square and radial PTCC packages and b. prototype of PTCC onto fabric [5]

Insulation of the conductive threads (Figure 108) is also important to prevent shorts and to preserve the quality of the textile. A way of insulating the conductive threads consists on applying 'puffy' fabric paint on the thread that needs to be insulated [12] or by applying a tubular intarsia sewing technique, where a non conductive thread is sewn around the conductive thread. Conductive threads and or conductive fabric can be

insulated as well by sewing a piece of non conductive thread on top of them. This last approach though is not suitable for complex circuit configurations.

Figure 108. a. Exposed and insulated thread by couching and b. insulated thread by fabric paint [12]

A.2.4 Multilayering of fabric circuits

All the circuits mentioned above deal with circuits drawn or embroided on a single piece of fabric. However, when nontrivial circuits and connects need to be developed a multilayered structure is appealing. This is also necessary for achieving a simple outward appearance for easy circuit-user fabric interface. Each layer of the stack of interconnects is made by e-broidery or printing or any of the other methods described so far. Then, the insulating fabric layers are placed between the layers with circuitry and the vias (conductive paths that connect the layers) are stitched between layers using more conductive thread. This concept is illustrated by (Figure 109).

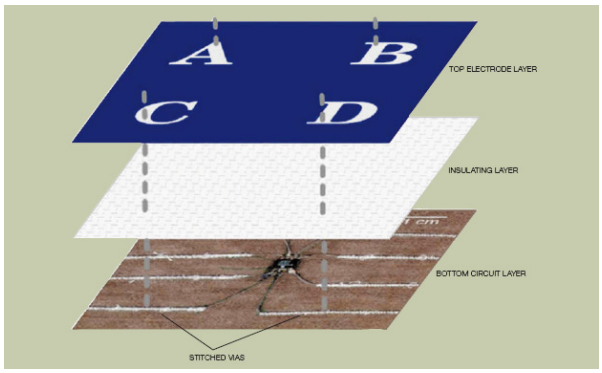

Figure 109. Concept of fabric multilayer connection [5]

The insulating fabric is also applied for the printed on conductive fabric circuitry. To continue the circuit on each layer, a similar 'ironing' process needs to be carried in order to print the conductive path on the fabric substrate. A conductive fabric insulated by a non conductive fabric both in a layered circuit are shown in Figure 110.

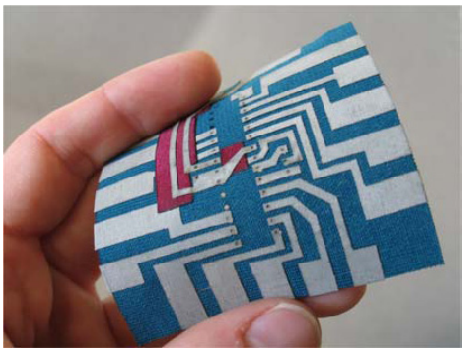

Figure 110. Conductive fabric (light blue) printed on Substrate (dark blue) insulated by a non-conductive fabric (purple) [28]

A.3 Some novel enabling technologies for e-textiles

A.3.1 A completely washable and durable material-QTC

In the need of new materials to comply with the requirements of textile mechanical characteristics, some novel solutions need to be provided. An example of an ideal

material that conducts on applied pressure, that is completely rubbery, completely washable, and very light is the quantum tunneling composite or QTC [82, 83]. This composite is made of carbon nanoparticles embedded in a polymer matrix. But its conduction mechanism is not the commonly known percolation but instead, electrons pass from atom to atom by the quantum tunneling effect.

In classical physics, an electron cannot pass a potential barrier without having enough energy to overcome it. In quantum tunneling however, the electron has a probability to appear at the other side of the potential barrier by the tunneling effect, in which the electron wave decays exponentially. This approach makes use of the wave characteristic of electrons, in addition to its particle characteristics (Figure 111). The reason for this to happen is the shape of the carbon particles. These nanoparticles have spikes. These spikes allow the electron density to be very high at the spikes or edges making a current possible under enough nearness. The nearness of the spiky particles is produced when one presses on it. The actual particles may never touch each other, they are trapped in the polymer matrix, however, the electrons can pass from one particle to the other by the accumulation of potential at the spikes ends and therefore by the tunneling effect that is produced.

Other polymer fillers to build QTC's can be Ni, Cu, Ag, Al and Fe [82, 83]. This is shown in Figure 112. This technology is being used in rollable computer keyboards that are being commercialized by Elektex (Figure 113) [84]. Each key has a layered combination of the quantum composite and conductive fabric.

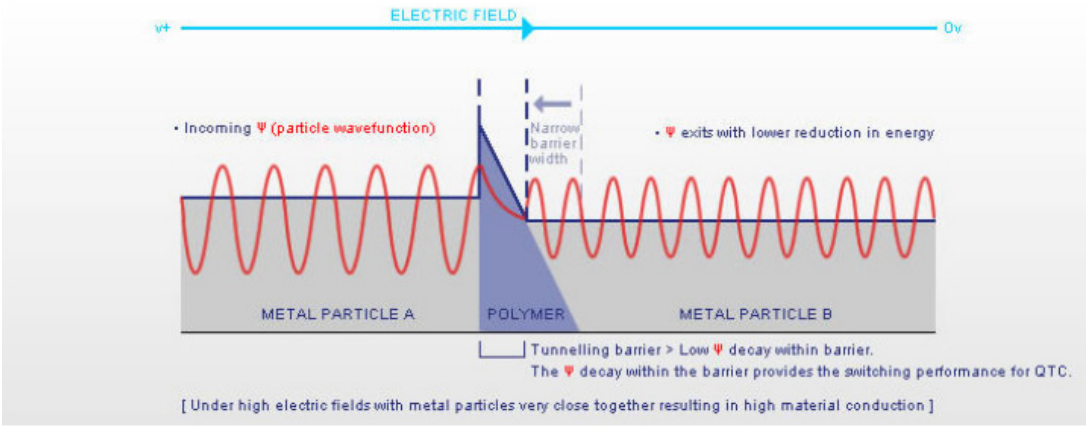

Figure 111. QTC quantum tunneling effect [84]

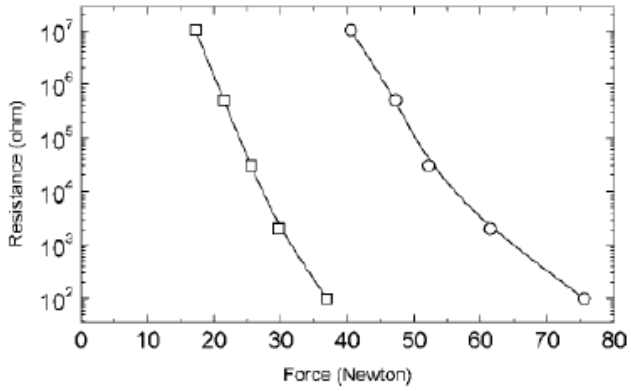

Figure 112. Resistance (Ohms) vs Force (N) in a Si–Ni type 287 QTC-Conduction under applied force [82, 83].

The quantum composite is placed in between two layers of conductive fabric, under applied pressure there is a passage of current which closes the circuit.

Figure 113. a. Electron current at tunneling (left) and b.Eleksen Keypad (right) [84]

The fabric technology used in making these keyboards is shown in Figure 114. This fabric sensor basically consists of two conducting layers separated by an insulating layer. The intensity of the current gives the level of pressure applied to the sensor. The first layer is knitted as a spacer fabric in which individual spacer threads extend between the first and second planar portions. The second fabric layer includes conductive threads that run in a second direction. The first and second planar portions have conductive threads running on different directions. When a force is applied over the surface the spacer threads collapse in that region and allow electrical conduction to occur between the first planar portion and the second fabric layer.

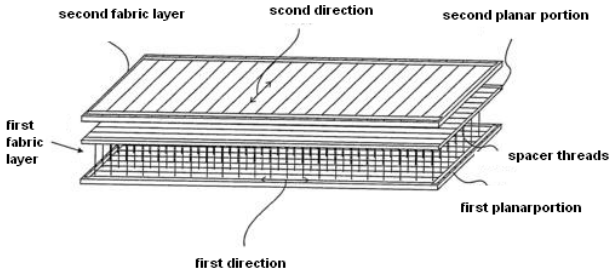

Figure 114. Elektex fabric sensor technology [85]

A.3.2 Energy harvesting technologies embedded in fabrics

Another packaging and interconnection technology for deep integration of electronics into textiles can be used to harness a micromachined thermoelectric generator chip (Figure 115). The human body produces several tens of watts of heat. Miniaturized thermoelectric generators, can harness part of this energy and convert it into electrical power. These generators are built in a silicon chip and consist of a large number of thermocouples, electrically connected in series and arranged to make best use of a given

area. Due to the Seedbeck effect, a temperature difference between both ends generates a voltage and an electrical current passes through a designated load. An output power of 1.6microwatts can be obtained from a 7.0 mm2 chip containing 16000 micro-thermocouples, which is enough to power devices such as a wrist watch (Figure 116) [86].

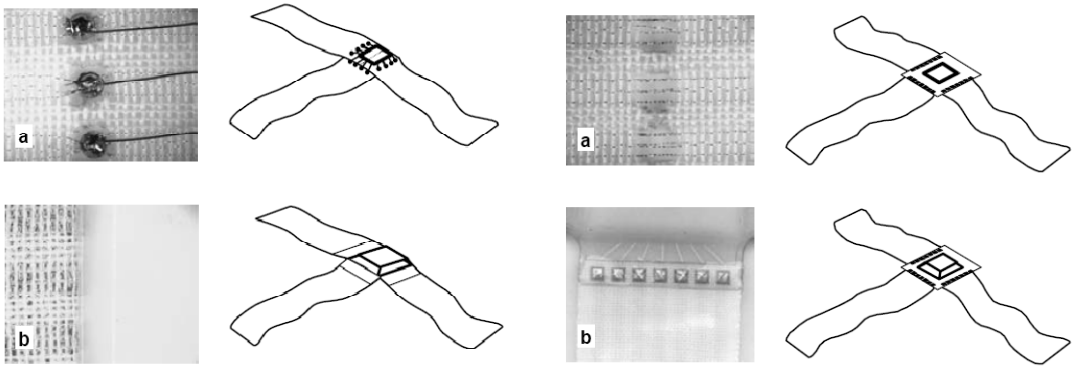

Encapsulated temperature silicon chip plate bonded **Flexible PCB cable bonded**

Figure 115. Micromachined thermoelectric generator chip: a. Encapsulated chip and b. Flexible PCB cable [86].

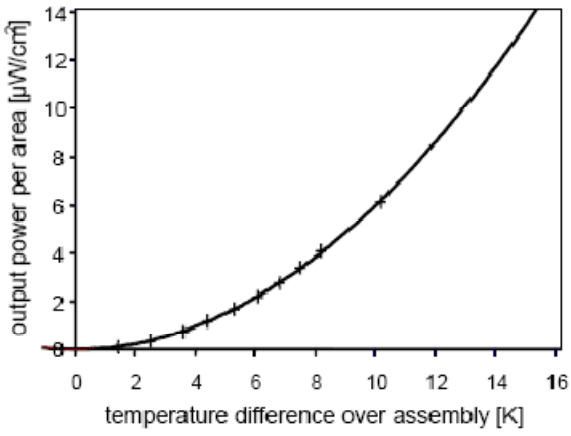

Figure 116. Measured output power of the thermoelectric generator chip [86]

The connection lines consist of a polyester narrow fabric with several warp threads replaced by copper wires which are coated with silver and polyester. The electrical connections are created by removing the surrounding textile material with a laser. The resulting holes in the fabric are then soldered with tiny contact plates and thin bonding wires before the module is encapsulated. Another possibility is to replace the contact plates by a thin flexible printed circuit board, which is attached to the polyester fabric before soldering. The complete unit is molded forming a hermetically sealed casing protecting it against mechanical and chemical stresses caused by wearing and cleaning the textile.

A.3.3 Carbon Nanotubes in textiles

Research in materials science such as the nano-textiles is currently also a research target. Carbon nanotubes (Figure 117) are injected into a rotating bath of PVA-aqueous polyvinyl alcohol, and then washed or can be grown by electrophoretic deposition into forming yarns and these can later be woven into the textiles to either increase the mechanical strength of the fabric or to increase the conductivity if they are used as conductive lines [87].

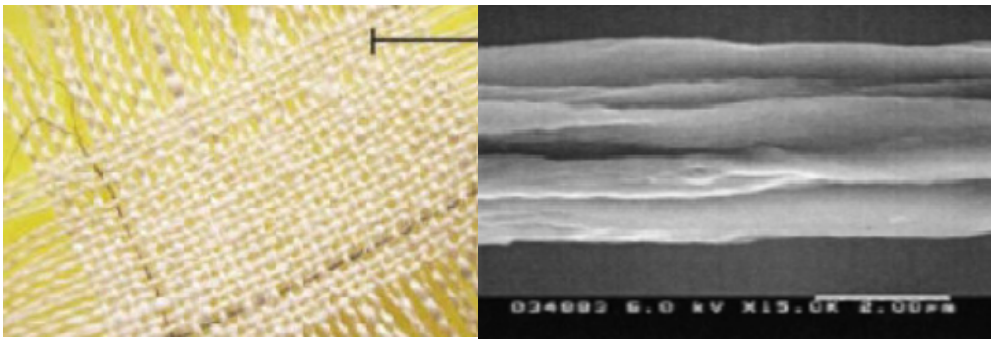

Figure 117. Carbon nanotubes into textiles: a. carbon nanotube thread sewn into non conductive fabric and b. micrograph of the nanotubes [87].

A.3.4 More enabling technologies

Flexible electronics technologies can be adapted to complement smart fabrics technologies. For instance, a stretchable silicon circuit with a mesh design, wrapped onto a model of a fingertip is shown in Figure 118. An array of organic transistors interconnected by printed bucky gels and supported by a thin sheet of PDMS is shown in Figure 119.

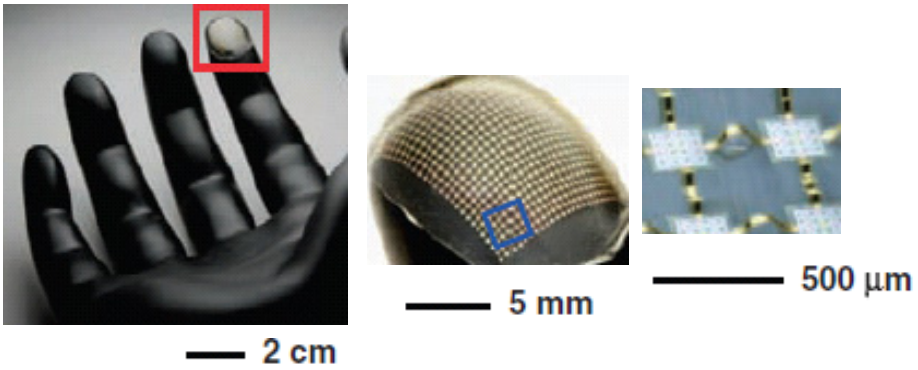

Figure 118. Stretchabble silicon circuit in different levels of amplification [88].

Figure 119. Flexible transistors [88].

Another enabling technology in the area of flexible electronics and flexible macroelectronics is e-paper, which intends to emulate the ink appearance of ordinary ink

on paper to generate flexible large area displays. Many more enabling technologies are current being developed and researched on.

Appendix B. Human foot anatomy and characteristics

B.1 Foot and lower limb anatomy, characteristics and dynamics

B.1.1 Foot anatomy and articulation

Given the premise for this thesis, which entails the possibility of tracking the motion of the foot, we proceed to looking at some of its anatomic aspects in some detail.

The human foot consists of 26 bones connected by tough bands of ligaments. The bones of the foot can be viewed as grouped into three main categories: tarsal, metatarsal and phalanges. The seven rounded tarsal bones are as follows: internal, middle, and external cuneiform bones, navicular, cuboid, talus, calcaneus, and lie below the ankle joint to form the instep. Five metatarsal bones form the ball of the foot. The 14 phalanges (toes) are divided into two in the great toe and three in each of the others. In each of the toes, with exception of the great toe, the first bone (from top to bottom) is called the proximal phalanx, then the middle phalanx and at last comes the distal phalanx. The foot bones form two perpendicular arches that normally get in contact with the ground only at the heel and ball of the foot. This arched structure helps to support the body's weight.

In terms of the main joints: the ankle joint, consists of all the bones and tendons around the talus, while the metatarsophalangeal joint includes all the meta-phalanx joints of the five fingers. This last one is also referred to as the MTP joint (Figure 120) and is the first joint that connects the toe to the middle portion of the foot. Following that one, is the proximal interphalangeal joint (PIP joint) and the last joint is the distal interphalangeal

joint (DIP joint). An encapsulation of ligaments surrounds each joint and holds the set of bones together.

Figure 120. Human foot: meta-joints [36]

As for the muscles involved in gait, there are hip, knee and ankle muscle groups involved; however we will focus on the ones for the leg and ankle which deal directly with the present study. The leg muscles [37] (on the sagittal plane) consist of a *dorsiflexor*: Tibialis anterior and two *plantarflexors*: Gastrocnemius and Soleus. On the frontal plane there are the following muscles; *inverter*: Tibialis anterior, posterior and the *everter*: Peronei. A detailed figure showing tendons and muscles is shown in Figure 121. Many other muscles are involved in foot motion, including the flexor hallucis brevis, and the large abductor hallucis, they are all illustrated in Figure 121.

All the muscle figures provide a view of the motion mechanism of the foot. It can have motion in 3D but also has limited angle range given by its anatomic constraints; for instance, the movements allowed at the metatarsophalangeal joint are flexion, extension,

abduction and adduction. Also, given the common architecture of the muscles, which increase in cross-section when exerting force or in motion, one could use the locations on the foot where certain major muscles make skin surfaces larger when in motion to place strain sensors.

This concept is illustrated in Figure 122, which clearly shows how a change in muscle cross-section can produce a change in skin surface. All other muscles which can contribute to a change in volume, and therefore to a change in skin surface, shown in Figure 121.

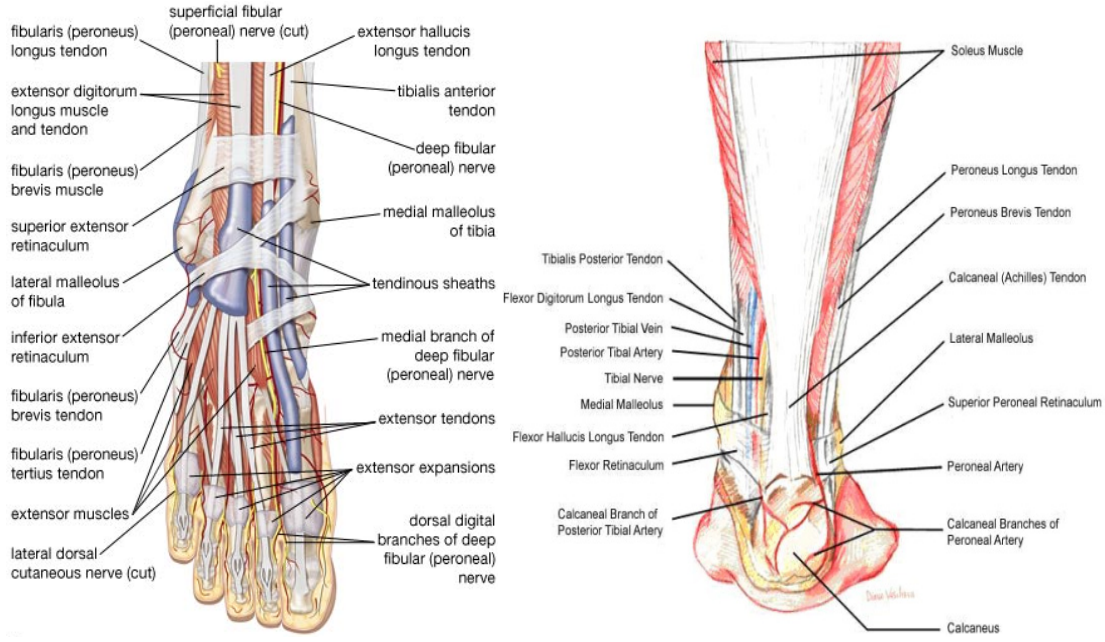

Figure 121. Foot muscles (detailed) front view (left) [89], back view (right) [90]

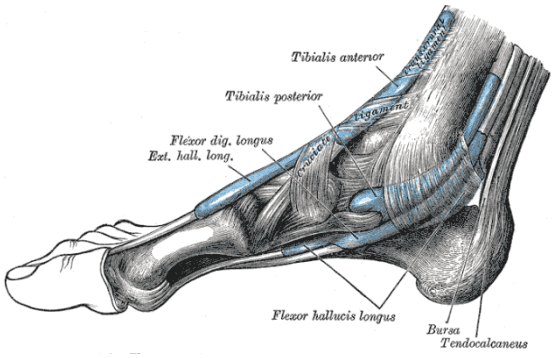

Figure 122. Muscles change in cross-section when strained [91]

B.1.2 Some anthropometric considerations

The science of biomechanics is usually divided into: rigid body dynamics and tissue mechanics. The former studies the body segments as if they were rigid uniform bodies linked by frictionless joints. The second one refers to the study of how forces deform tissues. Anthropometric data [92] is given within the rigid body dynamics framework since it deals with body segments. In general, anthropometry refers to the measurement of the human individual for the purposes of understanding human physical variation. A standardized approach is to consider that each of the body segments have a uniform density with mass concentrated at the center of mass. Anthropometric data of the human body entails segment length, mass, center of mass distance, and radius of gyration of different body segments such as the head, shank, trunk, etc… The human foot has its own set of measurements as well.

Five dimensions can be used to describe the anthropometric characterization of the foot [92]. These dimensions are: foot length, joint girth, maximum foot width, heel width and circumference, this is shown in Figure 123. All these characteristics have an inter-

correlation, which is expressed in Table 6. It is to be noted that all these characteristics can also correlate to the stature of the person. There is dependence of stature and foot length and on maximum foot width, as shown in Figure 124 and Figure 125. Also, the influence of birthplace and a person's style of life are indicative for some foot dimensions. This is also true in variations of ethnicity. The mean shape is based on homologous modeling. All these characteristics can serve the purpose to identify an individual's foot. The sensors to be used in the later part of this study and their angle output, associated to gait phases, could aid in identifying correlations, if any, of the major anthropometric parameters to normal/abnormal gait characterizations obtained with those sensors.

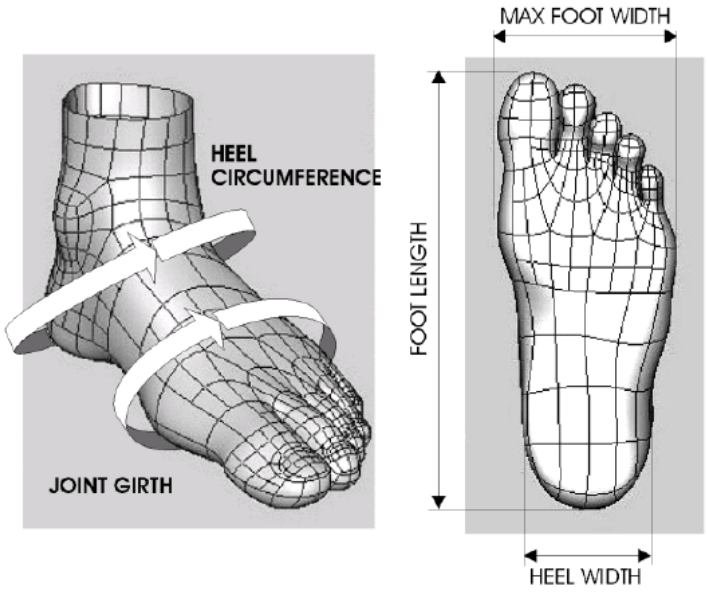

Figure 123. Five foot dimensions [92]

Table 6. Intervariable correlation coefficients (among average values) [92]

	Foot length	Joint girth	Foot Width	Heel Circumf.	Stature
Foot length	1	0.665	0.560	0.410	0.930
Joint Girth		1	0.925	0.829	0.78
Foot Width			1	0.865	0.721
Heel Circumf.				1	0.609
Stature					1

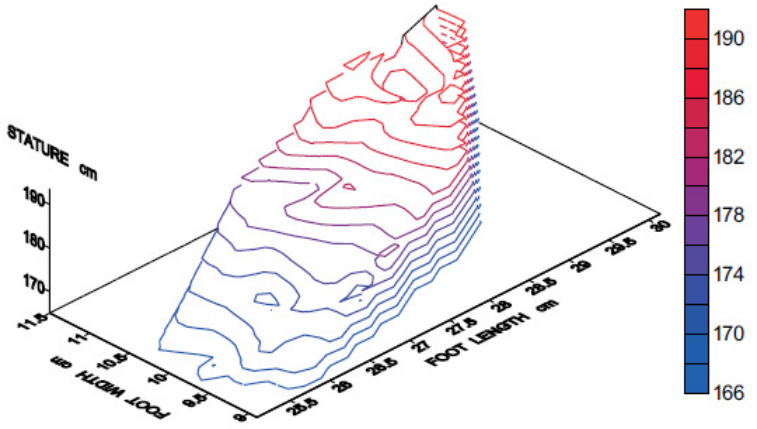

Figure 124. Stature dependence on foot length and on maximum foot width [92]

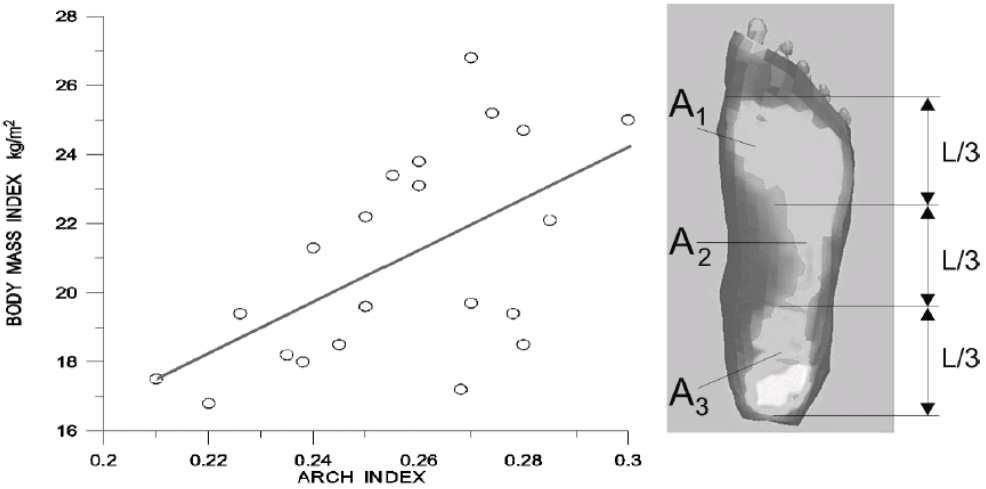

Figure 125. Body mass index vs arch index [92]

B.1.3 Human Motion

The biomechanics of human motion were already being conceptualized and mathematically enabled by the end of the 19th. The start of photography led to the documentation of human motion; currently, with computer technology it is possible to build models based on information acquired from visual systems. Optical three-dimensional techniques are currently being widely used for characterization of human motion.

B.1.4 Human Gait

Gait is the study of the pattern of motion of the limbs of animals, including humans. A complete gait cycle is shown in Figure 8. From the literature, it has been said that the driving aim of gait is to minimize vertical and horizontal motion of the center of mass, to maximize the energy efficiency. This mechanism is complex and is determined by several factors, such as pelvic rotation, and leg segment rotations. Three sets of physical variables are important in studying human locomotion: kinematic (velocities, positions), dynamic (forces and moments), and bioelectrical (muscle activity). Efforts have been made to characterize gait in all these variables theoretically and experimentally but always with the axiom of minimizing the energy expenditure via cost of transport, or metabolic cost, or energy expenditure.

Early works such as that of Atzler and Herbst [93], suggest an optimal relationship between walking speed and step length, showing that there is a minimum energy expenditure at each velocity (in excess of rest level) and an optimal frequency for energy

optimization. Other models like Cotes and Meade [94] developed a relationship which suggests that energy expenditure may be a linear function of lift work when step frequency is taken into account. Important biped models include those of Alexander [95] and those of McGeer [96], usually using geometrical simplified models (from the rigid body perspective) which are versions of the complex anatomical mechanism.

Another important concept to find the minimum energy is that of minimizing work and rate of work or power. For Cavagna and Margaria [97], the total external work is equal to Wext=Wv+Wf, where Wv is the work against gravity and Wf is the work due to forward velocity changes. In other words, from a conservational perspective, it suggests that there is an exchange of potential energy (when center of mass is vertically displaced) and kinetic energy (when translational motion of the center of mass occurs). The center of mass (CoM) acquires its maximum elevation during swing phase and is lowest during double support. Kinetic and potential energy interchange during one gait cycle; when the 'CoM' is at its highest or maximum potential energy, it also has the least velocity. When at its lowest, it has the maximum forward velocity. Therefore the total external work accounts for the interaction of these energies which should mirror each other for a perfectly conservative model; however it is the mismatch which causes the actual energy requirement for sustained locomotion. Also, according to Alexander, the external work done when the 'CoM' is lifted (+Work) turns to be lost at heel strike (- Work). In addition to this external work, the internal work (Wint) accounts for the motion of the limbs relative to the center of mass, located slightly above the hips.

Other results, such as that of Cavagna and Franzetti [98] show that the smaller the external power the greater the step frequency and the greater internal power the greater the step frequency. The determination of the gait frequency could be determined by energy minimization, such as the work of Minetti et all [99] indicates, concluding that the chosen frequency at a given velocity could be found by the minimization of external power alone. Minetti exposes as well that a potential source of inaccuracy between the mechanical demand and the metabolic expenditure, or inefficiency, may be in the neglected muscular force component in the lateral direction to support the hip during swing phase.

The musculoskeletal forces exerted during walking are considered of little importance during the swing phase, due to Electromyographic (EMG) studies on the leg undergoing swing. However, EMG studies can be used to measure muscle activity during the entire gait cycle. The metabolic, energetic and electromyographic aspects of gait are rather presented as part of the background information on human gait, i.e. its origin or cause, but these will not take part in the studies presented later in this document. This thesis is mainly concerned with complementing the information gathered on 2D plantar pressure insoles by the determination of out-of-plane foot motion characterization parameters, such as the variation of the main sagittal angle of the foot when in motion.

Gait analysis main techniques and limitations

Gait analysis entails systems to capture kinematics, and motion characteristics during gait. The kinematics comprises a description of motion in terms of the angles,

displacements, velocities and accelerations of the body segments and joints. Several techniques are available to achieve such measurements. Systems can measure relative changes or they can measure global changes. Potentiometers and electrogoniometers measure the relative change of angle. However, for global measurements, where the absolute motion of body segments is measured, a fixed reference system is needed. This can be done with four general techniques which were mentioned in section 1.6: 1. Optical: Such as in Vicon Motion Systems, CODA, Optotrak, etc,,, 2. Electromagnetic: Such as FasTrak, 3. Ultrasonic: Such as Zebris, and 4. Inertial: Such as a combination of inertial MEMS. Muscle activity can be obtained by EMG as mentioned before, or it can be deduced from the kinematics by using Newton's equations and constructing inverse dynamics. In this process, a link-segment model of the foot is constructed and each of the lower limb segments is treated as a rigid body.

There are limitations however to optical 2D gait analysis, instead, 3D techniques are now accepted as standard. This is due to several reasons; two of the major ones are parallax error and perspective error. The parallax error occurs when objects move away from the optical axis of the camera. Perspective error is the apparent change in length of an object when it moves out of the calibrated plane. Optical 3D gait analysis eliminates these errors by using skin markers and placing them on the underlying bone. In a 3D setting, an arrangement of cameras is needed such that the cameras are positioned so that at least two of them see each marker at any given time. Infra-red light sources around each camera reflect from the retro-reflective markers and result in a bright spot in each image. These spots are then combined to generate the 3D trajectories. This system needs

previous calibration of the volume in which the subject will move. This is done by placing a rod, or a cube, with markers at a known distance from one another, in front of the cameras. The only drawback of this powerful system can be caused by an inaccurate placement of the reflective markers. Also, these systems are quite expensive in their simplest form, more complex optical systems involve in as many as 70 cameras at the same time for capturing complex motions.

B.1.5 Foot kinematics and characteristics during gait

The actual motion of the foot is way more complex than considering it being a simplified model of two or three segments. The approximate axes of rotation of the major foot joints were shown in Figure 126, All the other types of foot motion, such as the different directions in which the foot may be flexed or rotated can be found in Table 7.

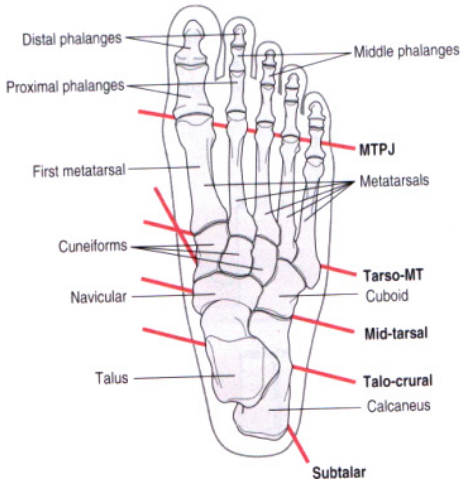

Figure 126. Major human foot joints [37]

To model foot motion with visual systems one could go on either extremes, for example a too complicated route would require placing of markers on each of the 26 bones but it is doubtful to assume that this configuration could actually reflect the underlying bone

motion. A reasonable way is to treat the foot as three functional segments: rear, mid and forefoot and place the markers accordingly.

Table 7. Summary of the various terminologies used for foot kinematics [37]

	Term	***Definition***	***Synonyms***
JOINTS	Ankle joint	Tibiotalar+fibulotalar+tibiofibular joints	Talocrural joint
	Subtalar joint	Talocalcaneal+talonavicular joints	
	Ankle joint complex	Ankle+subtalar joints	Often, confusingly,also termed 'ankle joint'
	Midtarsal joint	Talonavicular+calcaneoucuboid joints	Transverse tarsal joint, Chopart's joint
	Tarsometatarsal joint	Between cuneiforms/cuboid and metatarsals	Lisfranc's joint
	Metatarsophalangeal joint	Joints between each of the five metatarsals and proximal phalanx	Midfoot break, metatarsophalangeal break
FOOT MOTION	Extension	Sagittal plane motion (toes up)	Dorsiflexion
	Flexion	Sagittal plane motion (toes down)	Plantarflexion
	Abduction	Transverse plane motion(forefront rotates externally)	
	Adduction	Transverse plane motion(forefront rotates internally)	
	Eversion	Frontal plane motion at the subtalar joint (sole faces laterally)	Hindfoot eversion, pronation, valgus
	Inversion	Frontal plane motion at the subtalar joint (sole faces medially)	Hindfoot inversion, supination, varus
	Valgus	Everted hind or forefoot	
	Varus	Inverted hind or forefoot	
	Pronation	Eversion+dorsiflexion +abduction	Eversion, valgus
	Supination	Inversion+plantarflexion+adduction	Inversion, varus
	Forefoot supination	Frontal plane motion at the metatarsophalangeal joint (dorsiflexion of medial toes more than lateral)	Midfoot break, forefoot varus

More refined studies consist of dividing the foot into more segments, such as the one in [99], where the foot is divided into: hindfoot, talus, midfoot and medial and lateral

forefoot segments. This model also adds to the number of joints; six joints are defined. Miniature electromagnetic tracking such as the 'Flock of Birds' system can yield more sophisticated models, where it is possible to measure motion within the foot.

B.2 Posture and gesture monitoring works (mainly carbon printed sensors)

Posture is an arrangement of the body and its limbs, a gesture is a sequence of postures with semantic content. These studies are usually carried on the human hand or on the entire body. Some of the techniques used are optical, either planar (photographic, video graphic) or 3D and some others deal with clothes which have been sensorized for that purpose. This last approach deals with e-textiles, which can be either intrinsically sensorized or extrinsically modified to give sensor outputs with appropriate inputs. E-textiles will be reviewed in a later section of this document. As part of the extrinsically sensorized textiles, the coated textiles become 'smart' by applying piezoresistive, piezoelectric or piezocapacitive materials, usually polymers due to their elastic properties. Different polymeric materials can be used as coatings, it also depends on the sensing property that they have. For example, the piezoresistive properties are present in polymers which can partially or totally conduct electric current. The polymer then can be intrinsically conductive, such as pi-conjugated polymers or it can be a doped polymer where conductive particles are added and dispersed in it. The conductive particles may be conductive or semi-conductive. Each coating material has its own advantages and disadvantages.

In particular, carbon based polymers on stretchable fabrics can provide a perfect body sensor due to its compliant qualities. These sensors have been placed on gloves, leotards, and other garment sections in the work of de Rossi et al [32]. In these works, the sensors are printed on Lycra, a fabric which has been knitted with spandex in order to enhance resilience properties. However, these sensors present a drift which gives the signal a long settling time, in addition to nonlinearities which become a challenge for real-time processing, as mentioned in section 1.3. The output depends on both the velocity and second rate of change of the sensor length. A first important observation from this figure is that the sensor increases in resistance even when the strain is released (Figure 127).

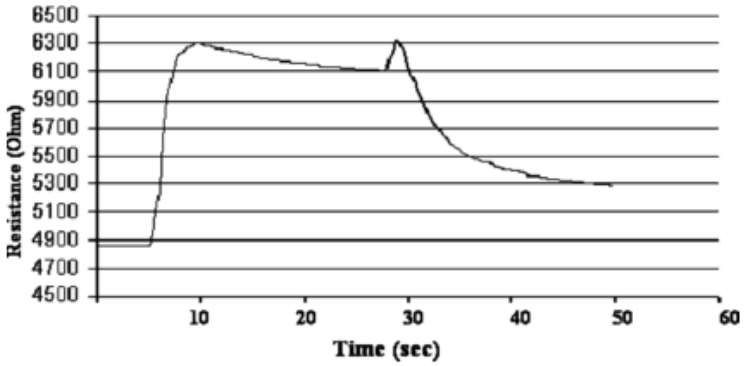

Figure 127. Carbon sensor response to square strain input [34]

This behavior is typical of these types of sensors. The second thing to notice is the roll off resistance at the end of the signal, which shows the drift. According to the work of [33, 34], the drift can be predicted by acquiring the poles of a linear system that models the behavior of the sensor. These poles are then used to predict the final value of resistance (c_0) after the settling time. The positive peaks indicate that the approximation of its behavior should have a square component in terms of the length of the sensor as an input. The behavior of the system can be portrayed as shown in Equation 6.

$$g(t) = a_1 l(t) + a_2 \frac{dl(t)}{dt} + a_3 \frac{dl(t)^2}{dt}, \qquad l(0) = l_0, \frac{dl(0)}{dt} = \dot{l_0}$$

Equation 6. sensor model

Where the input is the length of the sensor and the output is the g(t), the constants a1, a2 and a3 are experimentally obtained and depend on the nature of the input. One could solve this equation by computing a value of g(t) from an associated linear system and by using as boundary conditions at every numerical iteration, the last values of l (t) and its derivative. The value of g(t) can be obtained from Equation 7, where x and xdot are known by reading the resistance signals coming from the sensor and using the estimated poles for the construction of the matrix A (Equation 8). The estimation of poles w1 and w2 are obtained through an exponential regression of the data (Equation 9).

$$\dot{x} = Ax + \begin{bmatrix} 0 \\ g(t) \end{bmatrix}, \quad [\dot{x} - Ax]_2 = g(t)$$

Equation 7. Linear system- value of g(t)

Where

$$A = \begin{bmatrix} 0 & 1 \\ -w1 * w2 & -(w1 + w2) \end{bmatrix}, x = \begin{bmatrix} R(t) \\ \dot{R(t)} \end{bmatrix}, x_0 = \begin{bmatrix} R_0(t) \\ \dot{R_0(t)} \end{bmatrix}$$

Equation 8. A matrix and state vectors

$$y(t) = c_0 + c_1 e^{w1*t} + c_2 e^{w2*t}$$

Equation 9. Regression with two poles w1, w2

The drift difficulty can be solved by having a hardware differentiator which will add up a combination of ‘a’ times the signal, plus ‘b’ times its first derivative and ‘c’ times its second derivative, and equal the sum to a constant c0, or the settling value of resistance. This can be seen in Equation 10, where the constants a, b, and c can be calculated from the pole values.

$$a(c_0 + c_1 e^{-w_1 t} + c_2 e^{-w_2 t}) + b(-c_1 w_1 e^{-w_1 t} - c_2 w_2 e^{-w_2 t}) + c(c_1 w_1^2 e^{-w_1 t} + c_2 w_2^2 e^{-w_2 t}) = c_0$$

where

$$a = 1, b = \frac{1 + cw_1^2}{w_1}, c = \frac{w_2 - w_1}{w_1\ w_2^2 - w_1^2 w_2}$$

Equation 10. Finding Co, the settling value of resistance.

These findings are applied to a single sensor associated to a length l(t) and subsequently associated to an angle theta(t). However, when using the biomimetic approach for the posture and gesture detection using redundant networks of sensors, the treatment is completely different. A formal definition of posture requires a geometrical model of the kinematic chain under study. This can be done by fixing a certain number of Cartesian frames, one for each DOF considered and by relating them with the segments that compose the kinematic chain. A kinematic configuration consists of the set of the mutual positions of these Cartesian frames. Therefore, when a garment is worn by the user, the sensors on the garment acquire certain values that are strictly related to this configuration. If the number of sensors is large enough and adequate sensor locations are used then the

values obtained from the sensors can uniquely characterize the considered posture or configuration. A function F which maps the space of kinematic configurations (theta) into the sensor space (S), has to be constructed and defined in order for this model to be complete. After the function has been defined, its inverse is used to obtain angular data from sensor inputs.

Appendix C. Fabric construction

C.1 Fabric construction (materials, methods)

As was mentioned earlier, sensing characteristics can be given at many different levels within the fabric structure. In this section the standard construction of fabrics will be revised. Sensing characteristics can be given at any point of such a construction.

C.1.1 Fabric structure and smart fabrics

Fabrics have a hierarchical structure, bundles of fibers are spun, twisted or compressed to create yarns; yarns are woven, knitted, etc ... to create fabrics [100]. In previous sections we have seen that fabrics can be given capacitive, resistive, optical, and other properties. However, the main topic of this document deals directly with conductive characteristics given to fabrics (Figure 128).

Fabrics can be sensorized starting with the simplest fabric element, the fiber. This first path to smart conductive fabrics involves methods of creating conductive fibers which are completely made of conductive material or which are then twisted in with other non conductive fibers [101] to make a partially conductive yarn. For instance, as it was seen from the Textronics chest strap, knitted piezoresistive sensors have been developed; in this case, a conductive yarn is knitted on the non-conductive textile substrate [102], this

technique is also used to create conduction lines within the textile. Sometimes the textile's actual component fibers are conductive threads which allow it to be used as a circuit board. This usage is seen for instance in e-textiles, where circuit elements are soldered to the conductive fibers or yarns or threads.

Conductive coatings are also used for sensorizing fabrics. They can be inherently conductive, such as polypyrrole, polyaniline and PEDOT or doped, such as polymer matrices with conductive particles (i.e. carbon, metals) . As mentioned in section 1.3, previous work on this field has shown that the usage of a conductive carbon elastomer as a coating for stretchable fabrics enables them to be used as sensors in motion characterization and as strain sensing devices. There is also another coating method that deals with electrostatic self assembly of conductive nanoparticles onto fabric layers, where the surface of the fibers is infused with combinations of polymers and metals or metal oxides or semiconductors.

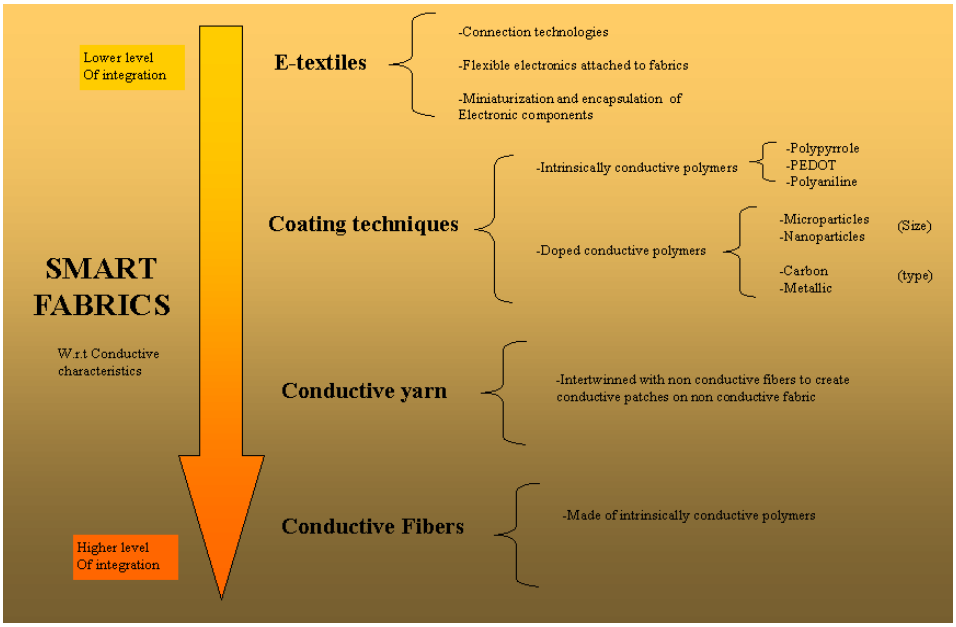

Figure 128. Schematic of the field of smart fabrics (conductive characteristics)

C.1.2 Origins of the fibers used to make fabrics (Natural or man-made)

As stated earlier, fabrics are constructed in a hierarchical fashion; fibers (which may come in filament or staples) are carded, combed, made into roving and then spun, twisted, etc… to form yarns (also known as threads) and yarns are woven, knitted, or compressed to create fabrics (Figure 129) [103]. Fibers are characterized by having a length at least 100 times its diameter and they can be natural or man-made. There are two major categories for fibers; Natural or man-made, a scheme of this categorization is shown in Figure 130.

Natural fibers can have vegetable, animal or mineral origins, such as cotton (vegetable), wool (animal), and asbestos (mineral), some of which are shown in Figure 131. Other commonly used natural fibers are linen and silk. Natural fibers are harvested, sorted, cleaned or milled in preparation for spinning, which is the previous step to the construction of yarns. Based on the type of construction of the yarns, they can be put together by different methods such as combing, carding, and drawing. Combing consists of making the yarn of the longest staple fibers, which later produces a smooth and close fabric structure. Carding involves the use of the shortest staple fibers, producing a coarse yarn surface and therefore a low fabric structure.

Man-made fibers (Figure 132) are fibers created by man through the use of technology. They can be grouped into regenerated fibers and synthetic fibers such as rayon

(regenerated fibers) and polyester (synthetic). Regenerated fibers are made from natural materials such as corn protein or petrified wood, which are chemically reformed to be turned into a usable fiber. The synthetic ones are produced from chemicals made from petroleum derivatives, nitrogen, hydrogen and carbon. The fiber forming ingredients of man-made fibers are extruded, twisted, or spun to form a long chain polymer. Other important synthetic fibers include nylon, acrylic, polyolefin and spandex.

Fibers

Fibers are 'units of matter characterized by flexibility, fineness and a high ratio of length to thickness' [104]. In individual textile fibers, the length/diameter ratio should be at least 1000:1, i.e. in cotton it is 1500:1 and in wool it is 3000:1. Also in natural fibers, the length variability is high; in cotton the variability is about 40% and for wool it is about 50%. Man-made fibers have off course lower length variability. Fibers of relatively short length are called staple fibers. All natural fibers come in staples, except silk. Silk is a natural filament fiber, which is a fiber of a long and continuous length. Man-made fiber staples are produced by cutting the continous filament strands that are produced when a liquid polymer solution is forced through a spinnerette and then hardens as such filament.

Staple fibers must be spun or twisted together to make a long continuous strand of yarn. However, depending on what their intended usage is, staples can also be used to form non-wovens or felted fabrics. The diameter of natural staple fibers is irregular and may vary along the length of the staple. The diameter of the man-made staple fibers is

uniform. Staples are used to make yarns. Yarns themselves can be knitted, woven or compressed in hundreds of patterns to create the final fabric.

Other important fiber characteristics are cross-section, shape, and fiber diameter. The variations in the cross-section form of the fiber will vary from one fiber to the other. These variations in the fiber shape will produce differences in the characteristics of fibers which will affect the covering power and light reflecting qualities of the fiber and/or yarn. The diameter of the fibers can be engineered to produce higher luster, or induce softness. Round or oval fiber shapes produce smooth, less surface area and poor covering power fabrics. Flat shaped fibers reflect more light than round fabrics. Dog bone/peanut produces a harsh fiber. Trilobal fibers produce a silk-like feel. A pentalobal fiber produces a bulkier fabric. Some fiber cross-sections are shown in Figure 133.

Yarns

A yarn is an agglomeration of fibers. Yarns are the next element in the hierarchical order; they are made from both natural and synthetic fibers of long (filament) or short (staple) lengths. Depending on the complexity of the combination of fibers they are made of, they can be composed of one or more strands of twisted or bonded fibers. Types of yarn include: spun (staple or short fiber) yarns, single (one strand or ply) yarns, filament (simple) yarns and plied (complex) yarns. That is, yarns may be constructed by using only staple, filament fibers (or strands), or by combining them.

Fibers **Yarn** **Fabric**

Figure 129. Hierarchical structure of fabrics: a. Fibers, b. Yarn, c. Fabric [103]

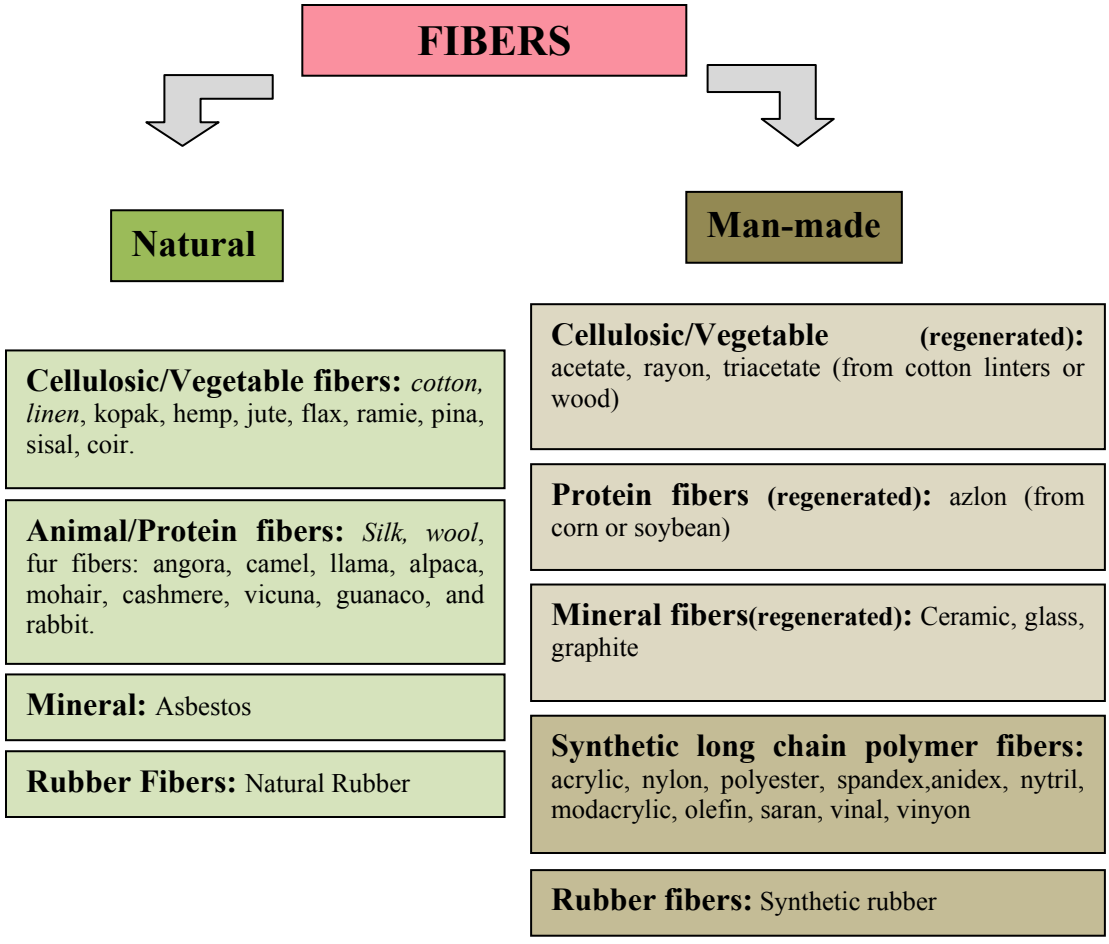

Figure 130. Fiber categorization

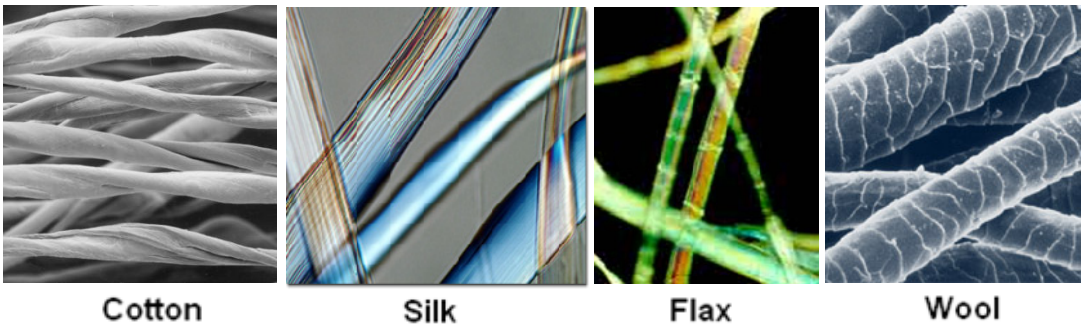

Figure 131. Some natural fibers: a. Cotton [105], b. Silk [106], c. Flax [107], d. Wool [108]

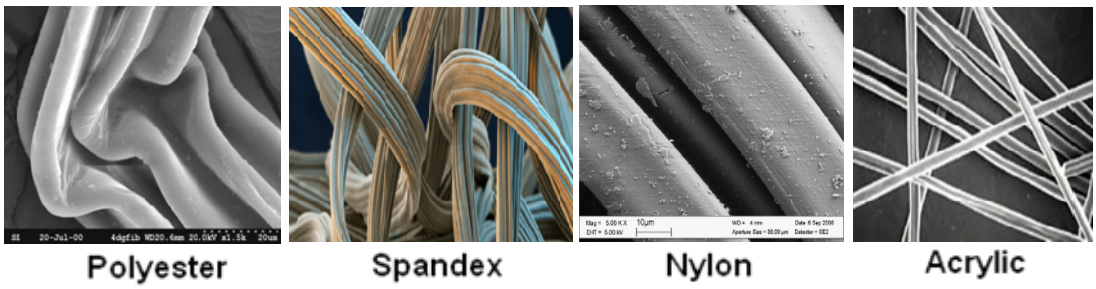

Figure 132. Some man-made fibers: a. Polyester [109], b. Spandex [110], c. Nylon [111], d. Acrylic [112]

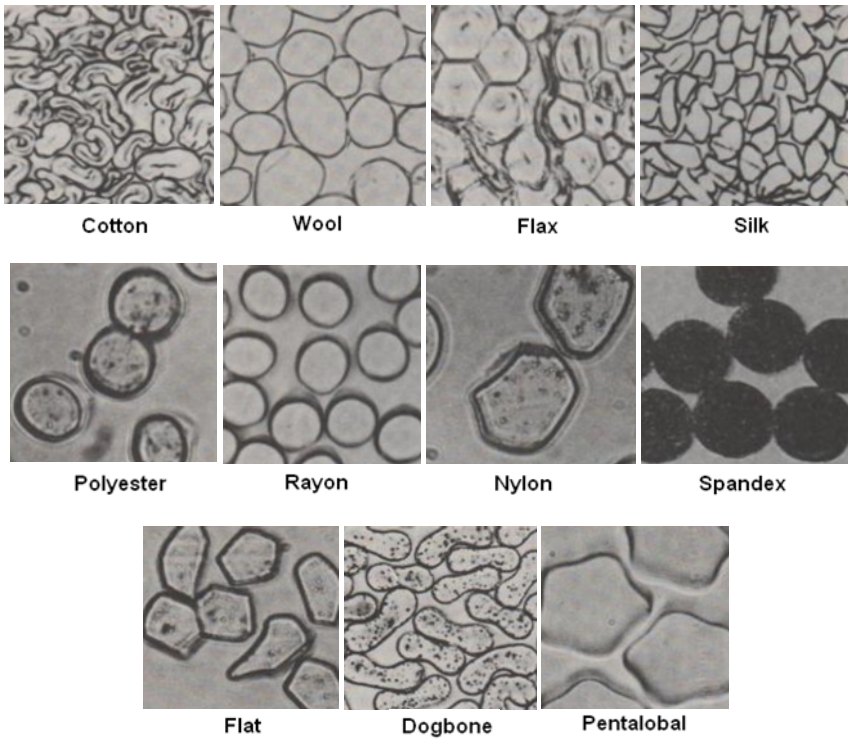

Figure 133. Cross section of some fibers: first row (natural fibers), second row (man-made and regenerated fibers), third row (cross-section shapes) [113]

Staple and filament yarns

Spinning is the process of drawing out and imparting twist to a mass of fibers. Filament fibers usually require less twist than staple fibers. Staple fibers are processed starting from a filament tow, that is, a long bundle of fibers in raw form. Spun yarns are then made of short staple fibers of a definite length. They are wider in diameter than the filament yarns and are usually highly twisted; however, they fall apart when they untwist.

The Filament yarns, classified into monofilament (single) and multifilament (plied), on the other hand are composed of long, continuous fibers (Figure 134). They are more uniform in diameter than the spun yarn and are loosely twisted; they do not fall apart when untwisted. These are stronger than the spun yarn of the same diameter. In general, it is stronger than the spun yarn of equal diameter. Therefore, the strength of the fabric is affected by the length of the constituent fibers. Complex yarns include the combination of one or more plies of yarn, a ply yarn is formed when two or more strands of yarn are twisted together. These can also be categorized according to how many twisting operations of the constituent yarns are present, i.e. cabled yarns are yarns with two or more components and more than one twisting operation [114].

Other characteristics that affect the strength of the final fabric are, i.e. number of plies in the yarn when it is a complex yarn, or whether the yarn is a core spun yarn, that is a central yarn with two or more types of fiber twisted around it. A core yarn consists of a core which could be spandex, rubber or any other type of yarn and an outer layer which is

usually texturized and of natural, manmade or blended fiber origin. The texture and elasticity of the yarn is partially determined by the outer layer.

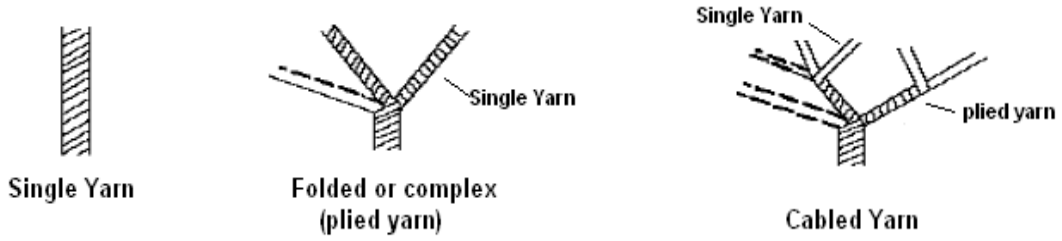

Figure 134. Basic types of yarn: a. Single Yarn, b. Plied Yarn, c. Cabled Yarn [114]

Strength characteristics are not only affected by the length of the constituent fibers of the yarn but also by the how the yarns are twisted. Yarns can be twisted in the S or Z direction (Figure 135); however, the yarn properties are affected only by the degree of twist. A fairly high degree of twist produces a strong yarn, low twist produces softer, more lustrous yarn and tight twist produces crepe yarns. In staple or spun yarns, the twist is given in units of turns per inch (tpi) [114]. As twist increases, the yarn strength and stiffness increase up to a certain degree and then begin to decrease at high twist levels. Yarns with extremely high levels of twist are called “crepe yarns”, which in turn possess a high level of torque (Figure 136). In woven fabrics, highly twisted yarns are noticeable by presenting a pebbled surface. On the other end, yarns with lower twist are softer to the touch and therefore more comfortable. Thread used for sewing is a tightly twisted ply yarn with a circular cross section.

There are other yarn properties that affect the final fabric; spun yarns have more spaces between fibers and therefore have better insulation properties, lower twist yarns also have more air space among them, and high twist yarns are more wind resistant.

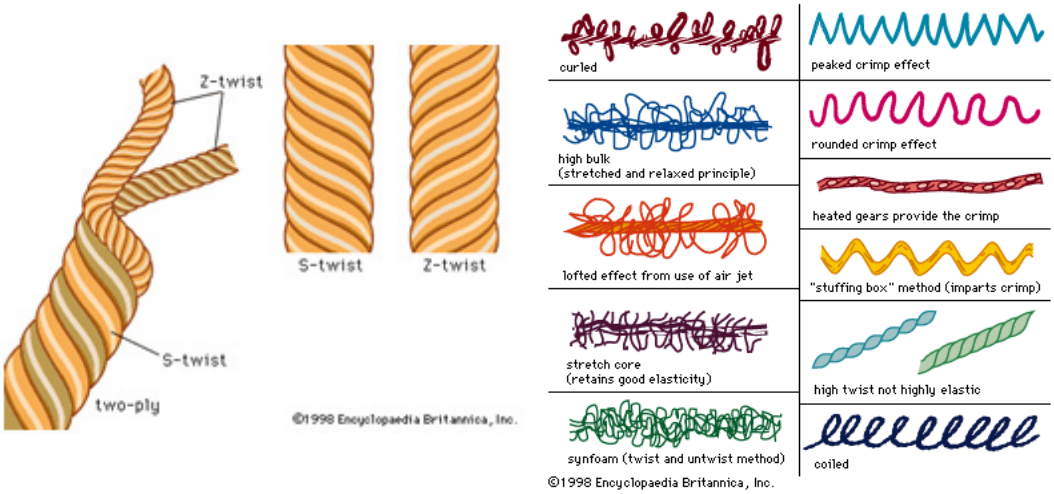

Figure 135. a. Twist given to yarns: S or Z, b. Examples of texturized yarn [114]

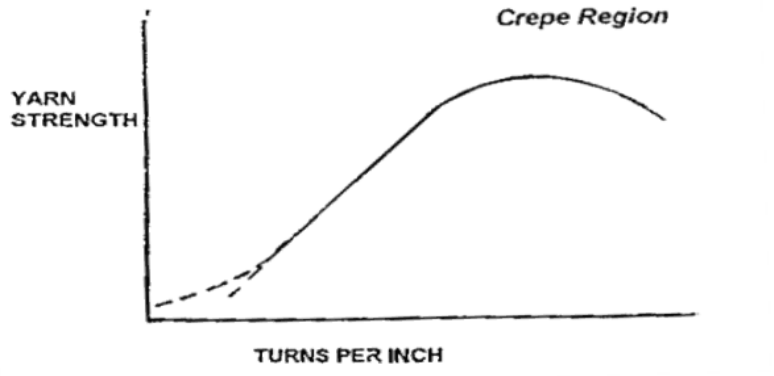

Figure 136. Strength of yarns according to degree of twist or turns per inch [114].

Novelty yarns, used to produce special effects include boucle (projecting loops), nub yarn (enlarged places), nubs (by twisting one end of a yarn around another many times at one point) and chenille (soft, lofty yarn with pile protruding on all sides).

Texturized yarns

Textured yarns are synthetic filament yarns that are made bulky or stretchy by heating or other techniques. They are the end result of physical, chemical or thermal manipulation of fibers and yarns so that they are no longer straight or uniform. This results in the modification of the arrangement of fiber and yarn. Texturizing produces a permanent change in the physical structure of the yarn (Figure 135). The fibers no longer lie parallel to each other. Texture characteristics vary from soft to crisp. They have greater covering power than untextured yarns, have stretch and elongation recovery properties, are softer than untextured yarns and have improved absorbency.

Knitting yarns

In yarns used for weaving the warp or lengthwise yarns are usually more tightly twisted, that is, stronger. Warp yarns are also smoother and more even than the weft or filling yarns. Knitting yarns have less twist than weaving yarns. Yarns used for machine knitting may be single or ply types, ply types are usually used for hand knitting.

Stretch yarns

Almost all natural and man-made fibers can be treated to produce yarns with some degree of stretch and recovery. Stretch properties may be applied to yarns by chemical or mechanical methods. The elasticity of the stretch yarn is controlled by the amount and type of twist in the yarn. Variation in the stretch may be obtained by modifying [113] the following properties:

- Amount of false twist
- Heat set temperatures
- Texturizing thermoplastic continous filaments
- Degree of tension and feed roll mechanism
- S or Z twist or alternating both
- Single or plied yarns

Yarns with high stretch potential and good recovery properties are mostly made or mixed with spandex fibers.

Spandex fibers

Spandex is a manufactured fiber made of at least 85% segmented polyurethane. It is extruded as a monofilament or in a multiplicity of fine filaments which immediately coagulate to form one filament. It deteriorates under the effect of heat and sunlight. For instance, a spandex solution may be put into a spinnerette from which it emerges to form a filament yarn (Figure 137).

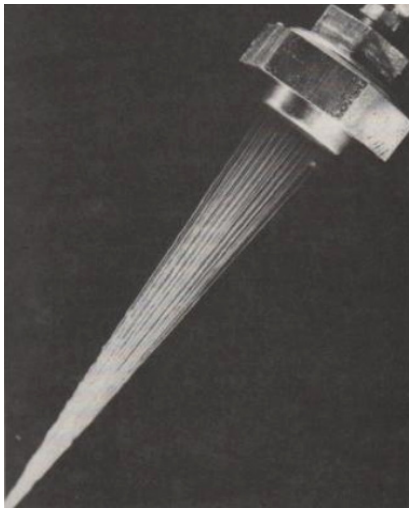

Figure 137. Solution emerging from spinnerrette to form filament yarn [113]

C.1.3 Yarn measurements and other properties

Linear Density or Fineness

Linear density is the fiber weight per unit length. The smaller the value of linear density the finer the fiber it measures. Yarn size measurement is done with the use of linear density or reciprocal of linear density, due to the accuracy with which the length and mass of the yarn can be measured. Linear density is frequently used to measure the fineness of fibers [115].

Quantities such as the diameter of the yarn cannot give accurate numbers because the yarns can be distorted by narrowing them. In terms of weight per unit length, it can be expressed in terms of Tex (g km^{-1}) which refers to the mass in grams per 1000 meters and Decitex (g $10km^{-1}$) which refers to the mass in grams per 10000 meters are used. When measuring objects with multiple fibers the term *'filament tex'* is used when referring to a single filament. The Denier is the other unit used and it is defined as the mass in grams per 9000 meters. Similarly, one can distinguish between the filament denier by *DPF* (Denier per filament) and the *total denier* which refers to the yarn. The fineness of fibers varies from about one decitex for fine viscous rayon, and even less for microfibers, to approximately ten decitex for coarse wools and even higher for man-made monofilaments. A fiber is considered a microfiber if it is 1 denier or less.

Linear density is also a good measure of the luster of a fabric since this number determines the number of individual reflecting surfaces per unit area of the fabric. Finer

fibers will produce more luster than coarser ones, which will generate a hard glitter. A chart with some common fibers and their linear density or fineness is presented in Table 8 [115].

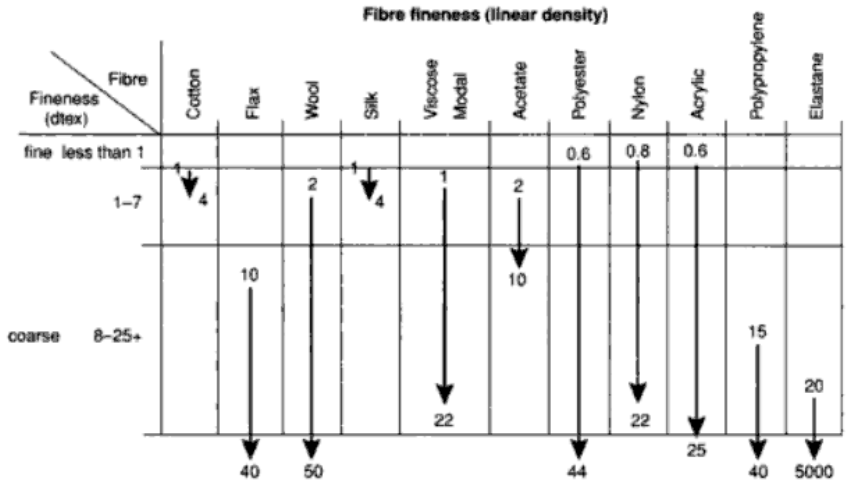

Table 8. Linear density of some common fibers [115]

Linear density has a strong correlation to the bending rigidity of fibers. For a given *yarn linear density* or for a *fabric weight* made from a given fiber; the resistance to bending increases as the linear density or fineness of the fiber increases. Fiber fineness is important in determining the stiffness of a fabric, and some other properties such as softness, handle and drapability qualities.

C.1.4 Tensile properties

The tensile properties of fabrics are ruled by the strength of its constituent fibers and by the degree of cohesiveness achieved in the twisting process to put them together. These mechanical properties directly affect some fabric properties such as: durability, low load

deformations (wrinkle recovery, drape, etc), resilience, stiffness, abrasion resistance, compressibility and softness. Stress strain curves for some of the most common fibers are presented in Figure 138.

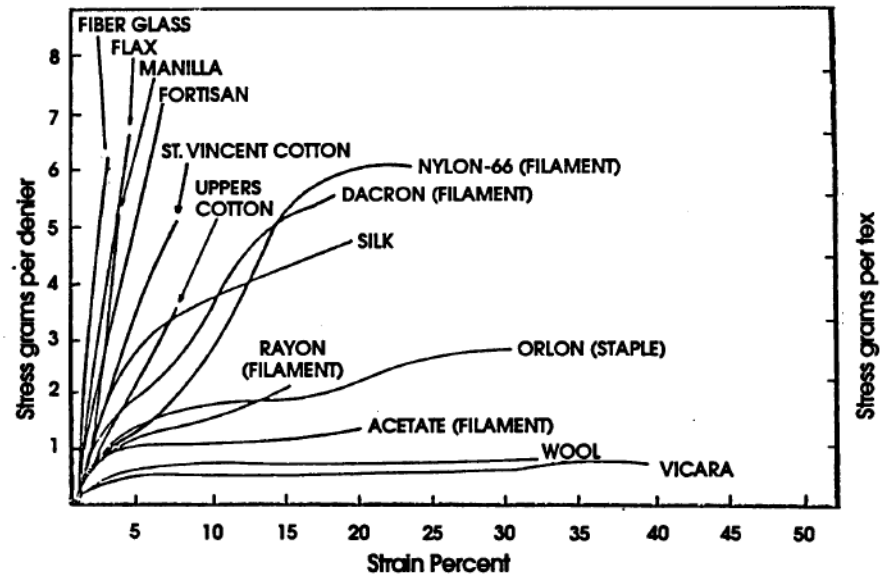

Figure 138. Typical stress strain curves for various fibers [104]

Fiber density

This property controls the covering power of a fiber in a fabric. In a given weight of fabric, the lower the density the greater the volume of fiber present. Therefore fabrics made from yarns of low density fibers will have a fuller and bulkier appearance than those made with high density fibers. These are presented in the following chart (Table 9).

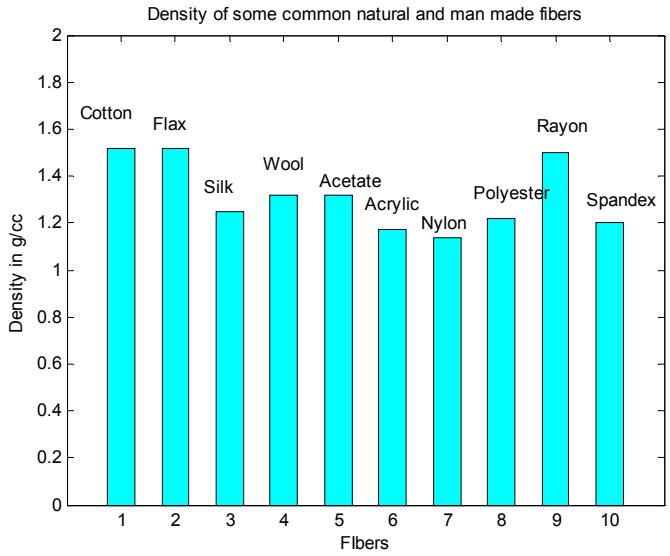

Table 9. Density of some common natural and man-made fibers [104]

Moisture absorption

Moisture absorption refers to the ability of the fiber to retain water. It shows how well a fiber absorbs water from the air, which also depends on the humidity (water content) of the air. Good water absorbing fibers help to prevent a buildup of static electricity in clothes. It can affect the dimensional stability of certain fibers. Also, when fibers gain water, their shape, size, stiffness and permeability might be affected. The amount of water absorption also affects the mechanical, frictional, and electrical (or static) properties of the fibers [104]. The following table (Table 10) shows the absorbency of some common natural and man-made fibers. In this figure, the moisture regain is expressed as a percentage of moisture free weight at 70F and 65% relative humidity.

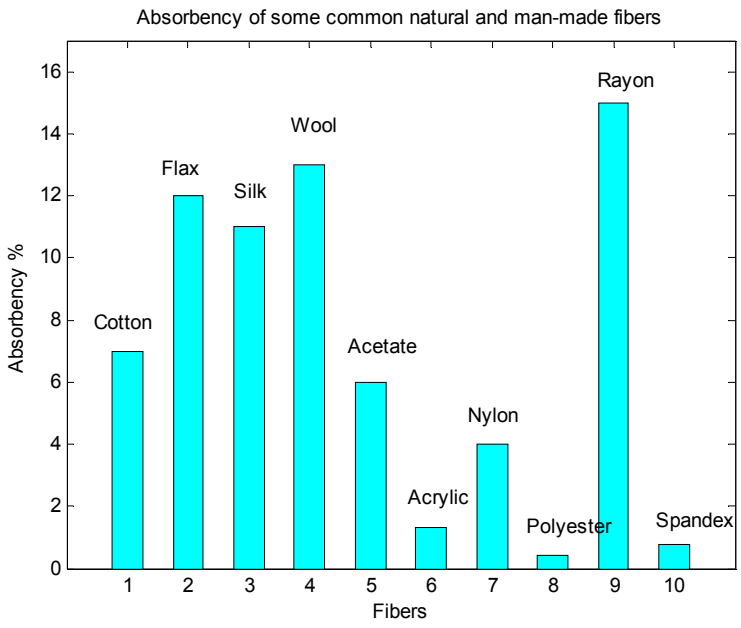

Table 10. Moisture absorbency of some common natural and man-made fibers [104]

Moderate changes in temperature

Temperature doesn't have a significant effect on the overall stability of the fibers. Synthetic fibers can be usefully deformed by heat and pressure; fabrics containing more than 50% of synthetic fiber are dimensionally very stable after heat setting. However, all textile fibers are susceptible to breakdown when exposed to very high temperatures.

Fiber Length

The shorter the fiber, the more fiber ends and therefore the more 'hairiness' which helps to trap air.

Biological resistance

It refers to the resistance that the fabric has to being decomposed by the enzymes of microorganisms.

Elasticity

It is a measure of how well a fiber returns to its original length after stretching.

Chemical resistance

Most natural textile fibers are inert, having a good resistance to mild alkalis and acids. They are practically insoluble in organic solvents and water. However, some man-made fibers such as the acetates are slightly soluble in organic solvents.

Tenacity and breaking extension

Defined as the force needed to break the fiber, strong fibers have a high tenacity value. A high tenacity value indicates that the fabrics made from these fibers are very durable. Breaking extension is the distance that the fiber will stretch before breaking. A comparison of the tenacity and percentage extension at break of some common fibers is presented in Table 11 [104].

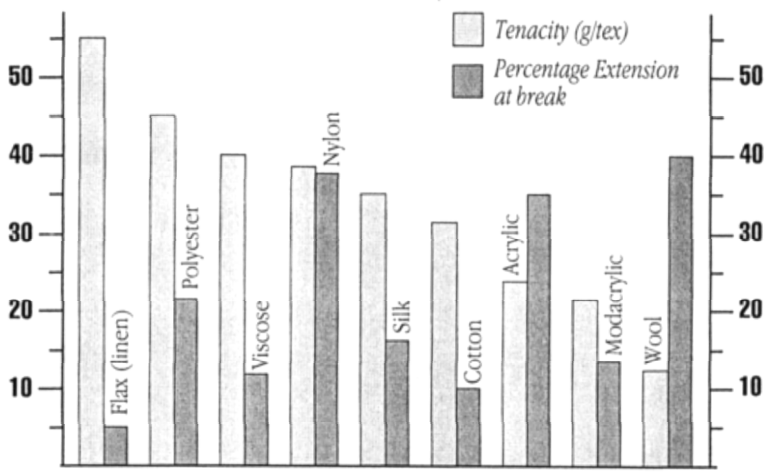

Table 11. A comparison of tenacity and percentage extension at break for the common fibers [104]

This amazing variety is either due to the intended functionality of the fabric or its aesthetic value. These construction processes and the origin of the fibers have an impact on the fabric final properties.

C.1.5 Comparison of the characteristics of the main fibers

The origin of the fibers ultimately affects the behavior and characteristics of the final textile. The characteristics of these fibers are important in the final properties of the textiles that they integrate. Natural fibers for instance have a tendency to be hydrophilic; they are good water retainers. Man-made fabrics, specially the synthetic ones are hydrophobic, that is they tend to keep dry and in general they are more compliant than natural fibers which are also non-resilient. The vegetable fibers, which are found in cell walls of plants, are cellulosic in composition. The animal fibers are protein in composition.

The major vegetable fibers are cotton and flax. Cotton grows in the seedpod of the cotton plant and its fiber is a single elongated cell. It resembles a collapsed and spirally twisted tube with a rough surface of about 200 to 400 turns of natural twist in one inch. The fiber appears flat, twisted and ribbonlike, with a wide inner canal (lumen) and a granular effect. Its chemical composition is of about 90% cellulose and about 6% moisture plus natural impurities. The outer surface of the fiber is covered with a waxlike coating which gives the fiber an adhesive quality. The natural twist of cotton fibers make them easy to spin into yarn. Cotton fibers that are treated by the process of mercerization undergo

swelling so they become straight and smooth. This produces a lustrous effect that is commercially valuable. The result of this process gives mercerized cotton. Flax, is a hair-like fiber with a cylindrical shape. The filaments are cemented together at intervals in the form of markings or nodes by 'pectin'. It is composed of about 70%cellulose and about 25% pectin plus woody tissue and ash. Flax fibers are more brittle than cotton fibers.

Cotton and linen with high absorbencies contribute to the cooling effect, desirable for hot weather clothing. Wool sheds water naturally, absorbs water slowly, and dries slowly, thermal and insulatory qualities. Rubber and spandex yarns may be produced as uncovered or bare yarns or as a monofilament core covered with another fiber. Rubber is used with other fiber yarns to produce elastics or fabrics.

A heuristic comparison of the main characteristics of some of the most common fibers is presented in Table 12 [115].

C.1.6 Types of fabric construction

The type of construction is also a constituent of the overall mechanical characteristics of the fabric. Figure 139 shows the different types of fabric construction from yarn elements. Woven fabrics are usually stronger than knitted ones. They are produced on anyone variety of simple or complex looms, which interlace the warp (0^0) fibers and weft (90^0) fibers in a regular pattern or weave style. The fabric's integrity is maintained by the mechanical interlocking of the fibers. Drape (the ability of a fabric to conform to a

complex surface), surface smoothness and stability of a fabric are controlled primarily by the weave style.

Table 12. Heuristic comparison of some of the main characteristics of common fibers [115]

Fiber	***Fineness***	***Length***	***Density***	***Moisture Absorp.***
Cotton	Medium	Staple	High	Good
Flax	Coarse	Long Staple	High	v.good
Wool	Fine/coarse	Staple	Medium	v.good
Silk	Medium	Filament	Medium	Good
Viscose	Fine/coarse	Filament	High	v.good
Acetate	Medium	Filament	Medium	Good
Polyester	Fine/coarse	Staple	Medium Good	v.poor
Nylon (polyam.)	Fine/coarse	Staple	Low	Poor
Acrylic	Fine/coarse	Staple	Low	v.poor
Polypropyl-ene	Fine/coarse	Staple	Lowest	Poorest
Elastane	Coarse	Filament	Low	v.poor

Fiber	***Biol. Resist.***	***Tenacity***		***Breaking extension***		***Elas-ticity***
		Dry	***Wet***	***Dry***	***Wet***	
Cotton	Poor	High	High	Low	higher	Poor
Flax	Poor	High	High	Lowest	Higher	Poor
Wool	Poor	Medium	Lower	High	Higher	Good
Silk	Poor	High	Lower	Medium	Higher	v.good
Viscose	Poor	Medium	Much lower	Medium	Higher	poor
Acetate	Good	Medium	Lower	High	Higher	good
Polyester	v.good	High	Lower	Medium	Medium	v.good
Nylon (polyam.)	v.good	High	Lower	High	High	v.good
Acrylic	v.good	High	Lower	Medium	Medium	v.good
Polypropyl-ene	v.good	High	High	High	High	Good
Elastane	Good	Low	Lower	v.high	v.high	highest

Figure 140 shows the three basic weave styles: Plain, Twill, and Satin. Other commonly used weaving styles include Basket, Leno and Mock Leno. In general, woven fabrics are firm, smooth, stable and maintain their stiffness. Other types of fabric construction, as shown in are nonwovens, where fibers are held together by gum or heat, such as Namada. Braided fabrics are created just like in braiding of hair and are mainly used to make trimmings and shoe laces. Nets are open mesh fabrics with geometrical shapes, the yarns may be knotted at the point of intersection. Tufting involves having a thread inserted on a primary base and is used to create dense insulating layers within a garment. There are also combinations of these last types, such as lace configuration.

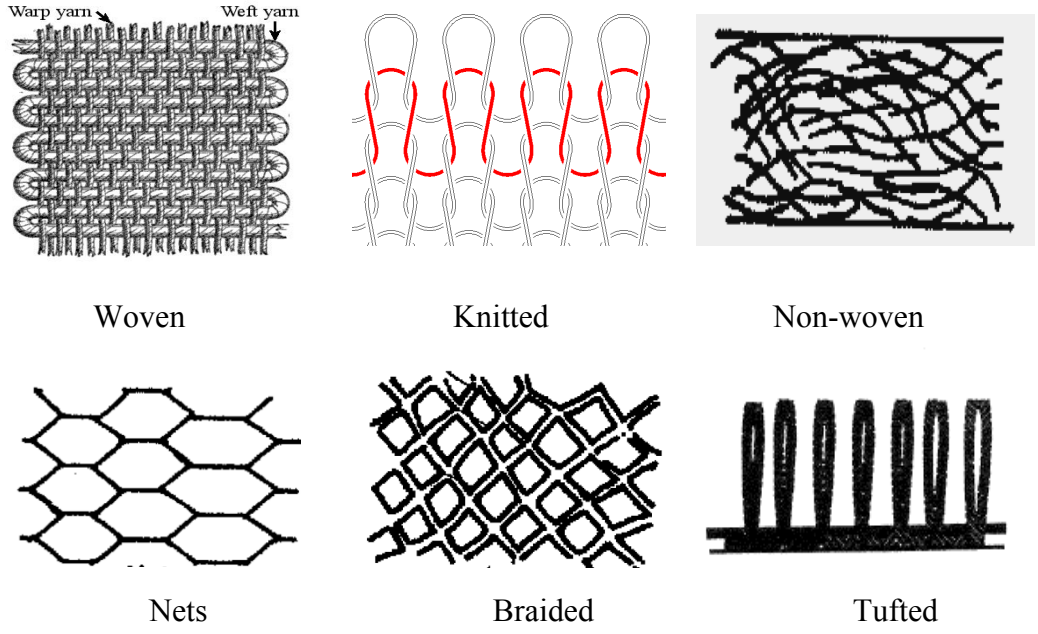

Figure 139. Basic types of fabric structure: a. woven [116], b. knitted, c. non-woven, d. nets, e. braided, f. tufted [117]

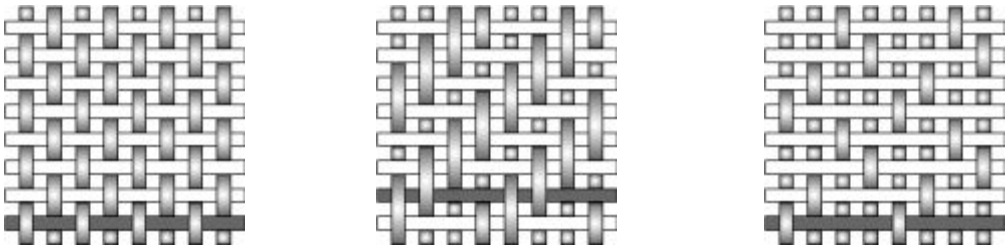

Plain Twill Satin

Figure 140. Basic types of weaving: a. plain, b. twill, c. satin [118]

In Plain weaving the fabric is symmetrical, has good stability but it is the most difficult to drape. Its high level of crimp imparts low mechanical properties. The twill weave provides a superior drape, reduced crimp and therefore higher mechanical properties. Satin weave has a high degree of drape, its low crimp gives good mechanical properties; however, it has low stability and is asymmetric.

Knitted fabrics are formed by the process of interlocking loops or forming loops with one or more yarns (Figure 141). Knitted fabrics are wrinkle resistant, stretchable and fitted to the body. They can be produced with one or more stitches which can be characterized by wale (vertical succession of loops) and courses (horizontal succession of loops). There can be flat knits or tubular knits, but there are hundreds of knit stitches and their combinations, most of which are used for aesthetic purposes. All these types of fabric construction can be the technological target for ultimate electronic integration into garments. Currently, the technologies have branched out ranging from a low level of integration to a high level of integration. They range from superficially added on electronics to components integrated within the textile yarn and even fiber integration. The knitted fabric structure is the one mostly used for the construction of socks. Some of

the basic stitches commonly used for knitting socks are shown in Figure 142. A second preferred construction is the woven type but is rather uncommon.

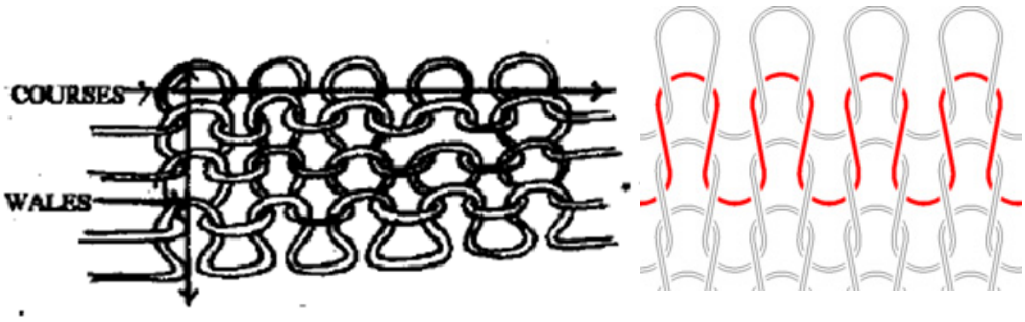

Figure 141. Knitted fabric structure: a. courses and wales [104], b. one course [117]

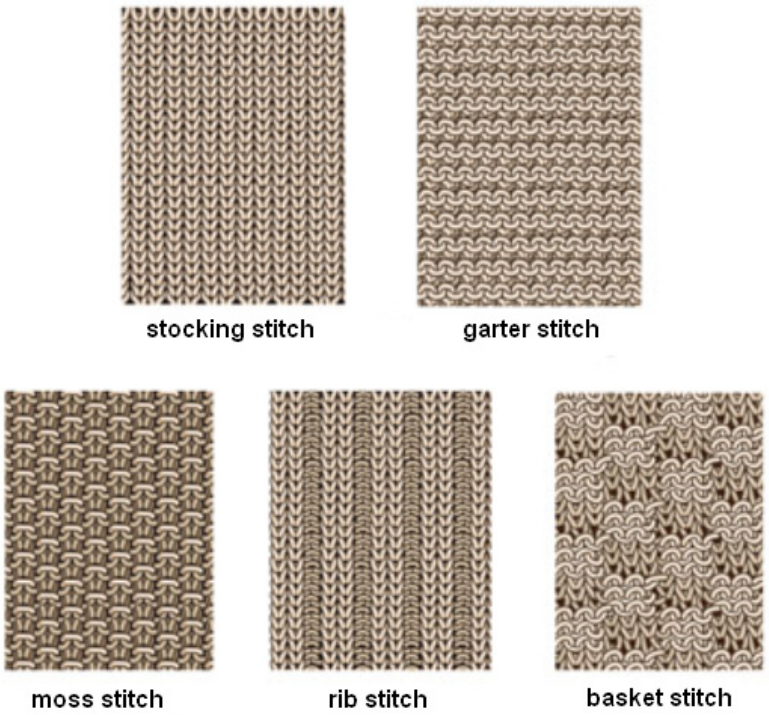

Figure 142. Knitted fabrics: some basic stitches [119]

C.2 Coating methods for fabrics

Fabrics can be given conductive properties by coating them with either intrinsically conductive materials or materials that have been doped with conductive particles. The doping particles can be of organic or inorganic origin.

Coating a layer of polymeric material on a textile imparts new characteristics to the base fabric. There are various methods used to apply polymer to textiles. For this thesis the method used was hand coating. However, there are many industrial-grade coating methods. They can be classified on the equipment used, method of metering and the form of the coating material. The various methods are as follows. First, fluid coating: coating material is in the form of paste, solution or lattices: it may consist of knife coaters, roll coaters, impregnators, and spray coaters. Second, coating with dry compounds (solid powder or film), comprise melt coating, calendering, and lamination. These processes may require expensive and dedicated equipment (Figure 143).

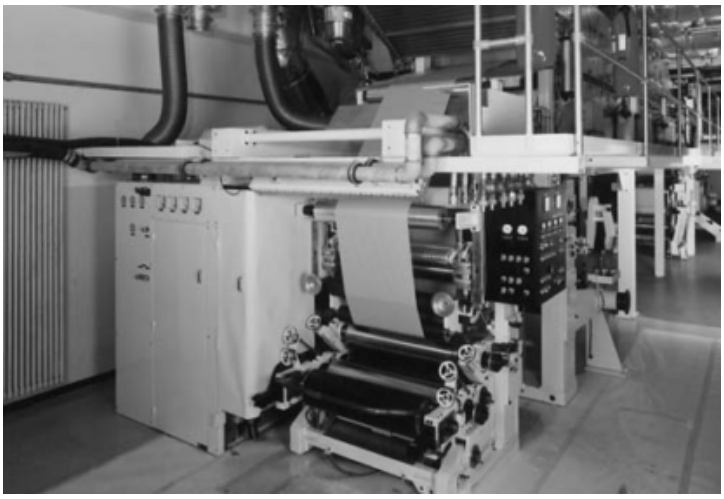

Figure 143. General view of a fluid coating plant.(Polytype, U.S.A) [120]

In gravure coating for example, engraved rollers are utilized to meter a precise amount of coating on the substrate. A setting like this is suitable for an extremely light coating and can handle higher viscosity materials (Figure 144).

Figure 144. A gravure coating plant [120]

There are many advantages in using these machines. For example, pre-tension is controllable as well as allowing the fabric to be coated under uniform tension. An oven is also usually incorporated for the curing phase, and a winding section for cooling. After this, the coated fabric can be wound up in rolls.

Bibliography

[1] "Smart shoes and smart socks for abnormal gait diagnosis and assistance" NSF grant # 08 00 501. Program manager: Dr. S.C. Liu.

[2] Glaros C., F.D.I., Likas A., and Stafylopatis A., A wearable intelligent system for monitoring health condition and rehabilitation of running athletes, in 4th International IEEE EMBS Special Topic Conference on Information Technology Applications in Biomedicine. 2003: UK.

[3] Tognetti A., L.F., Tesconi M., Bartalesi R., Zupone G., DeRossi D. Capture and classification of body posture and gesture using wearable kinesthetic systems. in Proc. of Euro. Conf. EACDA 2005. 2005. Pisa, Italy.

[4] Wagner, S., et al., Electrotextiles: Concepts and challenges. International Journal of High Speed Electronics and Systems, 2002. 12(2): p. 391-399.

[5] Post, E.R., et al., E-broidery: Design and fabrication of textile-based computing. IBM Systems Journal, 2000. 39(3-4): p. 840-860.

[6] Hasegawa, Y., et al. Novel type of fabric tactile sensor made from artificial hollow fiber. in Micro Electro Mechanical Systems, 2007. MEMS. IEEE 20th International Conference on. 2007.

[7] Sergio, M., et al., A textile-based capacitive pressure sensor. Sensor Letters, 2004. 2(2): p. 153-160.

[8] Gaudiana R, e.a., Photovoltaic Fibers, in Organic Photovoltaics VII. 2006, spie.

[9] Toivola, e.a., Photovoltaic Fiber. Thin Solid Films, 2009. 517(8): p. 2799-2802.

[10] McCall G.E., et al., “Flexor bias of joint position in humans during spaceflight”, Experimental Brain Research, vol. 152, n. 1, pp 87-94, 2003.

[11] Clement G., Reschke M.F. , “Neuroscience in Space”, Springer, 2008.

[12] Post E.R., a.O.M. Smart fabric, or “wearable clothing”. in IEEE First International Symposium on Wearable Computers, Digest of Papers. 1997.

[13] Phillips lumalive. Available from: http://www.lumalive.philips.com/

[14] Sahin O. et al. “Smart textiles for soldier of the future” Defense Science Journal, v 55, n2, p 195-205, April 2005

[15] Buechley, L. A construction kit for electronic textiles. in Wearable Computers, 2006 10th IEEE International Symposium on. 2006.

[16] Solar Jacket, Available from: www.gadgetheat.com

[17] Virginia Tech’s Hokie suit. Available from: http://blogs.zdnet.com/emergingtech/?p=727

[18] Chest strap, Available from: www.textronicsinc.com

[19] Golden-i headset, Kopin Corporation. Available from: http://www.gizmag.com/golden-i-headset/11666/

[20] MIThril, MIT Media lab human design. Available from: http://www.media.mit.edu/wearables/mithril/index.html

[21] Buechley LA. An Investigation of Computational Textiles with Applications to Education and Design. 2007.

[22] Eeonyx Corporation. Available from: http://www.eeonyx.com.

[23] Okuzaki, H., Y. Harashina, and H. Yan, Highly conductive PEDOT/PSS microfibers fabricated by wet-spinning and dip-treatment in ethylene glycol. European Polymer Journal, 2009. 45(1): p. 256-261.

[24] Nanosonic Inc. Available from: www.nanosonic.com.

[25] Sawhney, A., Agrawal, A., Patra, P., Calvert, P.,"Piezoresistive sensors on textiles by inkjet printing and electroless plating", Smart Nanotextiles , Proc.Mat. Res. Soc. Symp., v 920, p. 103-111, 2006.

[26] Kim, K. J., Chang, Y. M., Yoon, S. K., Hyun J., "A novel piezoelectric PVDF film-based physiological sensing belt for a complementary respiration and heartbeat monitoring system" ,Integrated Ferroelectrics, v 107, n 1, p 53-68, 2009.

[27] Carpi, F. et al., "Dielectric elastomers as electromechanical transducers", Piezocapacitive sensing, Elsevier Ltd., book, pp. 134, 2008.

[28] Buechley, L., Eisenberg M.," Fabric PCBs, electronic sequins, and socket buttons:Techniques for e-textile craft", Personal and Ubiquitous Computing, v 13, n 2, p 133-150, 2009

[29] Petkov, J., 'Measurement of body posture using multivariate statistical techniques', International Congress on Modeling and simulation proceedings, Australia 1999.

[30] Taya M., K.W.J., and Ono K., Piezoresistivity of a short fiber/elastomer matrix composite. Mechanics of Materials, 1998. vol. 28: p. pp. 53–59.

[31] Karaguzel B., "Printing conductive inks on nonwovens: challenges and opportunities", thesis, 2006.

[32] Tognetti A., B.R., Lorussi F., De Rossi D., Body segment position reconstruction and posture classification by smartTextiles. Transactions of the Institute of Measurement and Control, 2007. Vol 29(No. 3/4): p. pp 215-254.

[33] Lorussi F., S.E., Tesconi M., Tognetti A., and De Rossi D., Strain sensing fabric for hand posture and gesture monitoring. IEEE Transactions on information technology in Biomedicine, 2005. Vol.9 (No.3): p. p 372-381.

[34] Tognetti A., L., F., Tesconi, M. and De Rossi, D. Strain sensing fabric characterization. in 3rd IEEE Sensors Conf. 2004. Vienna.

[35] White, D. K., Wagenaar R. C., Ellis T. D., Tickle-Degnen L.. "Changes in Walking Activity and Endurance Following Rehabilitation for People With Parkinson Disease". Archives of physical medicine and rehabilitation, vol. 90, no.1, pp. 43-50, 2009.

[36] Foot bones. Available from: http://www.footankledr.com/

[37] Kirtley C., "Clinical Gait Analysis: theory and practice", Elsevier, 2006.

[38] 'Types of foot motion', Available from: http://www.dartmouth.edu/~humananatomy

[39] Fuller, P.W.W. "Life and work of Eadweard Muybridge", Proc. SPIE, v 3516, n1, p 4-14, 1999.

[40] Tognetti A., e.a. Characterization of a novel data glove based on textile integrated sensors. in IEEE Eng Med Biol Soc. 2006. New York City.

[41] Human gait. Available from: http://www.apas.com/ADI2001/adi/services/support/tutorials/gait/chapter1/1.1.asp

[42] Motion capture systems. Available from: www.vicon.com.

[43] Fastrak motion tracking system. Available from: http://www.polhemus.com/?page=Motion_Fastrak

[44] Zebrys gait analysis. Available from: www.zebris.de/english

[45] MEMS inertial sensors for gait analysis. http://www.xsens.com/en/mvn-biomech

[46] Meskers, C.G.M. et al.," Calibration of the 'Flock of Birds' electromagnetic tracking device and its application in shoulder motion studies" Journal of Biomechanics, v 32, n 6, p 629-633, June 1999.

[47] Electrogoniometer products. Available from: http://www.biometricsltd.com/gonio.htm.

[48] Donno, M., Palange, E., Di Nicola, F., Bucci, G., Ciancetta, F., "A New Flexible Optical Fiber Goniometer for Dynamic Angular Measurements: Application to Human Joint Movement Monitoring," *Instrumentation and Measurement, IEEE Transactions on* , vol.57, no.8, pp.1614-1620, Aug. 2008.

[49] Lee J. et al., "A Simple Optical Angular Sensors to Measure the Human Joint Angle," *SICE-ICASE, 2006. International Joint Conference* , vol., no., pp.1125-1126, 18-21 Oct. 2006.

[50] Svensson, W., Holmberg, U., "Foot and ground measurement using portable sensors," *Rehabilitation Robotics, 2005. ICORR 2005. 9th International Conference on* , vol., no., pp. 448- 451, 28 June-1 July 2005.

[51] Takeda, Ryo et al. “Gait analysis using gravitational acceleration measured by wearable sensors”, *Journal of Biomechanics,* vol 42, no. 3, pp. 223-233, 2009.

[52] Legnani G. et al., “A model of an electro-goniometer and its calibration for biomechanical applications”, Journal of Medical Engineering and Physics, Elsevier, vol.22, no. 10, pp. 711-722, 2000.

[53] ASTM Standard test method D 5278-98 (Reapproved 2004) for elongation of narrow elastic fabrics (static loading testing)

[54] ASTM Standard test method D 6614-07 for stretch properties of textile fabrics-CRE method

[55] ASTM Standard test method D 4964-96 (Reapproved 2004) for tension and elongation of elastic fabrics (constant-rate of extension type tensile testing machine)

[56] Niu, X.Z. et al., “Characterizing and Patterning of PDMS-Based Conducting Composites,” *Advanced Materials*, vol. 19, pp. 2682-2686, 2007.

[57] Hof, A. L. "A Control-release Ergometer for the Human Ankle." *Journal of Biomechanics* 30.2 (1996): 203-06.

[58] E. Ethridge, D.U., Electrotextiles. International Journal of High Speed Electronics and Systems 2002. 12(2).

[59] S. Wagner, E.B., W.B. Jordan, and J. Sturm, Electrotextiles: concepts and challenges. International Journal of High Speed Electronics and Systems, 2002. 12(2): p. 391-399.

[60] Zypad WL1100 by Eurotech group. Available from: http://www.zypad.com/zypad/home.aspx

[61] Timex data link, Timex Corporation. [cited; Available from: http://www.timex.com/

[62] Photovoltaic fibers invention. Available from: http://www.freshpatents.com/Photovoltaic-fibers-t20070412ptan20070079867php?3T3T type=description

[63] Quinn, B., "Techno fashion", book, Berg editorial, 2002.

[64] Voltaic systems. Available from:http://www.voltaicsystems.com/index.shtml

[65] Smart jacket. Available from: www.scottevest.com

[66] O'neil smart jacket. Available from: http://www.cellular.co.za/technologies/bluetooth/oneil/oneill_hub-jacket.htm

[67] Glowskin electroluminescent technology. Available from: http://www.safelites.com/glowskin.htm

[68] Canesis ltd. Textile research. Available from: http://www.techexchange.com/thelibrary/smarttextiles.html

[69] Adidas footscan. Available from: http://www.adidas.com

[70] Cetemsa R&D. Available from: http://www.cetemmsa.com/

[71] Numetrex cardio shirt. Available from: http://www.numetrex.com/

[72] Nike shoe application for ipod. Available from: http://www.apple.com/ipod/nike/

[73] Zephyr bioharness. Available from: http://www.zephyr-technology.com/products/bioharness-bt

[74] Excell, Jon, "Body clock" , 6T6T*Engineer*, v 293, n 7736, p 30-31, November 12, 2007

[75] Gebiom plantar pressure system. Available from: http://www.gebiom.com

[76] PPS digitacts human tactile system. Available from: http://www.pressureprofile.com/products-digitacts.php

[77] Sparkfun electronics. Available from: http:// www.sparkfun.com

[78] Stainless steel and polyester composite thread,Bekaert BK50/2. Available from: http://www.swicofil.com/bekintex.html

[79] Less EMF electromagnetic field shielding. Available from: http://www.lessemf.com

[80] Geisenberger, J. Zeller, K. "Textile Printing: A Challenge for Ink Jet Printing Technology", International Conference on Digital Printing Technologies, p 533-535, 2000.

[81] Tincher W.C. et al. "Inkjet systems for printing fabric", Textile Chemist and Colorist, v30,n 5, p 24-27, May 1998.

[82] Bloor D. et al. "A metal-polymer composite with unusual properties", Journal of Physics D: Applied Physics, v 38, n 16, p 2851-2860, August 21, 2005

[83] Bloor D. et al. "Metal-polymer composite with nanostructured filler particles and amplified physical properties." Applied Physics Letters, v 88, n 10, 2006

[84] Elektex conductive fabric. Available from: http://www.elektex.com/

[85] Fabric sensor patent, international application No. PCT/GB2004/004073 Available from: http://www.wipo.int/

[86] Jung S. et al. "Enabling technologies for disappearing electronics in smart textiles" Digest of Technical Papers - IEEE International Solid-State Circuits Conference, p 385-387, 2003.

[87] Carbon nanotube fabric. Available from: http://nanotechweb.org/cws/article/tech/22915

[88] Rogers A.J., "Materials and mechanics for stretchable electronics"Science 327, 1603, 2010.

[89] Muscles of the foot. Available from: http://www.medicalook.com/systems_images/Muscles_of_the_Foot.gif

[90] Anatomy of bones and ligaments. Available from: http://www.fairtrade-advocacy.org

[91] 'Foot muscles: Flexor hallucis longus'. Available from: http://www.wikipedia.org

[92] Agi A., Nikoli V., and Mijovi B., "Foot anthropometry and morphology phenomena" Ante Agic, Vailije nikolic Coll. Antropol. Vol.30, 2006.

[93] Atzler, E., Herbst, R., "Arbeitsphysiologische Studien", IIL Tell. Pfliigers Arch. ges.Physiol. vol. 215, pp. 291-328,1927.

[94] Cotes, J. E., and Meade, F., 1960, ''The Energy Expenditure and Mechanical Energy Demand in Walking,'' Ergonomics, 3, pp. 97–119.

[95] Alexander, R. M., 1995, ''Simple Models of Human Motion,'' Appl. Mech. Rev., 48, pp. 461–469.

[96] McGeer, T., 1990, ''Passive Dynamic Walking,'' Int. J. Robot. Res., 9, pp. 68–82.

[97] Cavagna, G. A., and Margaria, R., ''Mechanics of Walking,'' J. Appl. Phys., 21, pp. 271-278. 1966.

[98] Minetti, A., Capelli, C., Zamparo, P., Prampero, P. E. di, and Saibene, F., ‘‘Effects of Stride Frequency on Mechanical Power and Energy Expenditure of Walking’’, Med. Sci. Sports exercise, vol. 27, pp. 1194–1202, 1995.

[99] Jenkyn, T., Anas, K., Nichol, A., “Foot segment kinematics during normal walking using a multisegment model of the foot and ankle complex”, Journal of Biomechanical Engineering, v 131, n 3, March 2009.

[100] Corbman, B., ‘Textiles: Fiber to Fabric”. Fourth ed, ed. McGraw-Hill. Vol. Vol. 382. 1975.

[101] Cottet D., G.J., Kirstein T.and Troster G., Electrical characterization of textile transmission lines. IEEE Transactions on Advanced Packaging, 2003. 26(2): p. pp. 182-190.

[102] Pacelli M, C.L., and Paradiso R. Textile Piezoresistive Sensors for Biomechanical Variables Monitoring. in IEEE Conf Proc IEEE Eng Med Biol Soc. 2006.

[103] University, N.C.S. NC Textile Connect. Available from: http://www.nctextileconnect.com

[104] Carty, P. “Fibre properties” book, Pentaxion Ltd., 1996.

[105] Cotton fibers. Available from: http://www.itr-labs.com/2010/08/31/cotton-fibers/

[106] Silk fibers. Available from: http://micro.magnet.fsu.edu/primer/techniques/dic/dicgallery/wildsilksmall.html

[107] Flax fibers. Available from: http://www2.fbi.gov/hq/lab/fsc/backissu/july2000/images/flax.jpg

[108] Wool fibers. Available from:

http://www.csiro.au/science/WoolFibres.html

[109] Polyester fibers. Available from:

http://www.solarnavigator.net/composites/polyester_resin.htm

[110] Spandex fibers. Available from:

http://www.basf.de/en/intermed/industries/spandex/facilities.htm

[111] Nylon fibers. Available from:

http://www.emeraldinsight.com/content_images/fig/0580210205005.png

[112] Acrylic fibers. Available from:

http://www.awapaper.co.jp/e/products/es_m01a.html

[113] Gioello, D.A., Understanding fabrics: from fiber to finished cloth. 1982: New York: Fairchild publications. pp 42-206.

[114] Yarn classification. Available from:

http://smtradeltd.googlepages.com/YarnClassification.pdf

[115] Down, J.,Textiles technology through diagrams", book, Oxford university press, 2001.

[116] Woven structure. Available from: http://www.sarkisian.com/images/warpweft.jpg

[117] Basic types of fabric structure. Available from:

http://www. wikipedia.org

[118] Basic types of weaving. Available from:

http://www.recreationalflying.net/tutorials/scratchbuilder/composites.html

[119] Knitting stitches. Encyclopedia Britannica online, available from: http://www.britannica.com/

[120] Collier B.J., Epps H.H.,"Textile testing and analysis", Prentice Hall, 1999.